



TECHNISCHE UNIVERSITÄT MÜNCHEN

FAKULTÄT FÜR CHEMIE

PROTEINCHEMIE

**Insights into the regulation of Rab-AMPylation by the Legionella
enzyme DrrA**

Jiqing Du

Vollständiger Abdruck der von der Fakultät für Chemie der Technischen Universität
München zur Erlangung des akademischen Grades eines

Doktors der Naturwissenschaften (Dr. rer. nat.)

genehmigten Dissertation.

Vorsitzende: Prof. Dr. Cathleen Zeymer

Prüfer der Dissertation:

1. Prof. Dr. Aymelt Itzen

2. Prof. Dr. Kathrin Lang

Die Dissertation wurde am 23.11.2020 bei der Technischen Universität München
eingereicht und durch die Fakultät für Chemie am 21.12.2020 angenommen.

Im November 2020 vorgelegt von

Jiqing Du

aus Guangdong, China

geboren am 26.10.1987

Die vorliegende Arbeit wurde im Zeitraum von Oktober 2016 bis Oktober 2020 an der Fakultät für Chemie der Technischen Universität München und am Institut für Biochemie und Signaltransduktion am Universitätsklinikum Hamburg-Eppendorf unter der Anleitung von Prof. Dr. Aymelt Itzen durchgeführt.

Das folgende Manuskript ist im Rahmen dieser Arbeit entstanden :

Jiqing Du, Marie-Kristin von Wrisberg, Burak Gulen, Matthias Stahl, Christian Pett, Christian Hedberg, Kathrin Lang, Sabine Schneider, Aymelt Itzen (2020). **Rab1-AMPylation by Legionella DrrA is allosterically activated by Rab1.** *Nature Communications*. Under review.

Table of Content

Abbreviations.....	5
Abstract.....	6
Zusammenfassung.....	7
1. Introduction.....	8
1.1 AMPylation as a posttranslational modification.....	8
1.1.1 An overview of AMPylation.....	8
1.1.2 Structural and functional study of AMPylators.....	11
1.1.2.1 Enzymatic mechanism by Fic enzymes.....	11
1.1.2.2 Enzymatic mechanism by AMP-transferases.....	13
1.1.2.3 Enzymatic mechanism by pseudokinase SelO.....	14
1.1.3 Regulation mechanisms in AMPylators.....	15
1.2 <i>Legionella pneumophila</i> , the causative agent of Legionnaires disease.....	17
1.2.1 The regulation of <i>Legionella</i> T4bSS effectors.....	17
1.2.2 <i>Legionella</i> effector DrrA contains multiple functional domains.....	18
1.3 The vesicular transport protein Rab1b: the master regulator of the vesicular transport between ER and Golgi.....	19
1.3.1 Rab proteins act as molecular switches.....	19
1.3.2 Structural basis of Rab proteins.....	20
1.3.3 Rab1b: the master regulator of the vesicular transport between ER and Golgi.....	21
1.4 The coordination between DrrA and other Rab1b-targeted effectors.....	21
1.5 Novel target identification methods for Fic enzymes.....	22
1.6 Aim and scope of this thesis.....	24
2. Results.....	27
2.1 Non-canonical complex reveals Rab1b-AMPylation by <i>Legionella</i> DrrA is stimulated by active Rab1b.....	28
2.1.1 Biochemical characterization of DrrA AMPylation domain.....	28
2.1.1.1 Optimizing the expression and purification of DrrA AMPylation domain.....	28
2.1.1.2 The AMPylation domain of DrrA is a monomeric protein.....	29
2.1.1.3 The N-terminus of DrrA _{ATase} is critical for maintaining the AMPylation activity.....	30
2.1.1.4 Two different constructs of DrrA show similar kinetic features.....	32
2.1.1.5 Investigation of the interaction between DrrA and Rab1b by alanine screening.....	33
2.1.1.6 Probing the potential ATP binding mode in DrrA _{ATase}	35
2.1.2 Conceptual designs for trapping the non-canonical DrrA-Rab1b complexes.....	38

2.1.2.1 Complexes DrrA ₁₆₋₃₅₂ _L197C:TReND-1:Rab1b ₃₋₁₇₄ / Rab8a ₆₋₁₇₆ can be efficiently and specifically trapped in vitro.....	38
2.1.2 Structure of the DrrA: Rab8a-complex	41
2.1.3 Structural and biochemical analysis of the DrrA-Rab interaction in the non-canonical site of DrrA	44
2.1.4 AMPylation by <i>Legionella</i> DrrA is allosterically activated by active state Rab1b....	47
2.1.4.1 The C-terminus of the AMPylation domain may structurally stabilize the N-terminus for AMPylation.....	47
2.1.4.2 Rab1b binding in the NC-RBS may causes structural changes in DrrA	47
2.1.4.3 Rab1b-binding to the NC-RBS activates DrrA in vivo.....	48
2.2 Formation of the canonical complexes between DrrA AMPylation domain and Rab1b/8a.....	53
2.2.1 Design the potential cysteine substitutions for the DrrA-Rab1b/8a complex formation in the canonical site	53
2.2.2 Strategy for the purification of DrrA _{A176C} -Rab1b/8a complex	56
2.2.3 Biochemical characterization of DrrA _{A176C} -Rab1b complex.....	57
2.2.3.1 Crystallization of the covalent DrrA _{A176C} -Rab1b/8a complexes and the methylated DrrA _{A176C} -Rab1b/8a.....	57
2.2.3.2 Comparison of the catalytic activity of DrrA _{A176C} -Rab1b with the non-canonical complex	58
3. Discussion	60
4. Outlook.....	62
5. Materials and methods	63
5.1 Molecular biological methods.....	63
5.1.1 Polymerase chain reaction.....	63
5.1.2 Agarose gel electrophoresis.....	63
5.1.3 Gibson assembly	63
5.1.4 T4 SLIC	64
5.1.5 Quick change mutagenesis.....	64
5.1.6 Site-directed Q5 mutagenesis	64
5.1.7 Plasmid purification	64
5.1.8 Sequencing of vectors.....	64
5.2 Protein chemical methods	64
5.2.1 Recombinant protein overexpression	64
5.2.2 Production of <i>E. coli</i> cell lysates.....	65
5.2.3 Protein purification	65
5.2.4 Buffer exchange.....	66

5.2.5 In vitro AMPylation assay	66
5.2.6 Modification of Rab proteins with TReND-1	66
5.2.7 Formation of DrrA _{cys} -TReND-1 binary complex	66
5.2.8 ATPase assay	66
5.2.9 Cleavage of tag by TEV and PreScission protease	67
5.2.10 Nucleotide exchange for Rab1b and Rab8a	67
5.2.11 Preparative production of the DrrA:TReND-1:Rab complexes.....	67
5.2.12 Lysine methylation of DrrA ₁₆₋₃₅₂ and DrrA _{A176C} -Rab1b/8a complex.....	68
5.3 Analytical methods.....	70
5.3.1 SDS-PAGE	70
5.3.2 Coomassie staining of SDS gels	70
5.3.3 High resolution mass spectrometry (HRMS)	70
5.3.4 Temperature-scanning Circular Dichroism (CD) measurements	70
5.3.5 Determination of catalytic efficiencies for Rab1b and Rab8a	70
5.3.6 Enzyme kinetics of DrrA based on time-resolved tryptophan fluorescence	71
5.3.7 Analytical formation of DrrA:TReND-1:Rab complexes.....	71
5.3.8 Analytical size exclusion chromatography	72
5.3.9 ATP docking in DrrA ₁₆₋₃₅₂	72
5.4 Cell biology methods	72
5.4.1 Cultivation of H1299 cells	72
5.4.2 Transient transfection of H1299 cells	72
5.4.3 Collection of GFP-positive cells by FACS.....	73
5.4.4 Cytotoxicity analysis of DrrA-mutants by MTS assay	73
5.4.5 Fixation and imaging of H1299 cells.....	73
Reference	75
List of figures	98
List of Tables	102
Acknowledgement	103
Rights and permissions	104
Statutory declaration	105

Abbreviations

ER: Endoplasmic reticulum

Rab: Ras-related in brain

GEF: guanine nucleotide-exchange

GDI: GDP dissociation inhibitor

GAP: GTPase activating proteins

°C: Degree Celsius

P4M: Phosphatidylinositol-4-phosphate (PI4P) binding of SidM/DrrA.

LCV: *Legionella*-containing vacuole

DrrA: Defects in Rab1 recruitment protein A

AnKX: Ankyrin repeat-containing protein X

IbpA: Immunoglobulin binding protein A

HYPE: Huntingtin-interacting protein E

GS-AT: Glutamine synthetase adenylyltransferase

GS: Glutamine synthetase

Fic: Filamentation induced by cyclic-AMP

ATP: Adenosine triphosphate; ADP: Adenosine diphosphate; AMP: Adenosine

GDF: GDI displacement factor

GDP: Guanosine-5'-diphosphate; GTP: Guanosine-5'-triphosphate

GppNHp: Guanosine-5'-(β, γ)-imido]triphosphate

IPTG: Isopropyl β -D-1-thiogalactopyranoside

TCEP: Tris(2-carboxyethyl)phosphine

HEPES: (4-(2-hydroxyethyl)-1-piperazineethanesulfonic acid)

Tris: Tris(hydroxymethyl)aminomethane

Å: Angstrom

PI4P: Phosphatidylinositol-4-phosphate

FACS: Fluorescence-activated cell sorting

FBS: Fetal bovine serum

DMEM: Dulbecco's modified Eagle's medium

DAPI: 4, 6-diamidino-2-phenylindole

L. pneumophila: *Legionella pneumophila*

E. coli: *Escherichia coli*

TReNDs: thiol-reactive nucleotide derivatives

eGFP: enhanced green fluorescent protein

MTS: 3-(4,5-dimethylthiazol-2-yl)-5-(3-carboxymethoxyphenyl)-2-(4-sulfophenyl)-2H-tetrazolium

Amino acids are abbreviated with three or one letter codes in accordance with the recommendations of the International Union of Pure and Applied Chemistry (IUPAC) and the International Union of Biochemistry and Molecular Biology (IUB).

Abstract

In the course of infection, *Legionella pneumophila* secretes hundreds of effectors to hijack the host signaling machinery. To promote successful *Legionella* infection, the establishment and maintenance of a *Legionella*-containing vacuole are critical in the early phase of *Legionella* infection. DrrA, one of the early secreted *Legionella* effectors, is of importance for the recruitment of ER-like vesicles. During this process, Rab1b is redirected to the LCV from the host cytosol by the nucleotide exchange activity of the DrrA GEF-domain. Subsequently, DrrA utilizes ATP to AMPylate the Y77 residue in the regulatory switch II region of Rab1b. Although the molecular mechanism of GEF-action is well studied, the molecular mechanism underlying AMPylation by DrrA is uncovered yet. Together, the question about the physiological relevance between the GEF activity and the AMPylation event is not properly answered.

By using thiol-reactive nucleotide derivatives, two biochemically distinct enzyme:protein complexes between DrrA cysteine substitutions and Rab1 were covalently stabilized. The crystal structure of the non-canonical complex DrrA:Rab together with extensive biochemical characterization demonstrated that active Rab1b acts as an allosteric activator of DrrA through its binding to the non-canonical Rab1b binding site of DrrA AMPylation domain. This non-canonical Rab1b binding signal may be relayed into conformational changes in the DrrA AMPylation site, therefore the rearrangement of the active site may activate DrrA. As a result, DrrA AMPylation activity is primed by the GEF activity of DrrA, and further allosterically stimulated by active Rab1b. The double switches for turning DrrA AMPylation activity on may restrain AMPylation-mediated cytotoxicity to the LCV-surface, which renders AMPylation of Rab1 beneficial for the *Legionella* infection. Therefore, the allosteric activation of DrrA AMPylation activity by active Rab1b represents a yet unprecedented mechanism, which could shed light on other AMPylation enzymes.

Zusammenfassung

Im Verlauf einer Infektion durch *Legionella pneumophila* schleust das Bakterium Hunderte von Effektoren in die Wirtszelle ein, um bestimmte Signalwege des Wirts zu manipulieren. Insbesondere die Einrichtung und Aufrechterhaltung eines Subkompartiments, der Legionellen enthaltenden Vakuole (LCV), in der frühen Phase der Legionelleninfektion ist von entscheidender Bedeutung für eine erfolgreiche Legionelleninfektion. Einer der frühen sezernierten Legionellen-Effektoren ist DrrA, welches für die Rekrutierung ER-ähnlicher Vesikel von Bedeutung ist. Während dieses Prozesses wird Rab1b durch die Nukleotidaustauschaktivität der DrrA-GEF-Domäne vom Wirtszytosol zur LCV umgeleitet. Anschließend verwendet DrrA ATP, um den Y77-Rest in der regulatorischen Schalter-II-Region von Rab1b zu AMPylieren. Obwohl der Mechanismus der GEF-Wirkung gut untersucht ist, sind die molekularen Mechanismen, die der AMPylierung durch DrrA zugrunde liegen, noch wenig verstanden. Insgesamt ist die Frage nach der physiologischen Relevanz zwischen der GEF-Aktivität und der AMPylierung nur unvollständig beantwortet.

Durch die Verwendung thiol-reaktiver Nukleotidderivate wurden zwei biochemisch unterschiedliche Enzym:Protein-Komplexe zwischen DrrA-Cystein-Substitutionsmutanten und Rab1 kovalent stabilisiert. Die Kristallstruktur eines nicht-kanonischen DrrA:Rab-Komplexes zusammen mit einer umfangreichen biochemischen Charakterisierung zeigte, dass aktives Rab1b durch seine Bindung an die nicht-kanonische Rab1b-Bindungsstelle der DrrA-AMPylierungsdomäne als allosterischer Aktivator von DrrA wirkt. Dieses nicht-kanonische Rab1b-Bindungssignal bewirkt vermutlich Konformationsänderungen in der DrrA AMPylierungsdomäne, die daraufhin aktiviert wird. Die DrrA AMPylierungsaktivität wird somit einerseits durch die GEF-Aktivität von DrrA und andererseits allosterisch durch aktives Rab1b stimuliert. Dieser Doppelschalter zur Regulation der DrrA AMPylierungsaktivität könnte eine potenzielle AMPylierungs-vermittelte Zytotoxizität auf der LCV-Oberfläche einschränken, was die AMPylierung von Rab1 für die Legionellen-Infektion vorteilhaft macht. Daher stellt die allosterische Aktivierung der DrrA AMPylierungsaktivität durch aktives Rab1b einen neuartigen Mechanismus dar, der Licht auf andere AMPylierungsenzyme werfen könnte.

1. Introduction

During pathogen-host interactions, precise temporal and spatial regulations of host proteins are fundamental for infections. This signalling switch process can be orchestrated by proteins' binding, exchange of cofactors, and post-translational modifications (PTM). In order to hijack the complex signaling pathways in the host cells, PTMs are utilized by pathogens to regulate host proteins at the molecular level. Thus, to get insight into pathogen-host interaction, numerous PTMs are discovered and intensively studied. For instance, de/ubiquitination, ADP-ribosylation, phosphorylation, proteolytic cleavage etc. AMPylation, transferring adenosine monophosphate (AMP) moiety from adenosine triphosphate (ATP) to hydroxyl-bearing side chains of target proteins (Figure 1), is emerging as a PTM in playing fundamental roles in the course of pathogen infections. Therefore, the biochemical understanding of AMPylation will further increase the knowledge about pathogenesis, but also offers us a new perspective to re appreciate the host signaling pathways.

1.1 AMPylation as a posttranslational modification

1.1.1 An overview of AMPylation

Currently, AMPylation is shown as a widely shared PTM by diverse enzymes, which are including AMP-transferases, Fic (filamentation induced by cyclic-AMP) enzymes and pseudokinases. Interestingly, AMPylation was first revealed by the case study of glutamine synthetase adenylyltransferase (GS-AT, AMP-transferase) ¹. GS-AT, one member of the family of DNA polymerase β -like enzymes, is a bifunctional enzyme: its C-terminus functions as an AMP-transferase, whereas its N-terminus carries a reverse enzymatic activity: deAMPylation. The switch between AMPylation and deAMPylation is orchestrated by the cellular nitrogen level and the regulatory protein PII in *Escherichia coli*: in high level of nitrogen, PII activates the AMPylation activity of GS-AT while the level of nitrogen is low, UMP-modified PII inactivates the AMPylation activity of GS-AT ^{2,3,4}. Although GS-AT is well studied for its regulation in the cellular level of nitrogen in *E. coli*, no further seminal work has been done until the discovery of Fic enzymes.

The Fic gene knockout *E. coli* strain shows one abnormal phenotype: it forms filaments at high temperature. This observation leads to the identification of the first Fic protein ^{5,6}. Subsequently, bioinformatic analyses suggested that Fic enzymes, contains a conserved catalytic motif (HxFx(D/E)GNGR), that are widespread in all kingdoms of life ^{7,8}. However, the study of Fic enzymes' physiological functions at molecular level has not begun until recent years ⁹.

VopS, which contains a C-terminal Fic domain, can alter the transcriptional profiling in the host cells during the course of *Vibrio parahaemolyticus* infection. Such signaling

manipulation by VopS inactivated the NF- κ B pathway in the TLR receptor-independent manner, which further lead to apoptosis¹⁰. Moreover, VopS causes actin cytoskeleton collapse by AMPylation of the Rho family guanosine triphosphatases (GTPases), including Rac, Rho, and Cdc42. The modification of these proteins disrupts their binding to the downstream effectors and dampens the downstream signaling pathways¹¹. Later, the Fic domain-containing protein IbpA (immunoglobulin binding protein A) from the cattle pathogen *Histophilus somni*, caused cytotoxicity by its AMPylation activity. Interestingly, Cdc42 is AMPylated in Tyrosine 32 by IbpA, whereas Cdc42 is AMPylated in Threonine 35 by VopS. In general, the AMPylation of Cdc42 by IbpA and VopS was regarded as beneficial to the infection of the pathogens, since the Rho GTPases signaling pathways were reshaped by the pathogens. Intriguingly, the AMPylation of Cdc42 surprisingly initiated the innate immune response by forming the pyrin inflammasome¹². Therefore, it will be interesting to further investigate whether *Vibrio parahaemolyticus* and *H. somni* can employ unknown strategies to avoid being sensed by the pyrin inflammasome in the course of infection or not. Although these two Fic enzymes' physiological functions were well studied at molecular level, one important question about AMPylation is immediately raising up: is it possible that Rho GTPases or members in other subfamilies of small GTPases can be AMPylated by the AMP-transferase or Fic enzymes?

Indeed, *Legionella* effector DrrA, a member of AMP-transferases, was found to AMPylate Rab1b at tyrosine 77 in the regulatory switch II region¹³. Compared with the AMPylation of Cdc42, AMPylation of Rab1b shares similar physiological functions. AMP-Rab1b cannot bind to its interaction partners such as GDI (GDP dissociation inhibitor) and GAPs (GTPase activating proteins). Therefore, AMPylation of Rab1b leads to the inhibition of Rab1b's function in vesicular transport between endoplasmic reticulum (ER) and Golgi. Differently, DrrA modified Rab1b in the regulatory switch II region, one of the two regions, which are important for the binding of downstream effectors, and yet the AMPylation by IbpA and VopS occur in the regulatory switch I region. Notably, *Legionella* secretes another effector SidD, which can reverse the modification by deAMPylating Rab1b-AMP^{14, 15, 16}.

Although previous studies showed that the target substrates of AMPylation were restricted to small GTPases in the host, AMPylators can AMPylate diverse protein targets^{8, 9}. For instance, FicT toxin AMPylates DNA gyrase and topoisomerase IV in bacteria, which inhibits the growth of bacteria¹⁷. Moreover, the conserved Fic enzyme HYPE (Huntingtin-interacting protein E) in animals regulates the ER-resident Hsp70 chaperone BiP's functions by AMPylation and DeAMPylation^{18, 19, 20}. Therefore, AMPylation is not restricted to alter actin cytoskeleton and is also able to play an important role in other signaling pathways such as regulating unfolded protein response. Additionally, various studies proposed that HYPE's

AMPylation activity could be involved in the regulation of transcriptional machinery and the communication between the neuron cells⁹. Notably, HYPE was advised as one bifunctional enzyme by using the same catalytic center²¹, thus, such complex enzymatic regulations in one single Fic domain may further indicate HYPE can probably play more unknown roles in regulating the cellular signaling events.

Recently, one conserved pseudokinase SelO was confirmed as another class of AMPylators²². SelO modifies proteins (grxA and sucA) involved in redox biology. Moreover, the AMPylation of SelO plays a protective role against oxidative stress in *Saccharomyces cerevisiae*. These findings not only break the boundary between kinases and AMPylators, but also indicate that AMPylation can enable target proteins with more diverse functions than previously appreciated.

In a word, although significant progress has been achieved in the field of AMPylation, more and more putative AMPylators need to be characterized biochemically and structurally. Also, the molecular mechanisms and biological relevances of AMPylation remain to be uncovered. Thus, future studies should not only focus on AMPylation-mediated pathogenesis, but also concentrate on the crosstalk in host signaling pathways.

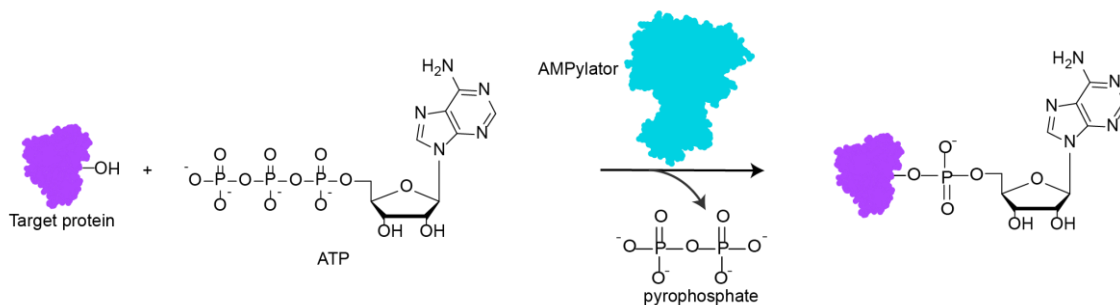


Figure 1 Schematic representation of AMPylation. Hydroxyl-bearing side chains of target proteins are AMPylated by AMPylators. ATP is the co-substrate.

1.1.2 Structural and functional study of AMPylators

The structural diversity of AMPylators leads to diverse enzymatic mechanisms of AMPylation. Hence, the enzymatic mechanisms by different subfamily of AMPylators will be discussed in the following.

1.1.2.1 Enzymatic mechanism by Fic enzymes

The diversified Fic motif sequences enable Fic enzymes adopt different co-factors. Interestingly, these co-factors contain a diphosphate moiety, e.g. ATP, other nucleotide triphosphates, or cytidine diphosphate (CDP)-choline⁸. With the assistance of divalent metal ions, Fic enzymes bind to the co-factors with its Fic motif (Figure 2A). During AMPylation, Fic enzymes cleave the P-O bond between the α phosphate and the β phosphate, which cleaved the cofactor into two distinct chemicals. Subsequently, the catalytic His will transfer the proximity-close one to the hydroxyl bearing group of the target protein^{8,9}. Therefore, the orientation of the cofactor relative to the Fic motif and the cofactor together determine the Fic-mediated modification. In this context, the modification can be diverse. For instance, IbpA transfers AMP from ATP to the protein substrate Cdc42 and releases the pyrophosphate. However, even utilizing the same cofactor ATP, the Fic enzyme Doc phosphorylates the protein substrate EF-Tu. Moreover, another peculiar Fic enzyme AnkX transfers the phosphocholine moiety of CDP-choline to its substrate protein Rab1b and Rab35^{23,24,25}.

Understanding the cofactor preferences Fic enzymes at molecular level is of importance. The Fic catalytic center together with the specific interactions outside the catalytic center discriminate the cofactor from others^{8,9,26}. In the case of AnkX, the complex structure of AnkX: CDP-choline shows that CDP-choline establishes elaborate interactions with the residues from the catalytic center and outside the catalytic center. Meanwhile, structural analysis indicated that binding of ATP to the catalytic center of AnkX is structurally excluded^{24,25}. Similarly, the limited space in the catalytic pocket of Doc forces ATP to be positioned in one inverse way, which results in phosphorylation instead of AMPylation^{27,28}. In the case of IbpA, one specific interaction between Glutamine 3757 and the adenine base enables ATP as a preferred substrate²⁹.

Structural studies have demonstrated the cofactor selection by Fic enzymes is elaborate, however, the knowledge about the substrate recognition by Fic proteins lags behind the urgent need. Currently, there are only two Fic enzyme-target substrate complexes reported^{25,29}. The first crystal complex is IbpA: Cdc42. In this complex, IbpA mainly interacts with Cdc42 by its N-terminal domain (referred as arm domain hereafter) (Figure 2B), which contributes to the substrate specificity. In addition to the arm domain mediated substrate recognition, the switch I region of Cdc42 extensively interacts with the so-called flap unit (Figure 2C). Such interactions not only bring the target Tyr residue into precise position for AMPylation²⁹, but

also contribute to substrate recognition. Intriguingly, the AnkX: Rab1b complex structure represents more distinctive features. After AnkX displaces the switch II region of Rab1b, the corresponding flap unit in AnkX is in the proximity of the switch II region of Rab1b. Such conformational changes render the S76_{Rab1b} of the switch II region into the correct position for phosphocholination. Therefore, displacing the switch II region efficiently is critical to prime the subsequent phosphocholination. Given that the switch II region is flexible in inactive state of Rab1b, it would be expected that AnkX prefers inactive state of Rab1b instead of active state of Rab1b²⁵. In conclusion, the flap unit in Fic enzymes is of importance for target substrate recognition. Additional interactions are also needed to discriminate its targets from other proteins. Therefore, further structural investigations can contribute significantly to the enzymatic mechanism by Fic enzymes.

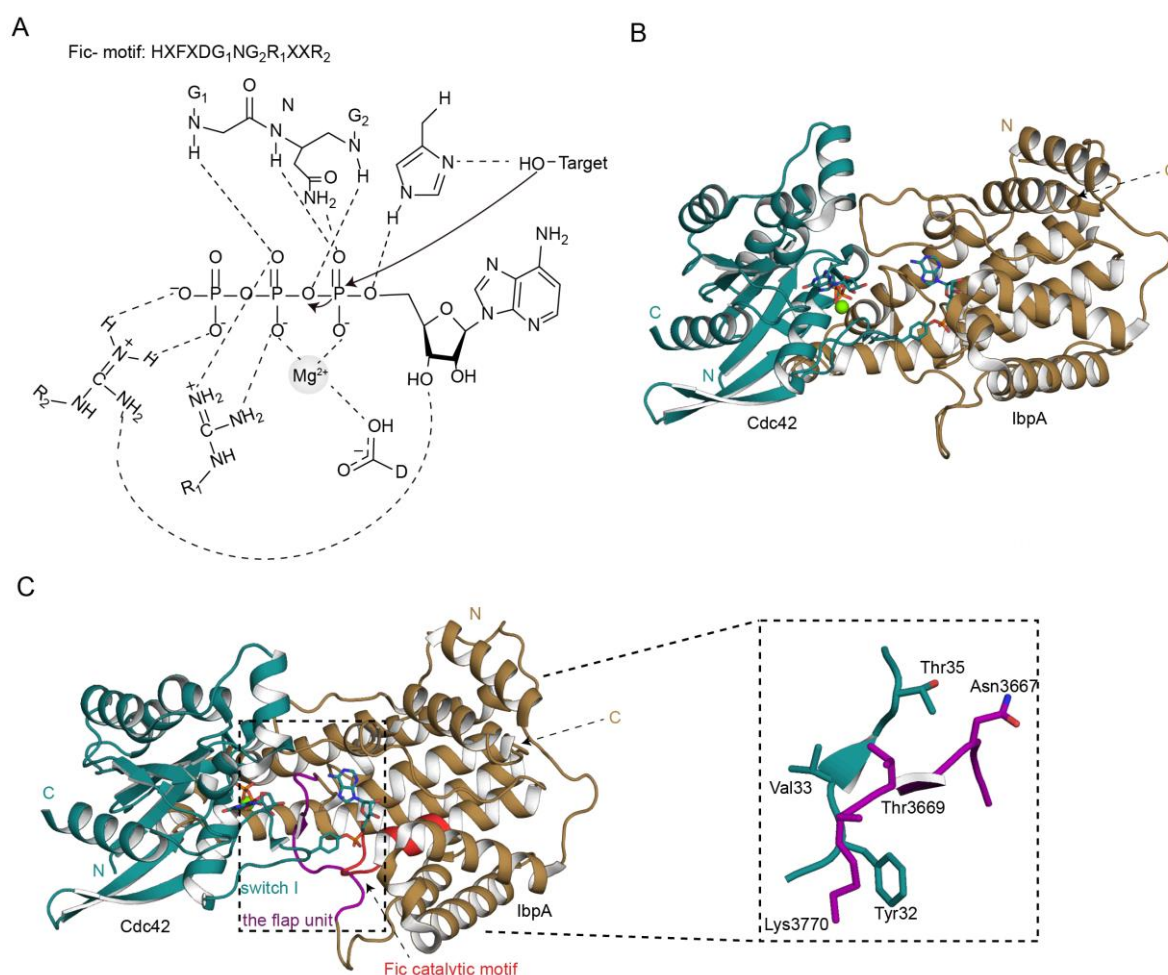


Figure 2 Enzymatic mechanism of Fic enzymes. **(A)** Schematic representation of the general binding mode of the co-factor ATP. **(B)** Cartoon representation of complex structure IbpA:Cdc42. The green sphere represents the Mg²⁺ ion. Stick binds to Mg²⁺ ion: GDP. Cdc42 is AMPylated in Tyr32 by IbpA. **(C)** Schematic representation of interactions between the flap unit and the switch I region of Cdc42 (PDB: 4ITR). Red region indicates the catalytic center of IbpA. Purple region indicates the flap unit in IbpA.

1.1.2.2 Enzymatic mechanism by AMP-transferases

In contrast to the Fic enzymes, the catalytic center of AMP-transferases is more divergent (GX₁₁DXD/E)^{1, 2, 3, 13}. Again, the divalent metal ion (e.g. Mg²⁺ ion) coordinates the interactions between the co-factor and the catalytic Aspartate residues (from the catalytic center (GX₁₁DXD/E)) for stabilizing the transition state (Figure 3). In general, triphosphate containing molecules are the co-factors of the AMP-transferases, especially ATP. Despite diphosphate containing molecules (e.g. ADP) can be transferred to the target proteins by the AMP-transferases, but kinetic studies show that they are not preferred co-factors³⁰. Surprisingly, the divergent catalytic motif shared by the AMP-transferases does not result in a diverse selection of the cofactors. Probably, there are additional interactions between the γ phosphate group of the co-factors and the AMP-transferases. Therefore, the AMP-transferases cleave the P-O bond between the two phosphates (α and β) of ATP during the AMPylation, and consequently cleaves the cofactor into two distinct groups: AMP and pyrophosphate. Subsequently, another Asp acts as the base to catalyze the AMPylation of the targets. Interestingly, the catalytic pocket of AMP-transferases is more flexible than Fic enzymes in space³⁰. Hence, despite different AMP-transferases adopt the different binding modes of ATP, these AMP-transferases carry the same function: transferring the AMP group to their targets.

AMP-transferases own another conserved feature: another polypeptide chain is required for their enzymatic activity. Lincosamide adenylyltransferase and kanamycin nucleotidyltransferase form homodimers to complement the active sites^{31, 32}. Prior to AMPylation, DrrA can bind to its cofactor ATP when Rab1b is present³³. Hence, AMP-transferases develop different strategies to regulate their active sites.

However, the knowledge about AMP-transferases' target recognition is limited, since the low affinity between the enzyme and target hinders the structural investigation. Only one of AMP-transferase: target complex was reported³⁴. In the complex of AadA: streptomycin, the conserved Asp residues is capable of Mg binding. The proximity-close Glu residue acts as the base for the nucleophilic reaction. Notably, structural analysis indicates that ATP's binding causes conformational changes in AadA. The regions in the C-terminus of AadA contribute to the interaction with streptomycin³⁴. Although the target in this reported complex is not a protein, the structural data provides critical information: first, ATP binding can cause conformational changes in AadA; second, the second Asp in the catalytic center of AadA is not the base for AMPylation. Therefore, it will be important to clarify whether these features are conserved or not in future investigation.

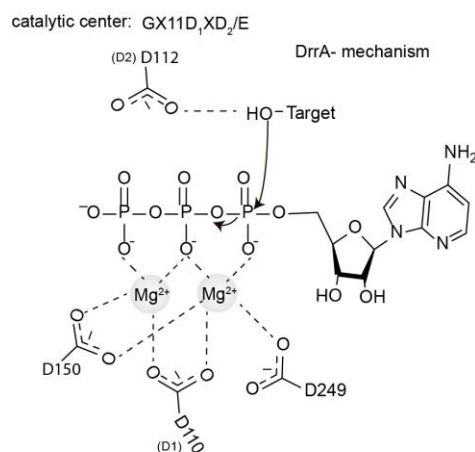


Figure 3 The potential AMPylation mechanism by AMP-transferases DrrA. Magnesium ions bridge the coordination between three aspartate residues and the triphosphate group of ATP. The second aspartate residue was suggested as the base to deprotonate the hydroxyl group.

1.1.2.3 Enzymatic mechanism by pseudokinase SelO

Pseudokinases, which were considered as inactive in phosphorylation, are now classified into AMPylators²². SelO adopts a kinase fold but is predicted as a pseudokinase, since it misses the catalytic base Asp residue in the HRD motif located in the catalytic loop.

Biochemical characterization indicates that SelO prefers ATP as the co-factor for AMPylation²². Similar to the AMP-transferases or Fic enzymes, a divalent ion is required to orient the phosphate groups of ATP. Strikingly, Mg²⁺ and Ca²⁺ are bound to the α and β phosphates in one reported crystal structure (PDB: 6EAC), which is never shown before in other classes of AMPylators. In order to precisely position the α and β phosphates of ATP, these two different divalent ions interact intensively with the distance-close Gln 253 and Asp 262. Importantly, more interactions contribute to coordinate the γ phosphate group of ATP. For instance, two invariant arginines (R176 and R183) interact with the γ phosphate. Additionally, lysine 113, stabilized by Glutamic acid 136 and arginine 176, also interacts with the γ phosphate (Figure 4).

Further understanding the enzymatic mechanism by pseudokinases is difficult since the pseudokinase: target protein complex is not reported yet. However, given that pseudokinases are highly conserved proteins in metazoans, future investigation in pseudokinases will not only deeper the molecular basis of AMPylation, but also stimulate more interesting discoveries of novel PTMs.

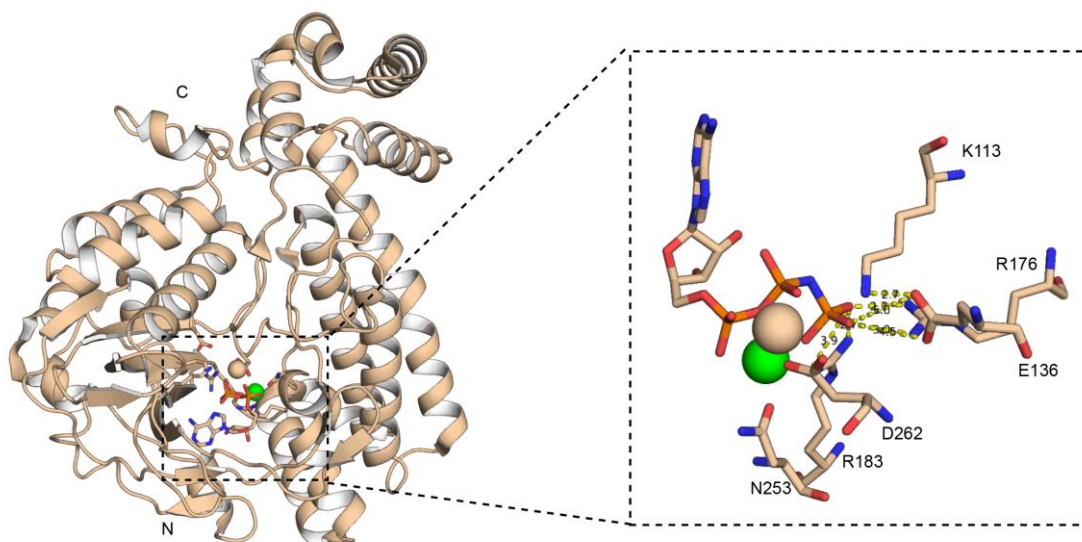


Figure 4 Representation of the interactions between ATP and pseudokinase SelO. The green sphere represents the Mg^{2+} ion. The sphere with wheat color represents the Ca^{2+} ion. Stick is ATP.

1.1.3 Regulation mechanisms in AMPylators

The potentially deleterious effects to the host cells (e.g. actin cytoskeleton collapse) by AMPylators indicate that AMPylation activity cannot be active constantly, and it has to be spatially and temporally regulated to limit its detrimental effects to the host cells.

Among all these previously reported AMPylators, the inhibitory mechanisms of Fic enzymes are well elucidated. It was reported that the presence of the inhibitory proteins (antitoxins) suppresses the AMPylation activity of Fic enzymes (toxin). Structurally, the inhibitory proteins will prevent the AMPylation activity by inserting a secondary structure element (e.g. an α -helix) into the co-factor ATP's binding pocket^{9, 26, 35}. In the toxin-antitoxin module, the inhibitory proteins are under degradation in certain stress conditions. Hence, the transcriptional regulation of the inhibitory proteins can turn the AMPylation activity of toxin off or on in a precise manner.

In addition to the toxin-antitoxin module, the intrinsic inhibitory α -helix (S/T)xxxE(G/N) in Fic enzymes can downregulate the AMPylation activity. Similarly, the inhibitory α -helix, referred to as inhibitory helix hereafter, obstructs the correct position of the ATP in catalytic center. In order to distort the ATP's correct binding mode, the Glu residue in this helix completes with the γ phosphate to form the ion bridge with the second Arginine from the catalytic motif³⁶. Consequently, this distorted conformation of ATP disables the nucleophilic attack to the hydroxyl residues of target proteins³⁶. In contrast to the inhibitory effect, the displacement of the α -helix can be reasoned as one activation mechanism of such Fic enzymes. Indeed, auto-AMPylation of the inhibitory helix renders this helix in a partly unfolded state, which

activates the AMPylation activity of NmFic³⁷. However, it has never been reported that auto-AMPylation by other inhibitory helix contained Fic enzymes can activate their AMPylation activity. Hence, probably the auto-AMPylation mediated activation by NmFic may be one unique sample. Notably, in vitro studies proposed that Fic enzymes can be turned on with the shift from the dimerization or oligomerization state to monomer state^{19, 37}.

In contrast to the Fic enzymes, AMP-transferases do not regulate the AMPylation by auto-modification or cycles from dimerization to oligomerization. In principle, AMP-transferases limit the AMPylation by deAMPylation^{2, 13, 14, 15}. As mentioned before, the AMPylation activity of GS-AT is under control by the regulatory protein PII. When the nitrogen level is low, UMP-modified protein PII stimulates the deAMPylation activity of the N-terminal domain in GS-AT. Conversely, when the nitrogen level is high, unmodified PII stimulates the AMPylation activity of the C-terminal domain in GS-AT. However, the regulation mechanisms in GS-AT by protein PII have never been shown in molecular level². Likely, modified or unmodified protein PII may bind to the central domain between the N-terminus and the C-terminus, and further regulate the catalytic centers in different domains. Nevertheless, the regulation mechanisms in GS-AT by protein PII can be different to the previously mentioned cases. Therefore, further structural investigation for studying the interaction between protein PII and GS-AT will be interesting.

Meanwhile, *Legionella* effector DrrA, another AMP transferase, shows comparable complexity in its regulation mechanisms with Fic enzymes³⁸. Initially, DrrA was found as the guanine nucleotide-exchange (GEF) protein for Rab1b, and amino acids from 340 to 533 are essential for maintaining the nucleotide exchange activity^{39, 40}. Later, its C-terminus was confirmed as a lipid binding domain^{41, 42}, which is used for its localization in the *Legionella*-containing vacuole (LCV). Once scientists reveal that DrrA AMPylates active state of Rab1b¹³, it immediately shows different regulation mechanisms in AMPylation from previously reported cases. First, DrrA-mediated AMPylation needs the GEF domain to recruit the Rab1b to the LCV, which brings Rab1b in close proximity to DrrA. At the same time, Rab1b needs to be activated by the nucleotide exchange from GDP to GTP. Notably, a set of *Legionella* effectors are participated to restrain the AMPylation activity by DrrA. SidD can specifically reverse the DrrA-catalyzed Rab1b AMPylation by deAMPylation of AMP-Rab1b. Subsequently, the *Legionella* effector LepB brings active Rab1b back into GDP-bound Rab1b, which can form a high-affinity complex with GDI to against DrrA-mediated AMPylation^{40, 43}. Additionally, Rab1b is shown to bind to the *Legionella* effector LidA with high affinity⁴⁴. Particularly, inactive Rab1b is phosphocholinated within the same switch II region by *Legionella* effector AnkX^{23, 25}. The competitions between DrrA, SidD and LidA may downregulate the AMPylation activity of DrrA. Likely, Rab1b phosphocholination by AnkX

could inhibit the Rab1b AMPylation by DrrA, since phosphocholinated Rab1b in GDP state is not a preferred substrate for DrrA.

The AMPylation regulation mechanisms underlying pseudokinase SelO are unique ²². Bioinformatic analysis indicates protein SelO contains mitochondrial target peptide. This peptide suggests its localization and potential functions. Biochemical study reveals that the SelO AMPylation activity is regulated by the formation of intramolecular disulfide bridge. Reduced disulfide increases the AMPylation activity of SelO, whereas increased disulfide decreases its AMPylation activity. Moreover, SelO replaces the disulfide-formed Cys with a Sec to enhance its redox potential, which enables SelO more sensitive to the redox or oxidative environment. Moreover, SelO can regulate its AMPylation activity by coordinating the position of the conserved activation loop in kinases.

In conclusion, the regulation mechanisms in AMPylators are diverse. Steric hindrances from intrinsically or extrinsically can downregulate or prevent Fic enzymes' AMPylation activity. Additional function-reverse domains or proteins restrict the AMP-transferases' activity. The cellular redox or oxidative environment switches pseudokinase SelO activity on or off. However, the known regulation mechanisms in AMPylators are mainly inhibitory ones. The unknown activation regulation mechanisms in AMPylators remain to be uncovered.

1.2 *Legionella pneumophila*, the causative agent of Legionnaires disease

The Gram-negative bacterium *Legionella pneumophila* is the causative agent of Legionnaires' disease. After uptake by human alveolar macrophages via phagocytosis, the pathogen establishes a replicative organelle referred to as the LCV, which is important for *Legionella* to escape from the lysosome degradation pathways ⁴⁵. The formation and maintenance of the LCV are mediated by *Legionella* effector proteins that are released by the bacterial Type IVb secretion system (T4bSS) from the bacterium into the host. In the following, the regulation mechanisms of *Legionella* T4bSS effectors will be discussed. Also, how the *Legionella* effector DrrA are regulated by *Legionella* will be briefly discussed.

1.2.1 The regulation of *Legionella* T4bSS effectors

To maximize the effectors' function and to suppress the innate immune response of the host in the replicative phase of infection, *Legionella* regulates its effectors in a temporal and spatial manner. First, the change in LCV phosphoinositide lipid (PI) composition by *Legionella* can regulate the distribution of the PI binding effectors. For instance, *Legionella* effector SidF can metabolize the PtdIns(3,4) P_2 and PtdIns(3,4,5) P_3 into PtdIns(4) P ⁴⁶. This activity is not only fundamental for recruitment of PtdIns(4) P -rich ER vesicles, but also important for the precise localization of SidC and DrrA. Additionally, host-lipidation machinery will be also hijacked by *Legionella* to facilitate its effectors' membrane localization ⁴⁷.

Legionella uses its effectors to directly reverse or suppress other effectors' enzymatic activities. DrrA are secreted by *Legionella* for AMPylation of Rab1b and deAMPylation of AMP-Rab1b, respectively^{13, 14}. Similarly, while AnkX acts for phosphocholination of Rab1b, another effector Lem3 functions for dephosphocholination of the modified Rab1b^{48, 49}. Recently, it was reported that *Legionella* effector SdeA ubiquitinates Rab33b in an E1 and E2 enzymes independent manner. Following, another two effectors were able to reverse the ubiquitination of Rab33b^{50, 51, 52}.

Some *Legionella* effectors are regulated directly by another effector. For instance, *Legionella* effector LubX targets SidH with ubiquitination⁵³. The effector SdeA's catalytic activity is inhibited by the SidJ's glutamylation⁵⁴. Of note, the activation of SidJ can be achieved in the presence of the eukaryotic protein calmodulin⁵⁵. Also, some *Legionella* effectors are regulated directly by host proteins. *Legionella* effector VipD lipase requires Rab5:GTP-dependent activation for its phospholipase A1 activity⁵⁶.

Surprisingly, *Legionella* recruits Cdc48/p97 to promote the dislocation of *Legionella* effectors and ubiquitinated proteins at the LCV⁵⁷, which is fundamental for *Legionella* intracellular replication. This unusual feature renders *Legionella* as one unique pathogen. Given that hundreds of effectors will be secreted in the course of infection, probably more unknown regulation mechanisms for the T4bSS effectors are not found yet. However, all of these mechanisms should have two important functions: First, to successfully manipulate the host signaling pathways; second, they must be regulated in a temporal and spatial manner.

1.2.2 *Legionella* effector DrrA contains multiple functional domains

Proteomic analysis shows that Rab1b, but not other small other Rab proteins, is recruited to the LCV³⁹. By a transposon-based screening, DrrA was identified as the effector responsible for Rab1b's recruitment³⁹. Such recruitment rerouted the ER-like vesicles to decorate the LCV, which is important to stabilize the LCV.

Subsequently, it was suggested that DrrA can act as the GEF protein and GDI-displacement factor (GDF) protein^{40, 58}. However, kinetic study indicates that the nucleotide exchange event starts when Rab1b is dissociated from Rab1b:GDI complex. Therefore, DrrA cannot function as one GDF, which can accelerate the dissociation of Rab1b from Rab1b:GDI complex. Although GEF activity cannot catalyze the displacement of Rab1b as a GDF protein, it was shown that the GEF activity is sufficient for the displacement of Rab1b from the Rab1b: GDI complex in the physiological conditions⁵⁹.

After that, the C-terminus of DrrA was found as a lipid binding domain, also called PtdIns(4)P-binding domain^{41, 42} (Figure 5). The specific recognition of PtdIns(4)P by DrrA ensures DrrA's localization to LCV. Also, such localization can orientate the GEF domain to

facilitate the Rab1b recruitment. Previous study shows that DrrA can cause cell-rounding phenotype when DrrA was overexpressed in the eukaryotic cells ¹³. Such cell-rounding phenotype in mammalian cells indicated cytotoxicity caused by full-length of DrrA in an unknown function. However, GEF domain together with P4M domain cannot cause cytotoxicity. Also, DrrA₆₁₋₆₄₇ is not toxic to the cells, suggesting that the cytotoxicity is not caused by the GEF domain and the P4M domain. DrrA was not suspected as one AMP-transferase until the DrrA₈₋₂₁₈ structure was solved ¹³. Structural analysis between DrrA₈₋₂₁₈ and the AMPylation domain of GS-AT suggested that N-terminus of DrrA owns AMPylation activity with the typical catalytic center (GX₁₁DXD/E). When Rab1b was found as the AMPylation target, then the crosstalk between these three domains were clearer than before: The C-terminus sets the stage for the following GEF activity and AMPylation. Then the GEF domain activates Rab1b and makes it ready for AMPylation. Once the active state of Rab1b is AMPylated, Rab1b is locked in the active state. The AMPylation by DrrA not only inhibits Rab1b's interactions with downstream effectors, but also extend its active state, which ensures that continuous recruitment of ER-like vesicles and hence supports *legionella*'s survival in the LCV ¹³.



Figure 5 Schematic representation of domain organization in full-length DrrA. Amino acid 1 to 340 is the AMPylation domain. GEF domain is from amino acid 340 to 533. The rest is the P4M domain. Picture is a copy from my previous manuscript to Nature Communications ⁶⁰.

1.3 The vesicular transport protein Rab1b: the master regulator of the vesicular transport between ER and Golgi

Small GTPases play important roles in cytoskeletal re-arrangement, vesicle trafficking, signal transduction and many other significant events in cells ⁶¹. Therefore, it is important to understand the biological functions of small GTPases. According to their different functions, small GTPases can be divided into the Ras, Rho, Rab, Arf/Sar, and Ran. Here the regulations and functions of Rab proteins will be discussed in the following.

1.3.1 Rab proteins act as molecular switches

Rab proteins, the largest subfamily of small GTPase, play crucial roles in vesicle trafficking and signal transduction through the interactions with downstream effectors. Rab proteins, as molecular switches, are active in GTP bound form and localized in a distinct compartment, or inactive in GDP bound form and localized in the cytosol in complex with RabGDI. Rab proteins nucleotide states are tightly regulated by the GEFs (guanine nucleotide exchange factors). Once activated by GEFs, Rabs' switch I and II structure become ordered

structurally, thereby enabling them to interact with the effectors for signal transduction and vesicle trafficking. Subsequently, Rab proteins are deactivated by GAPs followed by extraction from a distinct membrane by GDI (Figure 6). Therefore, precise temporal and spatial regulation of Rab activities by GEFs, effectors, GAPs and GDIs is fundamental for eukaryotic vesicle trafficking and signal transduction ⁶².

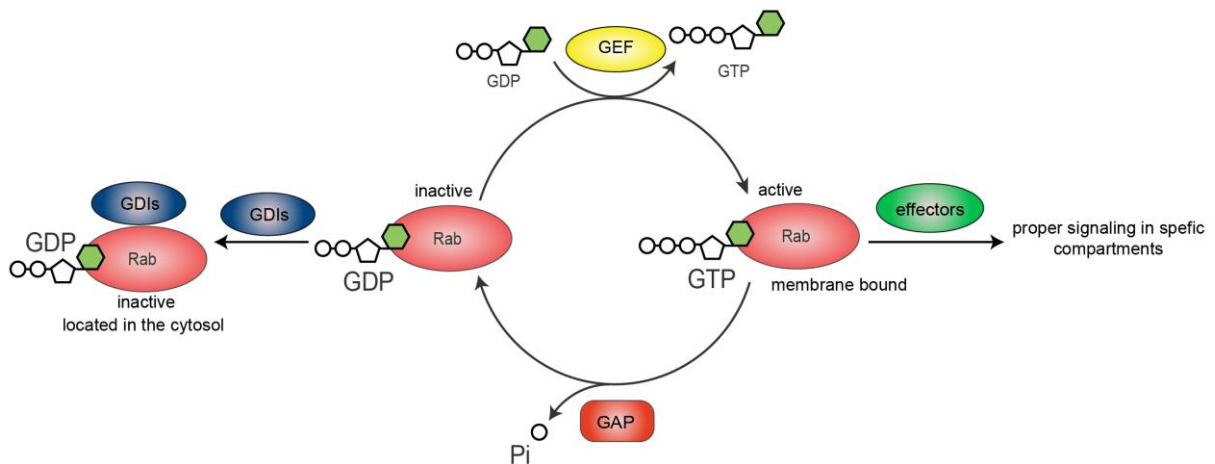


Figure 6 Switch cycling of RabGTPases. Inactive Rab proteins bind to GDIs in the cytosol. GEF proteins convert Rab protein to active state by nucleotide exchange. In the active state, Rab proteins interact with downstream effectors in defined compartments. The active Rab proteins are deactivated by GAPs-mediated intrinsic GTPase activity.

1.3.2 Structural basis of Rab proteins

Rab proteins have a fold consisting of a central six-stranded β -sheet surrounded by five α -helices ⁶². Rab proteins share conserved sequence motifs, which are important for coordinating the binding of nucleotides. In the presence of Mg^{2+} ion, the so-called p-loop contributes to the binding of the nucleotide's phosphates. Additionally, the G4 and G5 loops enable Rab proteins' specific binding to GDP/GTP instead of other nucleotides (Figure 7). Moreover, the distribution of Rab proteins in cells is under control by the prenylation of the Cys residues in the C-terminus. However, one has to notice that the structural heterogeneity shown by Rab proteins and the corresponding effectors further determine their different distributions and different signaling pathways in cells.

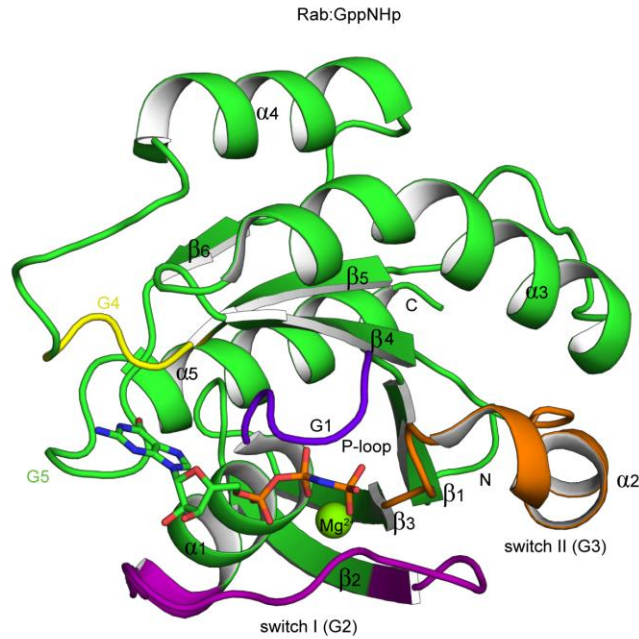


Figure 7 Cartoon representation of the structure of Rab proteins. Stick is GppNHp. Green sphere is Mg^{2+} . PDB: 1YZL ⁶³.

1.3.3 Rab1b: the master regulator of the vesicular transport between ER and Golgi

The study of Ypt (yeast protein transport 1) in the budding yeast *Saccharomyces cerevisiae* leads to the discovery of its mammalian homolog Rab1b ^{64, 65}. Like other Ras-related small GTPases, Rab1b activity is regulated by GEFs, GDIs, GAPs and GDFs ⁶⁶. Moreover, recent study indicates that TAK1 (TGF- β activated kinase 1)-mediated phosphorylation of Rab1b is necessary for the maintenance of normal Golgi apparatus structure ⁶⁷.

ER and Golgi apparatus play significant roles in the biosynthesis/ transport of proteins and lipids. Therefore, Rab1b-mediated membrane trafficking between them is critical for maintaining the balance of metabolic demands and further signal transductions ⁶⁸. Of note, Rab1b's function in ER-Golgi trafficking indicates that Rab1b has key roles in regulating autophagy, TORC1, Notch and integrin cell signaling pathways ⁶⁹.

1.4 The coordination between DrrA and other Rab1b-targeted effectors

Since DrrA is one effector in the replicative phase of legionella infection, its secretion and activity must fulfill two conditions: It must function properly to maximize its enzymatic activity

and must not cause cytotoxicity in the host. Therefore, it is not surprising that its expression level is not detectable after 4 hours of infection. Later, SidD is secreted to deAMPylate the AMP-Rab1b, which ensures that protein Rab1b can be accessible for LepB. Once the binding nucleotide of Rab1b is hydrolyzed from GTP to GDP by LepB, it can form a high affinity complex with endogenous GDI⁴⁰. Notably, two additional *Legionella* effectors (AnkX and LidA) are secreted to target on Rab1b^{23, 39}.

AnkX can modify GDP state of Rab1b with phosphocholination. Interestingly, phosphocholinated Rab1b can still bind to the GEF domain of DrrA²³. Likely, phosphocholination of inactive Rab1b probably represent a way to recruit Rab1b for its activation by the GEF domain of DrrA. As mentioned before, phosphocholinated Rab1b in GDP state is not a preferred substrate for DrrA-catalyzed AMPylation. However, phosphocholinated Rab1b in GTP state could be suitable for DrrA-catalyzed AMPylation. Therefore, understanding the physiological relevance between AnkX and DrrA in the *Legionella* infection will be important.

In the case of LidA, it was shown that LidA can bind to Rab1b or modified Rab1b (AMP-Rab1b or phosphocholinated Rab1b) with extremely high affinity⁴⁴. Albeit the physiological function of LidA is not clear, LidA probably functions as a safeguard protein to avoid causing cytotoxicity by preventing the modified Rab1b proteins mis-localized to the host cytosol.

In conclusion, AMPylation by DrrA needs to be well organized during the *Legionella* infection. Therefore, more effectors can be anticipated to regulate the AMPylation activity by DrrA. Also, there may be intrinsic regulations on AMPylation activity in DrrA.

1.5 Novel target identification methods for Fic enzymes

The greatest challenge in terms of characterizing those enzymes biochemically is that the target identification of AMPylators. Initially, Thr-AMP antibodies were applied for target identification⁷⁰. However, such antibodies failed to identify novel targets. Such antibodies are not specific against the epitope used for immunization, but also AMPylation is a diverse modification, which is including Threonine, Tyrosine and Serine AMPylation. Subsequently, ATP analogs were used for introducing reactive chemical handles or fluorescence chemicals^{71, 72, 73}. In a study, N6-propargyl ATP was first introduced to capture VopS-mediated AMPylation substrates from complex lysates⁷³. Similarly, a fluorescently labelled ATP analog was introduced to enrich VopS-mediated AMPylation substrates from lysates⁷². However, applications of these ATP analogs failed to discover novel AMPylator targets due to several limitations. Although such ATP analogs can be transferred to the targets by AMPylators, the competition between the endogenous high concentration of ATP and ATP analogs results in a low abundance of labeled targets. Meanwhile, labeling with ATP analogs yielded also

complex mass spectrometry data, which was not compatible in terms of novel target identification. Although novel targets of *Bartonella rochalimae* Fic enzyme Bep2 can be identified by using a stable isotope-labeled ATP, this is not applicable for general target identification of AMPylators⁷², since isotope-labelled chemicals are toxic. Therefore, it calls for novel target identification methods for AMPylators.

By engineering the chemical probes into mechanistically related classes of enzymes, activity-based protein profiling (ABPP) can be used as a functional technology for target identification⁷⁴. This technique offers a valuable advantage over traditional techniques that rely on abundance rather than activity.

Hence, macromolecular ABPP-like probes in AMPylators can be a novel target identification method for target identification. To this end, the synthetic thiol-reactive nucleotide derivatives (**TReNDs**) with attenuated chemical reactivity were designed: the combined reaction of the chloroacetamide with a strategically introduced cysteine in Fic enzyme and the AMP transfer by Fic enzyme to the target proteins enables the formation of a covalently trapped complex between the Fic enzymes and their target protein⁷⁵. Structural analysis on Fic enzymes shows that Fic enzymes share conserved structures in the active site: a loop and a helix are in proximity to the catalytic Histidine, which can be potential cysteine modification sites in the Fic enzymes. Therefore, the strategically design Fic_{cys} will react with thiol-reactive nucleotide derivatives to yield a binary complex. Subsequently, such binary complexes can be applied to covalently capture the target proteins to yield ternary complexes (Figure 8).

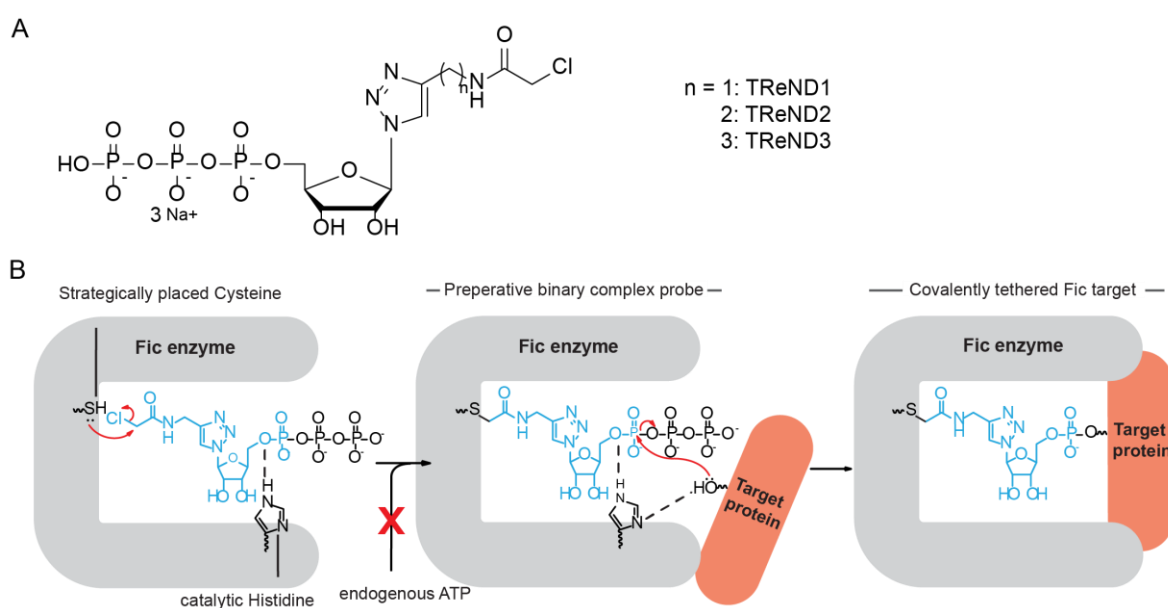


Figure 8 Chemical structures of TReND analogues and co-substrate-mediated covalent capture concept in Fic enzymes. **(A)** Chloroacetamide contained TReND analogues. The nomenclature of the TReND analogues is according to the linker length. **(B)** General strategy

of co-substrate-mediated covalent capture in Fic enzymes. The chloroacetamide reacts with the engineered cysteine yield a binary complex. Following, targets can be trapped by the AMP-transfer reaction. Figure 8B is a courtesy of Burak Gulen and has been reprinted with his permission.

1.6 Aim and scope of this thesis

In order to uncover the uncharacterized molecular mechanism underlying AMPylation by DrrA, this thesis will mainly focus on the characterization of the AMPylation domain of *Legionella* effector DrrA (hereafter referred to as DrrA_{ATase}) and the biochemical analysis of the covalent complexes DrrA_{ATase}-Rab1b/8a. (TReNDs analogues are designed and provided by Christian Hedberg, Umea University, Sweden)

The low affinity between the DrrA_{ATase} and Rab proteins posed a great challenge in terms of characterizing the DrrA: Rab complex. The TReNDs-mediated covalent capture approach has been successfully proven for Fic enzymes. Therefore, it is likely that this approach can be applicable in the case of DrrA_{ATase}, if TReNDs can be transferred to Rab1b by DrrA_{ATase} and a strategically designed cysteine can be introduced in DrrA_{ATase}. However, since DrrA_{ATase} is enzymatically and structurally different from Fic enzymes and the ATP binding mode in DrrA_{ATase} is unknown yet, the strategy for introducing the potential cysteine modification sites for covalent capture in DrrA_{ATase} will be different from the one in Fic enzymes. Previously, it was reported that ATP cannot bind to DrrA in the absence of Rab1b. Also, Rab1b's presence will change the conformation of DrrA_{ATase} in an unknown manner³³. Therefore, we reasoned that the strategically designed DrrA cysteine mutants would react with TReNDs in the presence of Rab1b, and further yield the DrrA-Rab complexes (Figure 9). However, the unknown ATP binding mode and the Rab1b-induced conformational changes in DrrA made the introduction of DrrA cysteine mutants difficult. Hence, I decided to first probe the unknown interface between DrrA_{ATase} and Rab1b by alanine screening and one genetic code expansion based method, which was provided by our collaboration partner Kathrin Lang from Technical University of Munich⁷⁶.

Eventually, a DrrA₁₆₋₃₅₂-L197C:TReND-1:Rab1b complex was yielded by extensive screening of cysteine substitutions in DrrA_{ATase}. However, the resulting crystals diffracted only poorly. Therefore, the TReND-linked complex with the GTPase domain of the close Rab1b-homolog Rab8a was also generated and submitted for structure determination. Surprisingly, the structure of complex DrrA₁₆₋₃₅₂-L197C:TReND-1:Rab8a was obtained at 2.1 Å resolution.

Interestingly, the structure of this complex suggested that DrrA_{ATase} contains two separate Rab-binding platforms. Therefore, the first part of this thesis focuses on biochemical characterization of DrrA, the identification of potential positions in DrrA_{ATase} for introducing the cysteine modifications and the formation of a ternary complex. Following, the previous unknown Rab1b binding site was confirmed by intensive biochemical, biophysical, and cell biological studies. In conclusion, this unrecognized Rab1b binding site acts as an allosteric regulation site since binding of active Rab1b can stimulate the AMPylation activity by three orders of magnitude.

Furthermore, structural analysis in the structure of DrrA₁₆₋₃₅₂-L197C:TReND-1:Rab8a complex reasoned that the second covalent DrrA-Rab complex can be obtained if the cysteine modifications were properly designed in the putative ATP binding pocket. Therefore, the second part of the thesis was focus on probing the potential positions in DrrA_{ATase} for the cysteine modifications in the catalytic site and the formation of the second complex. Indeed, DrrA₁₆₋₃₅₂ containing the A176C substitution formed a covalent ternary complex with Rab1b or Rab8a. However, structure determination of the complexes failed due a lack of well diffracting crystals. Nevertheless, by evaluating and comparing the catalytic activities of these two covalent DrrA-Rab complexes, we cannot only further confirm the significance of the allosteric regulation site, but also reason the sequence orders of DrrA-mediated AMPylation.

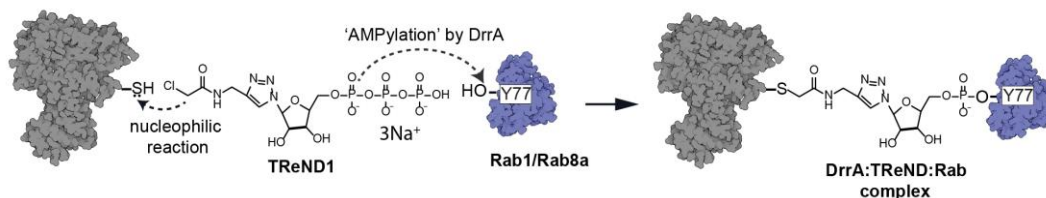


Figure 9 Trapping the DrrA:Rab complex via thiol-reactive nucleotide analog 1. Rab1b or Rab8a will be modified with TReND-1 at the AMPylation site Y77. The strategically designed cysteine will react with thiol-reactive nucleotide analog 1. Picture is a copy from my previous manuscript to Nature Communications ⁶⁰.

2. Results

This section is divided in two main parts according to two different DrrA-Rab complexes. The first complex, referred to as the non-canonical DrrA-Rab complex, allosterically regulates DrrA AMPylation activity by the binding of active Rab1b to the non-canonical site. Comparing the enzymatic activity of wt DrrA and these two complexes shows that the access of substrate molecules Rab1b is blocked in the second DrrA-Rab complex, named as canonical complex.

In the first part, biochemical characterization of DrrA and the non-canonical complex will be shown. By systematic investigation into the DrrA AMPylation domain, the construct of DrrA₁₆₋₃₅₂ was first optimized for further study. Surprisingly, the kinetic features of two different DrrA constructs (DrrA₁₆₋₃₅₂ and DrrA₈₋₅₃₃) are similar, which suggests that DrrA can have more than one Rab1b binding site in the AMPylation domain. Following, an alanine screening approach was used for probing the potential interactions between DrrA and Rab1b. Meanwhile, TReND-1 was used for detecting the possible ATP binding mode. Based on the obtained data and experiences from the study of Fic enzymes, strategies for covalent capture of the DrrA-Rab complex by TReND-1 were conceptualized. Covalent DrrA₁₆₋₃₅₂-L197C-Rab1b/8a complexes were successfully trapped. The structure DrrA₁₆₋₃₅₂-L197C-Rab8a was solved. Biochemical characterizations together with cell biology study were applied to further prove this non-canonical complex and depict its biological relevance of the unexpected allosteric binding of Rab1b.

In the second part, based on the analysis of the structure of first non-canonical complex, the second complex can be yielded by strategical design of cysteine substitution at A176 of DrrA. Interestingly, biochemical characterizations indicate that the catalytic center is blocked in this complex. Encouraged by this finding, we attempted to produce larger quantities of the ternary DrrA₁₆₋₃₅₂-A176C:TReND-1:Rab1b/8a complexes for structural investigations by X-ray crystallography. However, the low resolution and the complexity in the symmetry unit pose a great challenge in terms of solving the structures of DrrA₁₆₋₃₅₂-A176C:TReND-1:Rab1b/8a. Therefore, I also generated the methylated DrrA₁₆₋₃₅₂-A176C:TReND-1:Rab1b/8a complexes for structure determination. However, such methylated complexes did not yield any diffracted crystals. Probably, replacing Rab1b and Rab8a with other DrrA *in vitro* AMPylated small GTPases for a covalent complex can yield diffracted crystals in the future.

2.1 Non-canonical complex reveals Rab1b-AMPylation by *Legionella* DrrA is stimulated by active Rab1b

The *Legionella* enzyme DrrA tightly regulates Rab1b function and signaling via its GEF and AMPylation activities. Although the molecular mechanism of GEF action is well studied, the molecular mechanism underlying AMPylation by DrrA is poorly characterized. Attempts to characterize the AMPylation domain of DrrA failed, since the solubility of the AMPylation domain of DrrA previously has been poor. Therefore, I first attempted to express the AMPylation domain of DrrA in a soluble active form. Following, the AMPylation domain was extensively characterized biochemically. Based on the established data, potential cysteine substitutions were designed and tested for trapping covalent DrrA-Rab complexes, which was studied for elucidating the unknown molecular mechanism underlying AMPylation by DrrA.

2.1.1 Biochemical characterization of DrrA AMPylation domain

DrrA₈₋₅₃₃ is a well-established construct for studying the AMPylation activity and GEF action³⁰. However, the AMPylation domain of DrrA alone has never been successfully expressed in a soluble form by recombinant expression in *E. coli*. By structural optimization and introducing green fluorescent protein as the expression tag, active DrrA_{ATase} can be soluble expressed in *E. coli*. In this section, DrrA_{ATase} constructs were used or modified for further assays.

2.1.1.1 Optimizing the expression and purification of DrrA AMPylation domain

A previous study showed that DrrA₁₋₃₃₉, but not DrrA₁₋₃₀₀, caused AMPylation-related cytotoxicity in DrrA-expressing COS-7 cells¹³. Thus, it suggests that amino acids from 300 to 339 are important for maintaining the AMPylation activity in an unknown manner. Similarly, DrrA₆₁₋₆₄₇ cannot cause AMPylation-related cytotoxicity in eukaryotic cells³⁹. Hence, the first 60 amino acids in the N-terminus are also important to keep the AMPylation activity of DrrA. Bearing these in mind, we reasoned that if DrrA₁₋₃₄₀ can be solubly expressed in *E. coli*, protein DrrA₁₋₃₄₀ should be competent in AMPylation.

Halo tag can help protein expression in a soluble form in *E. coli*^{77, 78}. Thus, a Halo tag was recombinantly fused to the N-terminus of DrrA₁₋₃₄₀ for protein expression in *E. coli*. Indeed, active DrrA₁₋₃₄₀ can be expressed and purified from *E. coli*. In order to remove the Halo tag from DrrA, PreScission enzyme was used. Although Halo tag can be removed efficiently, the yield of this construct was poor (2mg from 2L LB expression). Meanwhile, DrrA₈₋₃₄₀ was generated and tested. Comparing to DrrA₈₋₅₃₃, which was expressed together with a His tag, these two constructs shared decreased AMPylation activity (Figure 10A). Presumably, these two DrrA constructs are structurally unstable.

Green fluorescent protein (GFP) has been widely used in cell biology as a reporter ⁷⁹. Recently, it was reported that GFP can be used as a scaffold for efficiency production of functional bacteriotoxic proteins in *E. coli* ⁸⁰. Thus, a GFP tag was introduced to the N-terminus of DrrA. It was reported that amino acids from 300 to 340 are important for maintaining the AMPylation activity. However, DrrA₈₋₃₄₀ is not active as DrrA₈₋₅₃₃. According to one previously reported DrrA fragment structure (DrrA₁₉₃₋₅₃₃, 3LOI) ⁵⁸, amino acid 340 is located in the middle of a long helix (from amino acid 321 to 360). This helix has extensive interactions with the N-terminal and C-terminal helices. Therefore, truncated construct DrrA₈₋₃₄₀ are not stable, since it will lose such interactions. Extension of the C-terminus of DrrA_{ATase} to amino acid 352 may yield a stable DrrA_{ATase} construct (Figure 10B). Indeed, the expression level of this construct (GFP-TEV-DrrA₈₋₃₅₂) was significantly increased in *E. coli*. Also, DrrA₈₋₃₅₂ was as active as His tagged DrrA₈₋₅₃₃ in AMPylating Rab1b (Figure 10C).

In conclusion, by using GFP protein as the expression tag for DrrA and extending the C-terminus of DrrA_{ATase} from amino acid 340 to amino acid 352, a stable and active DrrA₈₋₃₅₂ was generated for the first time.

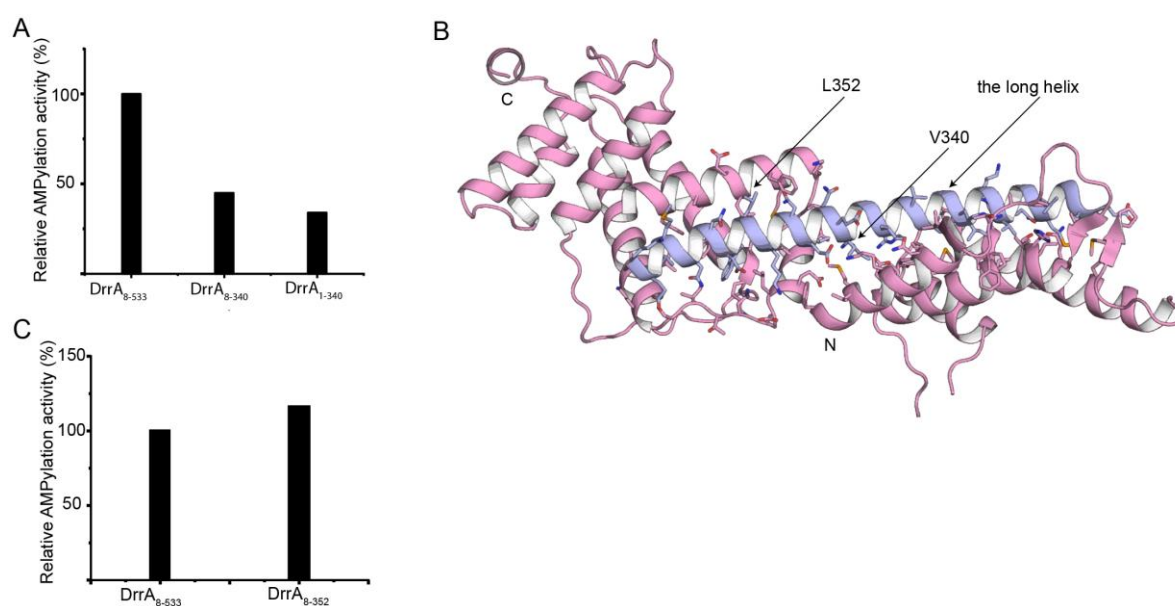


Figure 10 Expression, purification and characterization of the DrrA AMPylation domain. **(A)** DrrA₁₋₃₄₀ and DrrA₈₋₃₄₀ share decreased AMPylation activity. The k_{cat}/K_M value of His tag DrrA is $5.6 \times 10^5 \text{ M}^{-1} \text{ s}^{-1}$. **(B)** Interactions between the long helix (light blue) and the other helices (pink). PDB: 3LOI. **(C)** DrrA₈₋₃₅₂ is an optimized construct. The k_{cat}/K_M value of His tag DrrA₈₋₅₃₃ is $5.6 \times 10^5 \text{ M}^{-1} \text{ s}^{-1}$.

2.1.1.2 The AMPylation domain of DrrA is a monomeric protein

Fic enzymes can be shifted from the dimerization or oligomerization state to monomer state dependent on the concentration ³⁷, which further regulates their AMPylation activity.

Therefore, the DrrA was analyzed for oligomerization propensity. However, DrrA₈₋₃₄₀ samples with different concentrations (from 3 mg/ml to 46 mg/ml) shared the same monomer peak in analytical size exclusion chromatography (Figure 11A). Therefore, DrrA is different from Fic enzymes, which can be cycled between monomer and oligomer. (of note, before DrrA₁₆₋₃₅₂ was generated, DrrA₈₋₃₄₀ was extensively used.)

Prior to AMPylation, wild type Rab1b: GppNHp can regulate ATP's binding to DrrA in an unknown manner³³. Therefore, we further asked that the monomer state of DrrA can be regulated by Rab1b or not. In the presence of active Rab1b, DrrA₈₋₃₄₀ is still a monomeric protein. Further addition of ATP did not change DrrA's monomeric state (Figure 11B). Therefore, DrrA is not only a monomeric protein, but also a different AMP-transferase from others, which form homodimer to complement the active sites^{31, 32}.

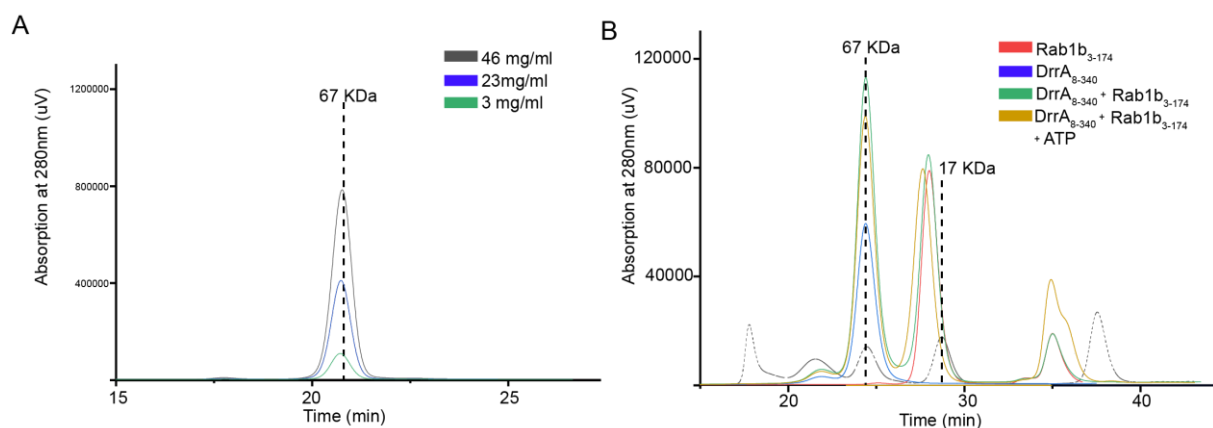


Figure 11 DrrA_{ATase} is a monomeric protein. **(A)** DrrA₈₋₃₄₀ shows the same monomer peak in analytical size exclusion chromatography in a concentration-independent manner. **(B)** DrrA₈₋₃₄₀ does not change its monomer state in the presence of Rab1b:GppNHp and nucleotide ATP.

2.1.1.3 The N-terminus of DrrA_{ATase} is critical for maintaining the AMPylation activity

Amino acids 8 to 15 cannot be visible in the structure model of DrrA₈₋₂₁₈ (PDB: 3NKU), which suggested that this region is flexible and not suitable for structure determination. At the same time, amino acids 16 to 30 displayed as a loop in the structure of DrrA₈₋₂₁₈. More stable DrrA constructs can be generated if these two flexible regions are removed. Thus, DrrA₁₆₋₃₅₂ and DrrA₃₀₋₃₅₂ were designed, purified, and tested. DrrA₁₆₋₃₅₂ is as active as DrrA₈₋₅₃₃. Notably, DrrA₁₆₋₃₅₂ is more active than DrrA₈₋₃₅₂. However, DrrA₃₀₋₃₅₂ decreased the AMPylation activity by a factor of 300 (Figure 12A). (Of note, since DrrA₁₆₋₃₅₂ is a stable and active construct than others, DrrA₁₆₋₃₅₂ will be used as the wild type protein for further assays.)

The catalyze center of the DrrA's AMPylation domain is spanning amino acids 97-112. Thus, the amino acids 15-30 are not part of the catalytic center. Consistently, ATP hydrolysis assay

indicated that construct DrrA₁₆₋₃₅₂ shared the same ATase activity as DrrA₃₀₋₃₅₂ (Figure 12B). Probably, some amino acids of this region appear to be important for recognizing the substrate Rab1b. Afterwards, we mutated some charged residues in this region based on the available crystal model DrrA₈₋₂₁₈ (PDB: 3NKU). Using a mutation analysis, we discovered that R24_{DrrA} is important for Rab1b recognition (Figure 12C). Furthermore, D22_{DrrA} and E23_{DrrA} likely stabilize R24_{DrrA} through intramolecular electrostatic interactions (Figure 12D). Notably, it is worth mentioning that R139_{DrrA} has polar interactions with a charged patch (D22_{DrrA} and E23_{DrrA}) in the N-terminus in previous structure (PDB: 3NKU)¹³. It appears that DrrA will keep R24_{DrrA} in the right orientation by stabilizing this charged patch through this dedicated interaction network. Presumably, this is also the reason why the reported construct DrrA₆₁₋₆₄₇ is deficient in AMPylation³⁹.

In conclusion, the AMPylation activity is not only dependent on the catalytic center, but also dependent on the N-terminus of DrrA_{ATase}.

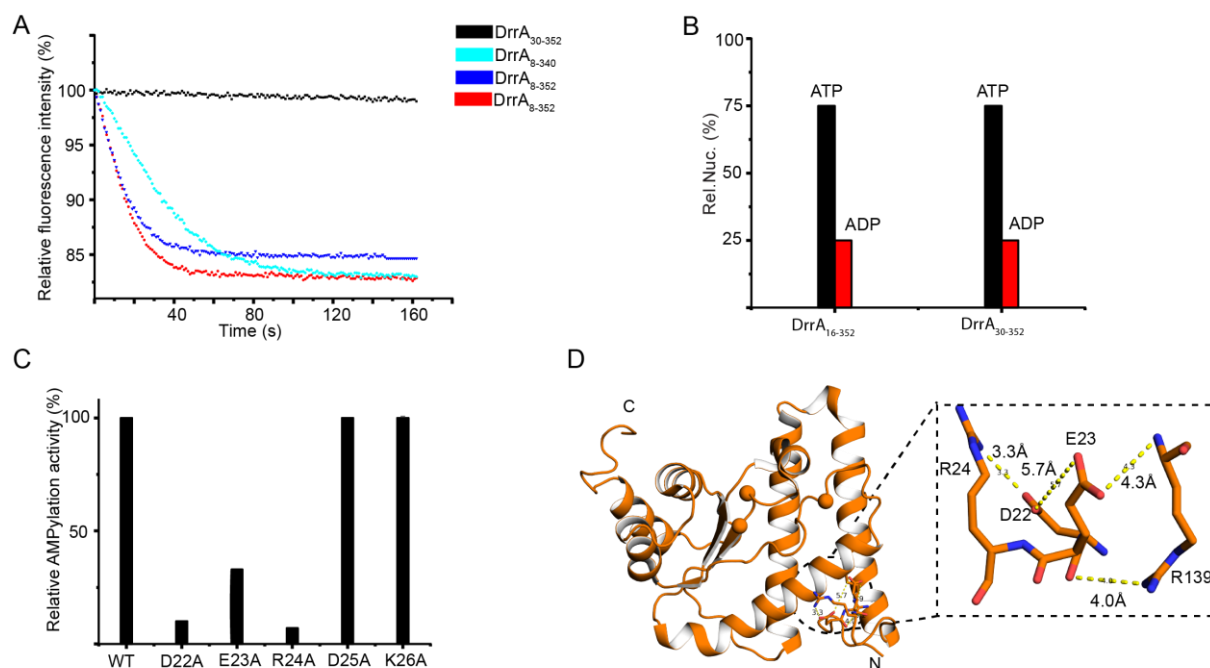


Figure 12 N-terminus of DrrA AMPylation domain plays a significant role in AMPylation. **(A)** Relative Tryptophan fluorescence change by different DrrA constructs. The k_{cat}/K_M value of DrrA₁₆₋₃₅₂ is $7.4 \times 10^5 \text{ M}^{-1} \text{ s}^{-1}$. The k_{cat}/K_M value of DrrA₃₀₋₃₅₂ is $2.4 \times 10^3 \text{ M}^{-1} \text{ s}^{-1}$. **(B)** DrrA₁₆₋₃₅₂ and DrrA₃₀₋₃₅₂ share identical ATase activities. 100 μM ATP and 5 μM DrrA constructs were incubated for overnight, samples were analyzed by reverse phase chromatography. **(C)** Important residues in the N-terminus of DrrA AMPylation domain for maintaining the AMPylation activity. R24_{DrrA} is important for interaction with Rab1b. **(D)** Interactions among D22_{DrrA}, E23_{DrrA}, R24_{DrrA}, and R139_{DrrA}. Orange spheres are catalytic Asp residues. PDB: 3NKU (orange).

2.1.1.4 Two different constructs of DrrA show similar kinetic features

Previously, the kinetic parameters of DrrA₈₋₅₃₃ catalyzed AMPylation were determined by time-resolved tryptophan fluorescence³⁰. The generated pyrophosphate during AMPylation inhibits the DrrA-catalyzed AMPylation³⁰, therefore measurements were taken in the presence of pyrophosphatase that hydrolytically cleaves PPi to phosphates. When Rab1b is in the active state, k_{cat} and K_M are determined to $53.4 \pm 3.9 \text{ s}^{-1}$ and $64.2 \pm 12.9 \text{ }\mu\text{M}$, respectively³⁰. While Rab1b is in the inactive state, k_{cat} and K_M are $0.78 \pm 0.01 \text{ s}^{-1}$ and $362.9 \pm 21.7 \text{ }\mu\text{M}$ respectively³⁰. Interestingly, a lag-phase in the AMPylation rate was observed at low Rab1b:GDP concentrations³⁰. Thus, the authors suggested that Rab1b may form dimers when the concentration is high as was shown for Rab9 and Rab27^{81,82}. However, there are also other possibilities, e.g. two Rab1b molecules bind to DrrA at two distinctive binding sites. Notably, the GEF domain in DrrA₈₋₅₃₃ can also provide the binding platform to the Rab1b protein. To exclude this possibility, the kinetic assay of DrrA-catalyzed Rab1b AMPylation was first performed with DrrA₁₆₋₃₅₂ (Figure 13A).

Indeed, the kinetic features between these two different DrrA constructs are similar. When Rab1b is in the active state, the values of k_{cat} and K_M are $104.7 \pm 5.1 \text{ s}^{-1}$ and $70.7 \pm 5.7 \text{ }\mu\text{M}$ respectively. However, fitting the data to a simple Michaelis-Menten model (i.e. to a hyperbolic function) was not feasible, hence a sigmoidal Hill-type function was instead employed (Figure 13 A). Since it was the first time to observe sigmoidal kinetic behavior for Rab1b: GppNHp, therefore we asked whether the presence of pyrophosphatase contributes to the sigmoidal kinetic behavior or not. The k_{cat} value, but not the K_M , decreased significantly. However, the sigmoidal kinetic behavior was still observed (Figure 13 B). Therefore, the GEF domain does not contribute to the sigmoidal kinetic. Thus, there can be two explanations for the sigmoidal kinetic behavior: the first one is that Rab1b forms dimers as previous suggested; the alternative one is that DrrA possess two separate Rab1b binding platforms in the AMPylation domain.

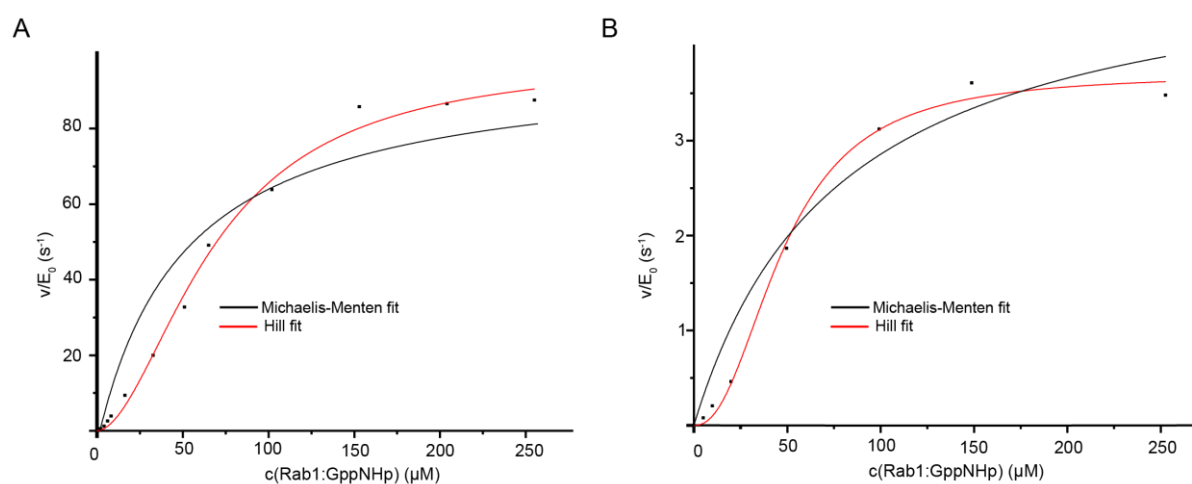


Figure 13 DrrA₁₆₋₃₅₂ show similar kinetic features with DrrA₈₋₃₄₀. **(A)** DrrA₁₆₋₃₅₂-catalyzed Rab1b:GppNHp AMPylation in the presence of pyrophosphatase. Sigmoidal dependence of AMPylation from active Rab1b-concentration. Red curve is the Hill-fit with the cooperativity parameter 1.8 ± 0.19 , black curve is the Michaelis-Menten-fit. **(B)** DrrA₈₋₃₄₀-catalyzed Rab1b AMPylation in the absence of pyrophosphatase. Sigmoidal dependence of AMPylation from active Rab1b-concentration. Red curve is the Hill-fit with the cooperativity parameter 2.2 ± 0.30 , black curve is the Michaelis-Menten-fit.

2.1.1.5 Investigation of the interaction between DrrA and Rab1b by alanine screening

In order to get the structure of DrrA-Rab1b complex, we first attempted to determine the structure of DrrA_{ATase} and the structure of DrrA_{ATase}:ATP complex. However, DrrA₁₆₋₃₅₂ with or without ATP has not been crystalized. In some cases, methylation of the exposed lysines can help proteins crystalize or diffract better⁸³. Given that multiple lysine residues are present in DrrA, attempts to crystalize methylated DrrA may work. However, methylated DrrA₁₆₋₃₅₂ or methylated DrrA₁₆₋₃₅₂ together with ATP failed to be crystalized (Figure 14). Thus, the interaction between DrrA and Rab1b may be deduced from systematic alanine screening on DrrA (Figure 15).

According to the above-mentioned data, alanine screening for further exploring the potential interaction mode between DrrA and Rab1b was performed. R139A_{DrrA} decreased the enzymatic activity by a factor of 1000. Structural analysis indicated that R139_{DrrA} should only interact with the charged patch (D22_{DrrA} and E23_{DrrA}), which is used for maintaining the proper orientation of R24_{DrrA}. Presumably, DrrA uses R139 to interact with the charged patch for further stabilizing the proper orientation of R24_{DrrA}. Again, the result demonstrated that R24_{DrrA} is important for the interaction between DrrA and Rab1b. Other alanine substitutions, such as D110, in the catalytic center lead to a loss of AMPylation activity. Interestingly, R246_{DrrA} and D249_{DrrA} also completely inactivated the enzyme. R246_{DrrA} and D249_{DrrA} may interact with the phosphate group of ATP, therefore R246A_{DrrA} and D249A_{DrrA} significantly

decrease their AMPylation activity. D177A_{DrrA} and R158A_{DrrA} were reported as active as wild type DrrA³³. However, our data indicated that these D177A_{DrrA} and R158A_{DrrA} decreased the enzymatic activity by a factor of 6 and 4, respectively. Since these two residues were not in the catalytic center they may interact with the adenosine part of ATP instead of interacting with the phosphate groups in ATP.

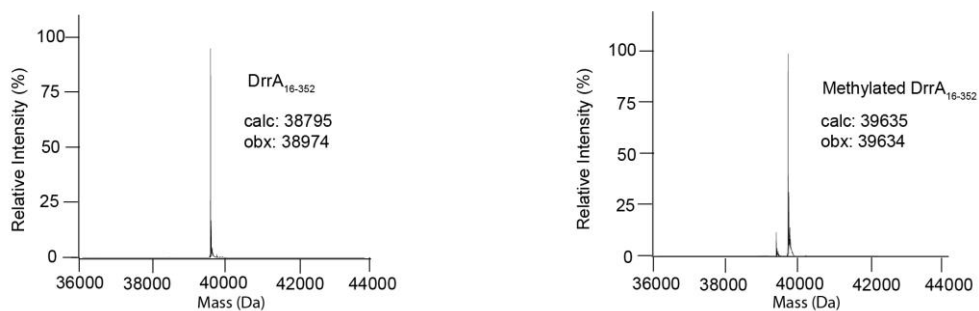


Figure 14 Mass spectrometry analysis of DrrA₁₆₋₃₅₂ and methylated DrrA₁₆₋₃₅₂. The increased mass indicated that all the 30 lysine residues in DrrA were methylated.

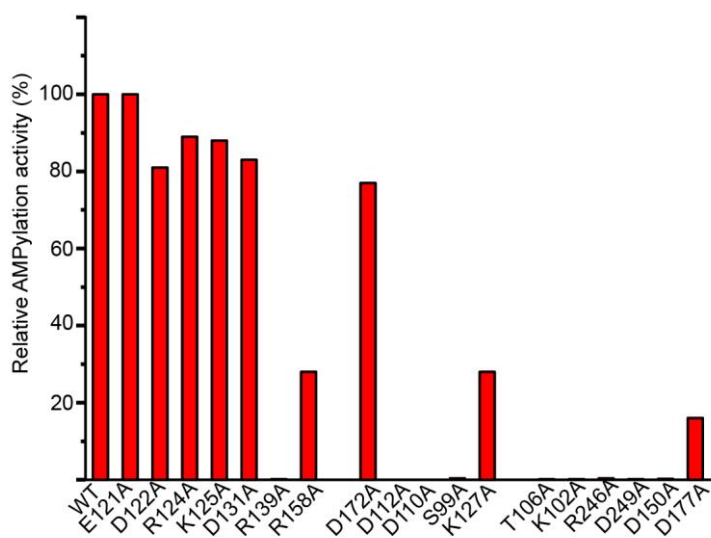


Figure 15 Profiling substrate recognition and catalytic residues in DrrA AMPylation domain. Alanine mutations in the putative catalytic center inactive DrrA. R139A (not located in the catalytic center) also inactive the AMPylation activity of DrrA.

2.1.1.6 Probing the potential ATP binding mode in DrrA_{ATase}

Although previous biochemical study can provide hints about the ATP binding mode in DrrA_{ATase}, designing the potential cysteine for covalent capture of DrrA-Rab remains challenging. The previous report indicated that ATP cannot bind to DrrA in the absence of Rab1b³³. Catalytically, DrrA is not efficient in ATP hydrolysis compared with other AMPylators, such as IbpA, BepA and VopS (Figure 16A). However, if ATP was incubated with wild type DrrA overnight, roughly 25% of ATP is hydrolyzed (Figure 12B). Presumably, TReNDs are incubated with DrrA cysteine constructs for a long period, these TReNDs can also bind to the catalytic pocket of DrrA. Therefore, if one perfect cysteine substitution in DrrA can be designed, the chloroacetamide handle of TReNDs can react with the designed cysteine mutations, and then DrrA_{Cys}-TReND binary complex can be yielded during overnight incubation.

To this end, TReNDs were tested as the co-substrate of DrrA. Surprisingly, only TReND-1 can be well recognized by wild type DrrA (Figure 16B). Therefore, we generated and purified numerous cysteine mutations of DrrA₁₆₋₃₅₂: N135C, Q138C, R246C, T106C, E107C, S109C, R158C, D177C, A180C, K223C, F228C, R246C and F250C. The designed DrrA cysteine mutations were incubated with high concentration of TReND-1 (1mM). However, mass spectrometry indicated that none of these cysteine mutants can yield a covalent product (Table 1). Therefore, A97C, S99C, L159C, T181C, S184C, and M253C were designed for DrrA- TReND-1 binary product formation. Again, none of these cysteine mutants yielded a covalent product (Table 1). Due to the lack of available structures, it was difficult to predict the ATP binding mode in DrrA. Also, conformational changes in DrrA were suggested before, which made the design of potential cysteine mutations more challenging. Thus, attempts to get the DrrA_{Cys}-TReND-1 binary product failed.

However, if the suggested ATP binding mode in a previous report is correct³³, then one of these mutations (K223C, F228C, F250C, and M253C) should yield the DrrA_{Cys}-TReND-1 binary product. Again, if R246 and D249 were interacting with the adenosine group, the R246A and D249A alanine mutants should not completely lose their enzymatic activity. Therefore, this suggested mode could be wrong, and probably the adenosine group of ATP should interact with the residues in the other side of the catalytic pocket (the region of R158 and D177) (Figure 16C).

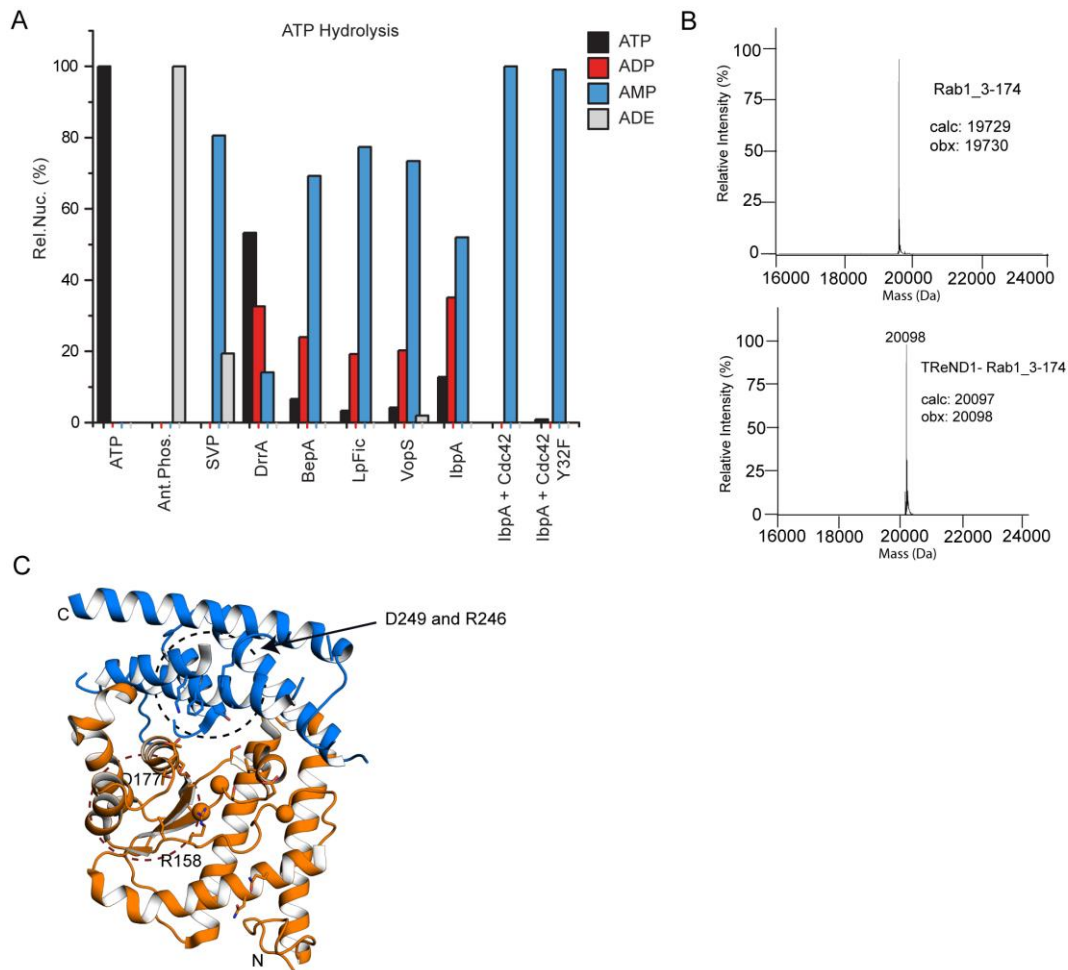


Figure 16 Detection of the potential ATP binding mode in DrrA AMPylation domain by forming DrrAcys-TReND-1 binary complex. **(A)** DrrA is deficient in ATP hydrolysis. Antarctic Phosphatase was used to generate adenosine as a reference. Snake venom phosphodiesterase was used to generate adenosine and AMP as another reference. **(B)** Rab1b can be modified with TReND-1 by wild type DrrA₁₆₋₃₅₂. **(C)** Schematic representation of the region of D249 and R246, and the region of R158 and D177. K223C, F228C, F250C, and M253C are located in the region of D249 and R246. Orange spheres are catalytic Asp residues. PDB: 3NKU (orange) and 3LOI (blue). Model is created by superimposing these two structures. Figure 16B and 16C are copies from my previous manuscript to Nature Communications⁶⁰.

Table 1 DrrA cysteine mutants for DrrAcys-TReND-1 binary complex formation. IbpA₃₄₈₃₋₃₇₉₇ I3455C can form a binary complex with TReND-1, and was used as a positive control. Wild type DrrA₈₋₅₃₃ was used as a negative control.

DrrA cysteine mutations	Mass data of DrrA cysteine mutations (da)	Mass data of DrrA cysteine mutations plus TReND-1 (da)
N135C	61600	61599
Q138C	61585	61584
R246C	61559	61557
T106C	61612	61612
E107C	61585	61587
S109C	59880	59880
R158C	61558	61559
D177C	61559	61600
A180C	61639	61639
K223C	61586	61586
F228C	59820	59820
F250C	61566	61567
A97C	61641	61642
S99C	61627	61627
L159C	61601	61601
T181C	61615	61611
S184C	61626	61625
IbpA ₃₄₈₃₋₃₇₉₇ I3455C	37737	38097
DrrA ₈₋₅₃₃	60422	60422

2.1.2 Conceptual designs for trapping the non-canonical DrrA-Rab1b complexes

By the application of site-specific incorporation of unnatural amino acids (UAAs) bearing bromoalkyl moieties (e.g. BrC6K) into the substrate protein Rab1b, researchers from Lang lab structurally characterized the interaction of the guanosine triphosphate exchange factor (GEF) domain of the *Legionella* effector enzyme DrrA/SidM with its substrate, the human small GTPase Rab1b. Notably, a possible mechanism of DrrA GEF-mediated GDP release of Rab1b was able to be proposed for the first time ⁷⁶. Therefore, we asked whether the DrrA_{ATase} can form a complex with BrC6K incorporated Rab1b. Indeed, one R69BrC6K based Rab1b:DrrA_{D82C} was obtained and further subjected to structure determination. Unfortunately, the resulting crystals did not diffract. (The BrC6K-based crosslinking assays were done and analysed by Marie Kristin von Wrisberg and Kathrin Lang.)

In parallel, I further designed the cysteine substitutions in DrrA to trap the DrrA:Rab complexes with TReND-1.

2.1.2.1 Complexes DrrA₁₆₋₃₅₂-L197C:TReND-1:Rab1b₃₋₁₇₄/ Rab8a₆₋₁₇₆ can be efficiently and specifically trapped *in vitro*

The kinetic data of DrrA₈₋₅₃₃ suggested that either two Rab1b molecules bind to DrrA or Rab1b forms dimer during AMPylation ³⁰. Interestingly, the information provided by our collaborators from the Lang group suggested that it is more likely that two Rab1b molecules bind to DrrA: one binds to the site which contains the catalytic center, the other one binds to a previous unrecognized site in the AMPylation domain. However, the difficulties in getting diffracting crystals by this UAA-based crosslinking assays suggested us to explore the interaction between DrrA and Rab1 with alternative mythologies.

To uncover the DrrA-mediated AMPylation mechanism at the molecular level, we further designed additional cysteine residues in DrrA for the formation of DrrA:Rab complex. For this purpose, the strategy for generation of such complex was adjusted from a recent publication ⁷⁵. The method was based on the previously report that the presence of Rab1b is critical for the binding of ATP and conformation change in DrrA ³³. Thus, DrrA₁₆₋₃₅₂ constructs bearing M169C, M174C, V175C (the putative catalytic site) and G198C, and L197C (opposite to the the putative catalytic site) substitutions were generated, then these mutants were tested with TReND-1 and GppNHp loaded Rab1b (Figure 17A and Figure 9).

Surprisingly, TReND-1, but not TReND-2 and TReND-3, successfully formed a covalent ternary complex with Rab1b₃₋₁₇₄ and DrrA₁₆₋₃₅₂-L197C, which can be clearly validated by denaturing SDS-PAGE (Figure 17B). ATP failed to covalently link Rab1b and DrrA or DrrA cysteine mutants. Thus, the TReND-1-mediated reaction was site-specific since other cysteine mutants did not yield the formation of a ternary complex (Figure 17B). Interestingly,

residue L197_{DrrA} is not located in the vicinity of the catalytic site. Instead, it is also located on the same surface patch as residue D82_{DrrA} opposite the catalytically active amino acid residues of DrrA (e.g. D110_{DrrA} and D112_{DrrA}) (Figure 17C). Of note, DrrA₁₆₋₃₅₂-L197C mutant can nearly yield the ternary complex in a quantitative manner.

In order to further explore the interaction mode between DrrA and Rab1b, the pure DrrA₁₆₋₃₅₂ L197C:TReND-1:Rab1b₃₋₁₇₄ complex (around 10 mg/ml) was subjected to structure determination by X-ray crystallography. However, the resulting crystals diffracted poorly as the UAA-based crosslinked DrrA₁₆₋₃₅₂:Rab1b₃₋₁₇₄. To uncover the DrrA-catalysed AMPylation of Rab1b at the molecular level, replacing Rab1 with other *in vitro* targets of DrrA for crystallization of the complex may serve as the last alternative strategy.

DrrA AMPylates Rab1b, Rab3A, Rab6A, Rab4B, Rab8a, Rab13, Rab14, and Rab37 *in vitro*¹³. Then Rab8a was first selected and tested, since Rab8a and Rab1b not only share 53% sequence identify, but also possess a very similar structure with an an RMSD (root-mean-square deviation) of 0.511 Å. Moreover, time-resolved tryptophan fluorescence assay indicated that DrrA AMPylates Rab8a with comparable enzymatic kinetics *in vitro* like for the AMPylation of Rab1b (Figure 17D and Supplementary Figure 1)¹³. Indeed, Rab8a can also form the ternary complex with DrrA₁₆₋₃₅₂-L197C efficiently, and the results can be demonstrated clearly by the SDS-PAGE and intact mass spectrometry analysis (Figure 17E).

In conclusion, using nucleotide analogues (TReND-1) with strategically designed DrrA cysteine mutants, DrrA:Rab complexes can be generated and submitted to structure determination, which opens an avenue for us to understand the molecular mechanism of DrrA-mediated AMPylation for the first time.

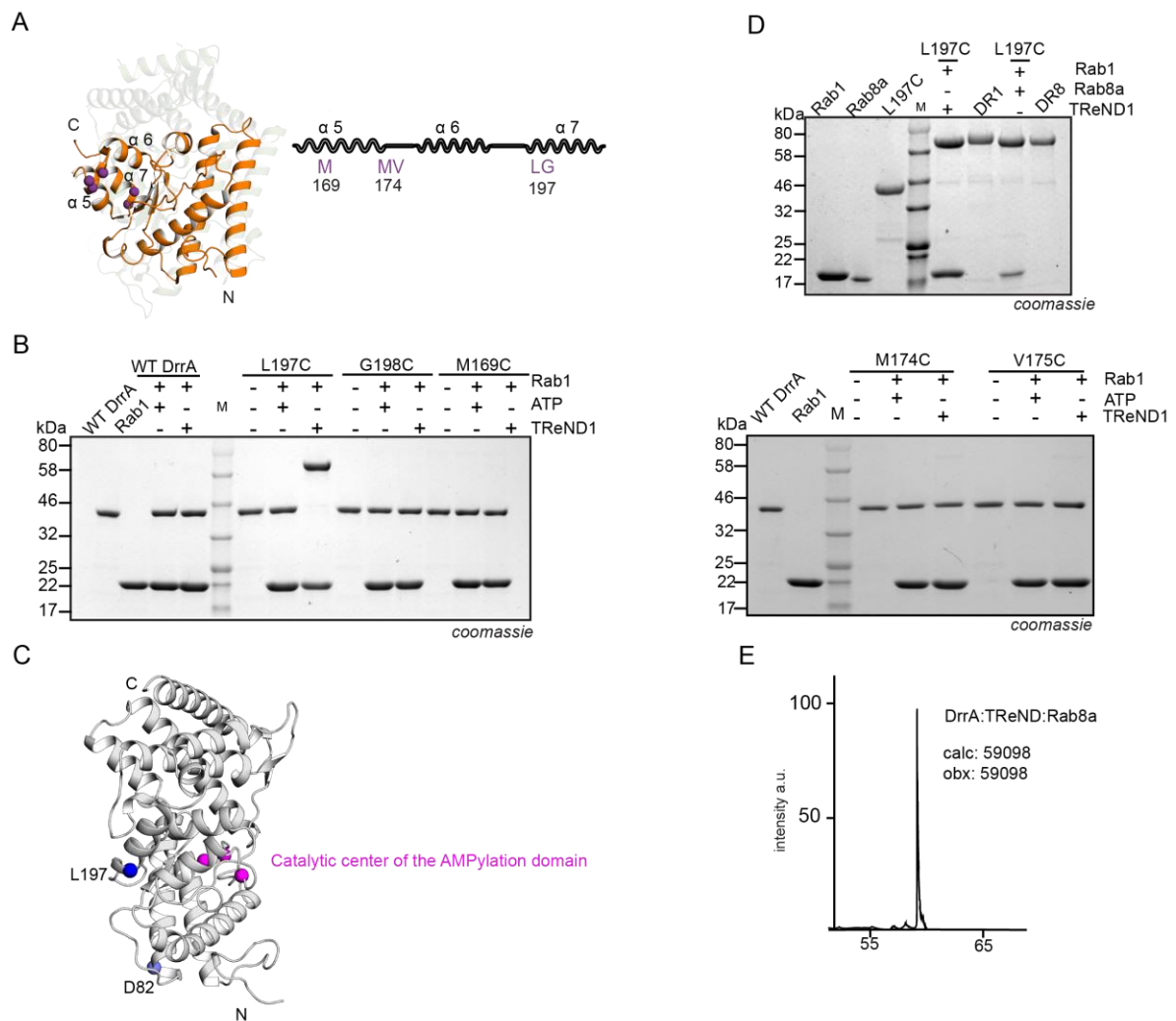


Figure 17 Conceptual design for stabilising the low affinity DrrA_{ATase}:Rab complexes. **(A)** Selection of Cys substitution sites (M169, M174, V175, L197 and G198, purple) in the model, and superimposition of DrrA₈₋₂₁₈ (PDB: 3NKU, orange) onto GS-ATase (PDB: 3K7D, light green background). **(B)** SDS-PAGE shift analysis of DrrA:TReND-1:Rab1b complex formation. **(C)** Demonstration of the positions of L197_{DrrA} (color blue) and D82_{DrrA} (color light blue). Pink spheres: the active site of DrrA_{ATase}. **(D)** SDS-PAGE shift analysis of preparative DrrA:TReND-1:Rab1b (DR1)/Rab8a (DR8) complex formation. **(E)** Intact mass spectrometry analysis of the DrrA:TReND-1:Rab8a complex. Picture is a copy from my previous manuscript to Nature Communications⁶⁰.

2.1.2 Structure of the DrrA: Rab8a-complex

In order to uncover DrrA-catalyzed Rab1b AMPylation at molecular level, the crystal structure of the DrrA₁₆₋₃₅₂:TReND-1:Rab8a₆₋₁₇₆:GppNHp complex (referred as DrrA:Rab8a in the following) was solved at 2.1 Å resolution (Supplementary Table 1, the structure of DrrA:Rab8a complex was determined by Dr. Sabine Schneider, details for structure determination can be found in Du J. et al. Nature Communications ⁶⁰). However, the DrrA:Rab8a structure clearly showed that Rab8a binds to the opposite site of the catalytic site. Therefore, the current Rab8a binding site in DrrA will be referred as the non-canonical (NC) Rab binding site (RBS), hereafter called NC-RBS or RBS2, and the catalytic site will be referred as the canonical Rab1 binding site, hereafter named as RBS1 in the following (Figure 18A and Figure 18D) ¹³.

First, the TReND-1 linker in the current DrrA:Rab8a complex is clearly defined. Importantly, the TReND-1 does not contribute to the interface in the current complex (Figure 18B).

The general structural features of the previously reported individual subunits of Rab8a: GppNHp, and DrrA fragments (e.g. parts of DrrA₈₋₂₁₈ and DrrA₂₁₀₋₅₃₄) can be seen in the DrrA:Rab8a complex (Figure 18A) ^{13, 58, 84}. Rab8a in the DrrA:Rab8a complex is consisting of a central six-stranded β-sheet surrounded by five α-helices ⁸⁴. Together with Mg²⁺, the so-called p-loop contributes to the binding of the GppNHp phosphate groups. Additionally, Rab8a shows a signature feature of small GTPases when it is in the GppNHp state: the regulatory switch I and II regions of Rab8a are ordered.

Although attempts to crystalize the full AMPylation domain of DrrA in the apo form failed, the DrrA structure from the current complex offers us the chance to study its structural features with previously determined structures of DrrA fragments ^{13, 58}. Indeed, the secondary structure elements are almost identical between the DrrA structure from current complex and the previously reported ones. Also, the DrrA structure from the DrrA:Rab8a complex represents a signature structure feature in the DNA polymerase β-like enzyme family: the catalytic center (GX₁₁DXD) displays a helix-loop-β strand fragment.

In the current complex, only ten residues from DrrA form polar interactions with the residues from Rab8a (Figure 18C and hydrophobic interactions can be seen in Supplementary Figure 2), suggesting the affinity between DrrA and Rab8a is low. Consistently, the small solvent-accessible area buried upon complex formation is only 648 Å² (using the Protein Interfaces, Surfaces and Assemblies (PISA) web service) ⁸⁵. Interestingly, nine of these interacting residues in DrrA are in the region of DrrA₈₋₂₁₈, only E264 is in the C-terminus of DrrA. Surprisingly, only two residues (Q60_{Rab8a} and R69_{Rab8a}) in the regulatory switch II region of Rab8a are contributing to the interactions between DrrA and Rab8a. The main interacting residues are from the regulatory switch I (E30_{Rab8a}, F33_{Rab8a} and N34_{Rab8a}), and the

interswitch region (D44_{Rab8a} and K58_{Rab8a}). Of note, amino acids R70_{DrrA}, Q71_{DrrA} and K74_{DrrA} seem to be located in the center of the current interface in the DrrA:Rab8a complex, which are simultaneously interacting with D44_{Rab8a} from the interswitch region.

Albeit structural analysis indicated that the catalytic Asp residues in DrrA₈₋₂₁₈ are positioned significantly different from the one observed in the current complex, the ones in DrrA in the current complex share very similar positioning with the ones in GS-AT (Figure 18E). Interestingly, the catalytic Asp residues in DrrA₈₋₂₁₈ are unlikely capable for the coordination of Mg²⁺ and the binding of ATP. Differently, the catalytic Asp residues in the DrrA from DrrA:Rab8a complex are ordered and likely competent for the binding of ATP and Mg²⁺ (Figure 18E). Indeed, the C-terminus of DrrA keeps the full AMPylation domain structurally intact, but the factors, which contribute to the disordered catalytic center in DrrA₈₋₂₁₈, need to be further investigated.

Furthermore, by structural alignment between free Rab8a:GppNHp and Rab8a from the DrrA:Rab8a complex, significant global structural changes was not observed⁸⁴. Similarly, superimposing AMPylated Rab1b with Rab8a, an RMSD of 0.623 Å was yield, suggesting almost identical structures (Figure 18F). Therefore, remarkable conformational changes in Rab1b should not be induced when Rab1 binds to the non-canonical Rab binding site of DrrA

13

In conclusion, by using TReND analogues, the DrrA:Rab8a crystal structure was determined at high resolution. Furthermore, the non-canonical Rab binding in current complex may reveal a previously unrecognized Rab binding site in the AMPylation domain of DrrA.

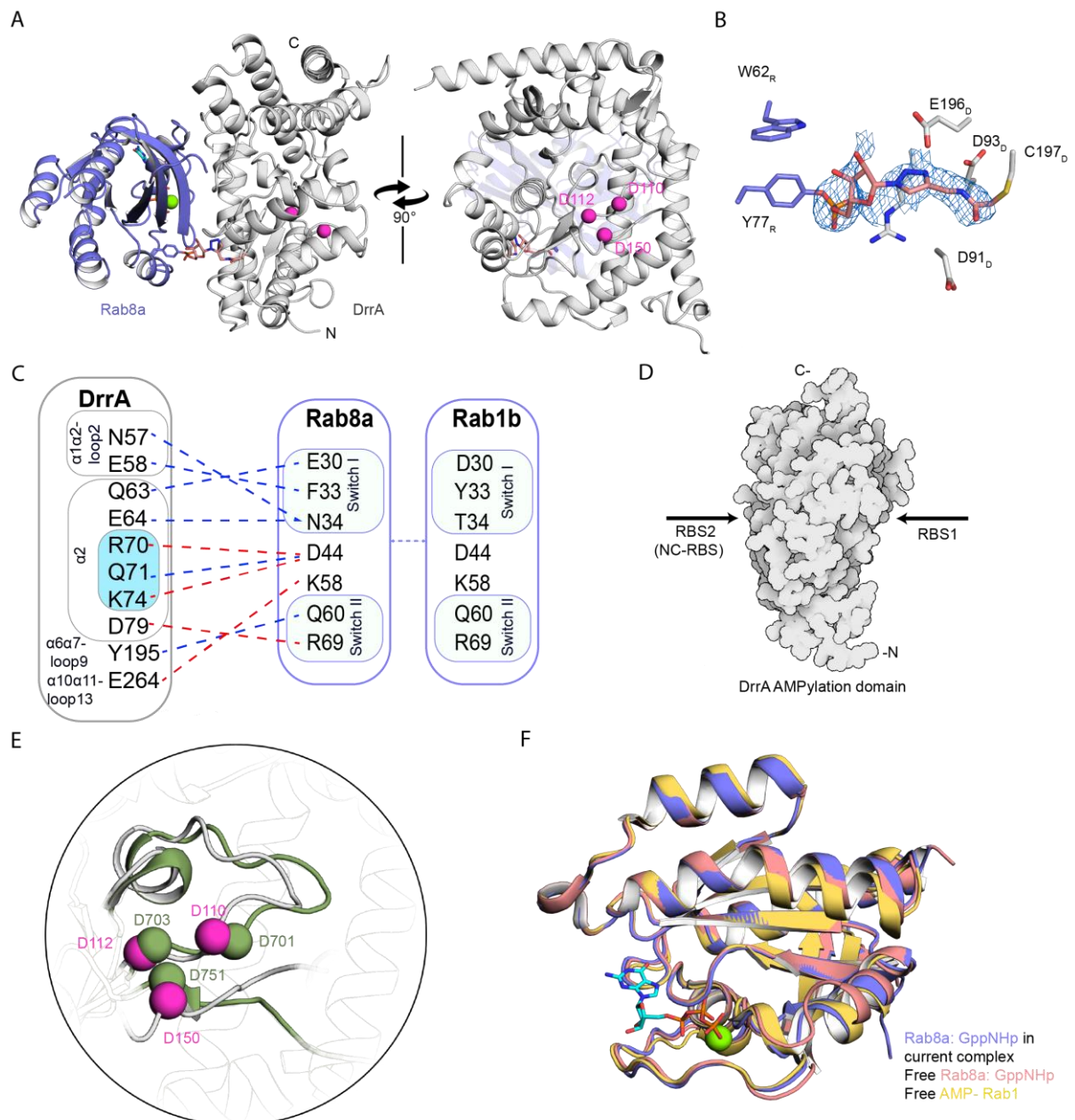


Figure 18 Structure of the DrrA:Rab8a complex. **(A)** Orthogonal views of the Rab8-DrrA complex. Pink spheres denote the catalytic Asp residues of DrrA. The green sphere represents the Mg^{2+} ion. **(B)** Linker density from the unbiased simulated-annealing omit DFO-Fc electron density map contoured at 2.5σ . The R subscript denotes Rab8a, and the D subscript denotes DrrA. **(C)** Schematic representation of the Rab8-DrrA interface. Interactions are shown with dashed lines; hydrogen bonds are blue and salt bridges are red. The corresponding interaction residues in Rab1b are shown in the panel on the right. Important residues for maintaining enzymatic activity are coloured cyan, and ‘ α ’ represents α -helix. **(D)** Demonstration of the conventional site (RBS1, containing the catalytic centre) and non-conventional site (RBS2, the back face of the catalytic centre). **(E)** Structural comparison between the catalytic centre in GS-ATase (PDB: 3K7D, green) and the catalytic centre in DrrA in the DrrA-Rab8a complex. The catalytic centre of DrrA includes D110_{DrrA}, D112_{DrrA} and

D150_{DrrA}. The catalytic centre of GS-AT includes D701_{GS-AT}, D703_{GS-AT} and D753_{GS-AT}. (F) Structural superposition of free AMP-Rab1b:GppNHp (PDB: 3NKV, yellow) and Rab8a (PDB: 4LHW, pink) with Rab8a (blue) from the complex with DrrA. Green spheres indicate Mg²⁺ ions, and GppNHp is shown in stick representation. Picture is a copy from my previous manuscript to Nature Communications⁶⁰.

2.1.3 Structural and biochemical analysis of the DrrA-Rab interaction in the non-canonical site of DrrA

Indeed, Rab8a binds to the non-canonical site of DrrA may suggest unknown regulation mechanisms. Alternatively, the current complex is only formed artificially by the application of TReND-1. Therefore, structure-guided mutagenesis was performed to answer the above-mentioned questions.

It is worth mentioning that the corresponding interaction residues in Rab proteins may also interact with the residues from the catalytic site of DrrA. Thus, I only generated the alanine substitutions of DrrA residues involved in the DrrA:Rab8a interface. Prior to determine the AMPylation efficiencies of these generated alanine mutants, the thermal unfolding of the alanine substitution proteins was monitored via the change in circular dichroism (CD) signal (of note, the thermal unfolding of DrrA constructs can never been precisely determined by other techniques). DrrA₁₆₋₃₅₂ is a stable construct as demonstrated with a high melting point ($T_m = 60.1^\circ\text{C}$). Compared with the melting point of wt DrrA₁₆₋₃₅₂, only D79A_{DrrA} shows a significant decrease of the 4.2°C in the melting point (Figure 19A). Structural analysis suggests that D79A_{DrrA} loses its original polar interactions with K36_{DrrA} and Y40_{DrrA}, therefore destabilizes the protein as a significant decrease in the melting point. For the other alanine substitutions, they either show almost identical melting point (e.g. N57A, R70A, K74A, and E264A), or represents changes within 2.5°C (e.g. Q63A, E64A, Q71A, R194A, and Y195A) (Figure 19A). Therefore, these generated alanine mutants are biochemically stable as the wt DrrA₁₆₋₃₅₂.

Subsequently, the AMPylation efficiencies of these generated alanine mutants were determined by using the change in time-resolved tryptophan fluorescence. Since this interface represents a previously unrecognized Rab binding site, careful evaluation of DrrA alanine substitutions toward to Rab8a and Rab1b will be necessary. Although Rab8a is not a physiological AMPylation substrate for DrrA in the course of *Legionella* infection, the current observed DrrA-Rab8a interface was still validated by checking the AMPylation activity of these DrrA mutants toward GppNHp-bound Rab8a with time-resolved tryptophan fluorescence. Indeed, the DrrA mutants showed decreased AMPylation activity toward Rab8a, except Q63A and E64A, which exhibit increased AMPylation rates. Especially, R70A, Q71A, K74A and Y195A impaired the AMPylation activities remarkably (Figure 19B).

Then the AMPylation activities of these DrrA mutants toward GppNHp-bound Rab1b were investigated ³⁰. Interestingly, E264A showed 5-fold decrease activity toward Rab8a, while E264A only slightly impaired its enzymatic activity toward Rab1b by a factor of 2. Also, both Q63A and E64A exhibited increase activities toward Rab8a, but only Q63A exhibited increase activity toward Rab1b. Albeit some of DrrA alanine mutants showed different enzymatic activities toward Rab8a and Rabab, R70A, Q71A, K74A and Y195A also impaired the AMPylation activities remarkably toward Rab1b. Of note, R70A_{DrrA} and Q71A_{DrrA} displayed significant reduction in the AMPylation activity with a factor of 1000 (Figure 19C). Since R70_{DrrA}, Q71_{DrrA} and K74_{DrrA} are not only interacting with each other with polar interactions, but also further interacting with D44_{Rab1b/Rab8a}. Therefore, any alanine mutants in position 70, 71, and 74 may not only completely disrupt the network between them, but also abolish their interactions with D44_{Rab1b/Rab8a}, which may lead to a strong decrease in the AMPylation rates as a final consequence.

Again, the generated results were further validated by using proximity-enabled crosslinking of Rab1b bearing BrC6K mutants and corresponding Cys-mutants in DrrA ⁶⁰.

In summary, the mutagenesis studies toward Rab8a:GppNHp and Rab1b:GppNHp demonstrate that the non-canonical binding of Rab protein should regulate the AMPylation activity of DrrA.

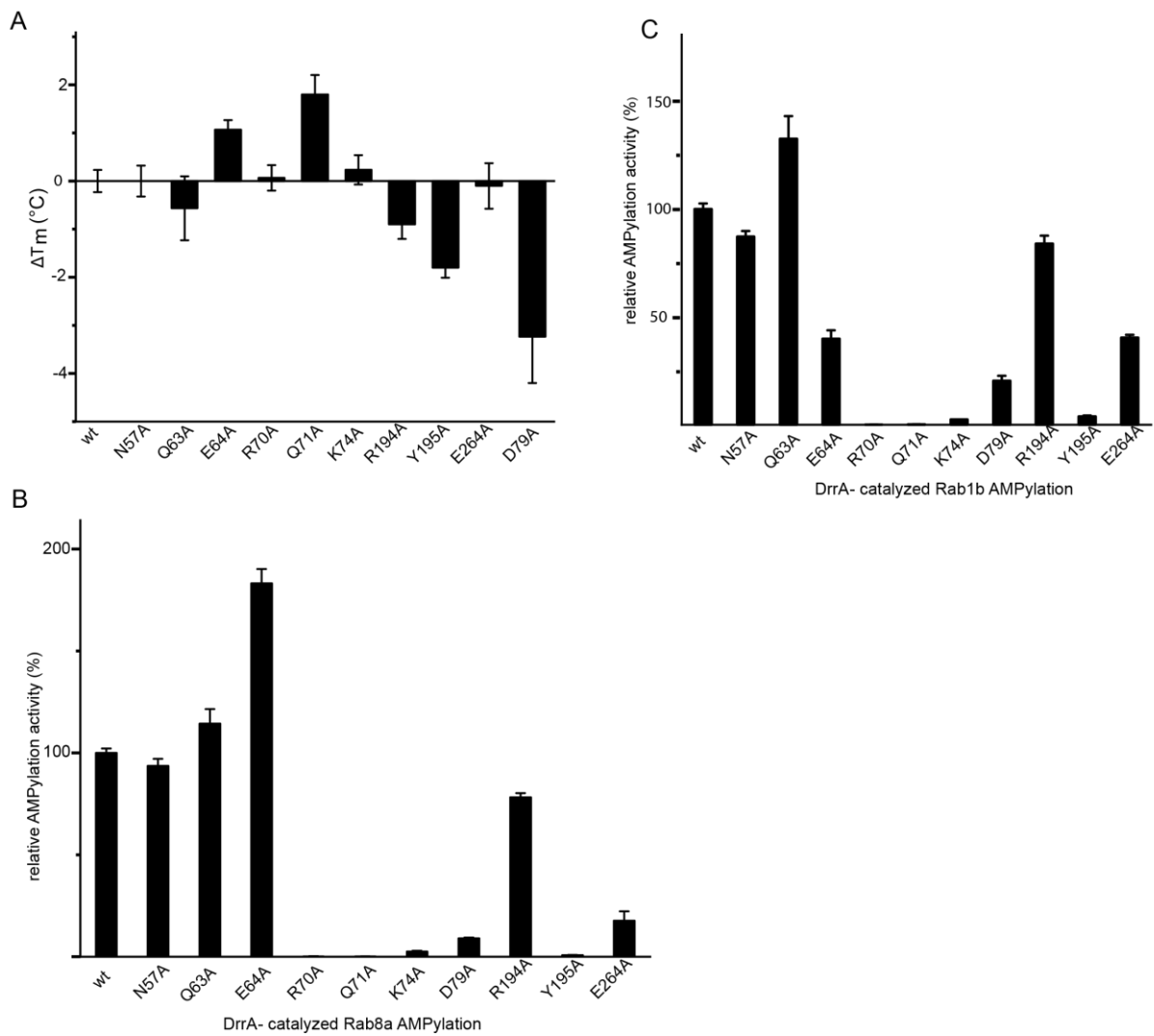


Figure 19 Confirmation of the NC-RBS complex interface. **(A)** Melting point (T_m) determination of DrrA and DrrA alanine mutants by circular dichroism (CD). The melting point of wt DrrA is 60.1°C . Data are means \pm standard error of the mean (SEM) from three independent experiments. **(B)** Determination of Rab1b-AMPylation rates in vitro by DrrA with mutations in the non-conventional site. The k_{cat}/K_M value of wt DrrA toward Rab8a:GppNHp is $9.0 \times 10^5 \text{ M}^{-1} \text{ s}^{-1}$ ($\pm 1.2 \times 10^5 \text{ M}^{-1} \text{ s}^{-1}$). Data are means \pm standard error of the mean (SEM) from three independent experiments. **(C)** Validation of the non-conventional (NC) site from DrrA mutation: AMPylation rates. The k_{cat}/K_M value of wt DrrA toward Rab1b:GppNHp is $8.0 \times 10^5 \text{ M}^{-1} \text{ s}^{-1}$ ($\pm 2.0 \times 10^4 \text{ M}^{-1} \text{ s}^{-1}$). Data are means \pm standard error of the mean (SEM) from three independent experiments. Picture is a modified copy from my previous manuscript to Nature Communications⁶⁰.

2.1.4 AMPylation by *Legionella* DrrA is allosterically activated by active state Rab1b

Even though we confirmed the presence of an NC-RBS in the complex crystal structure by complementary approaches⁶⁰, the functional relevance of Rab1b binding to the non-canonical site remains unclear. Therefore, we further investigated the roles of Rab1b's binding in the back site of DrrA to answer the question about its physiological relevance.

2.1.4.1 The C-terminus of the AMPylation domain may structurally stabilize the N-terminus for AMPylation

Although attempts to crystalize the apo form of the full AMPylation domain failed, DrrA fragments (e.g. DrrA₈₋₂₁₈ and DrrA₁₉₃₋₅₃₃) were reported before^{13, 58}. To understand the conformational changes between DrrA₁₆₋₃₅₂ and DrrA₈₋₂₁₈, we first asked whether the C-terminus of DrrA may contribute to the structural changes in DrrA or not. To this end, the DrrA structure from the current complex was served as a relevant model, and the previous reported N-terminal part and C-terminal parts were superimposed to this model (DrrA₈₋₂₁₈ and DrrA₂₁₈₋₃₄₀, referred as part-N and part-C respectively in the following) (Figure 20A)^{13, 58}.

Indeed, extensive contacts between part-N and part-C are present (Supplementary Figure 3). Interactions between the part-c and the catalytic center in the part-N can be observed (Supplementary Figure 3). Therefore, such interaction may help the secondary elements in the part-N correctly fold. Also, Rab binding to the non-canonical site also regulate the AMPylation activity of DrrA. However, most interactions between DrrA and Rab8a are formed from the part-N (Supplementary Figure 3 and Figure 17C). Although E264_{DrrA} is from the part-C, its interaction with K58_{Rab} is not important for maintaining the AMPylation activity (Figure 18C). Thus, Rab1 binding to the non-canonical site should not influence the proper folding of the part-C.

Taken together, constructs that lack of part-C cannot stabilize the region in part-N necessary for catalysis, which renders these constructs deficient in AMPylation, which are further supported that the fact that constructs lacking part-C or portions (eg. amino acid 300-340 or amino acid 218-340) do not possess AMPylation activity, and do not cause AMPylation-mediated cytotoxicity in COS7 cells¹³. And Rab1 binding to the non-canonical site regulate the AMPylation activity of DrrA with another unknown way.

2.1.4.2 Rab1b binding in the NC-RBS may causes structural changes in DrrA

Significant global structural differences between DrrA₈₋₂₁₈ and DrrA₁₆₋₃₅₂ were not observed (Figure 20B). Instead, the obvious structural differences in the catalytic center can be observed (Figure 20C). The relative positions of the catalytic Asp residues (D110_{DrrA}, D112_{DrrA}, and D150_{DrrA}) in DrrA₈₋₂₁₈ are disordered. Furthermore, the helix α 3 is in the middle of D110_{DrrA} and D150_{DrrA} (Figure 20C). In contrast to that, the helix α 3 in DrrA₁₆₋₃₅₂ is

relocated into the inner part of the protein catalytic pocket. Consequently, D110_{DrrA}, D112_{DrrA} and D150_{DrrA} are coordinated together, which renders the catalytic center capable of Mg²⁺ binding and ATP binding. Notably, it is worth mentioning that DrrA can bind to ATP when Rab1 is present³³. Therefore, Rab binding to the non-canonical binding site of DrrA regulates the AMPylation activity of DrrA by repositioning the active site of DrrA.

To prove that DrrA has two separate Rab binding sites, then I performed the kinetic experiments with DrrA₁₆₋₃₅₂ and Rab1b:GppNHp by time-resolved tryptophan fluorescence. Consistent with the previous observation, a lag phase in the kinetic curve was observed when Rab1b concentration was low (Figure 20D). Also, analysis of the data via the sigmoidal Hill-type function, not Michaelis-Menten function, yields a better fit. Importantly, the resulted cooperativity parameter is 1.7 ± 0.16 , suggesting that Rab1b allosterically stimulates the AMPylation activity of DrrA, and DrrA has two separate Rab binding sites. To further prove the above suggested allosteric regulation by the AMPylation domain of DrrA, I performed the kinetic experiments with full-length DrrA₁₆₋₆₄₇ and Rab1b:GppNHp by time-resolved tryptophan fluorescence. Remarkably, identical kinetic features were observed in the full-length DrrA₁₆₋₆₄₇-mediated AMPylation kinetic assay with the cooperativity parameter ($n = 1.6 \pm 0.20$) (Figure 20E).

Indeed, the detailed conformational changes by Rab1 binding in the NC-RBS of DrrA should be further investigated in the future. However, together with our kinetic study, mutation analysis, crosslinking assays and structure analysis, one can propose that Rab1b binding in the NC-RBS may causes structural changes in DrrA, which may regulate the AMPylation activity of DrrA.

2.1.4.3 Rab1b-binding to the NC-RBS activates DrrA *in vivo*

Inspired by the above findings, the allosteric stimulatory function of Rab1 was further tested *in vivo*. Previously, the DrrA-catalyzed AMPylation can cause cytotoxicity when AMPylation-competent DrrA constructs were overexpressed in mammalian cells. Therefore, the cell viability can direct reflect the AMPylation activity of selected DrrA alanine mutants¹³. Given that the expression levels of DrrA constructs and long incubation time in mammalian cells, only alanine mutants, which impaired the AMPylation activity significantly, were selected for *in vivo* test. Meanwhile, the GEF domain is necessary for producing active Rab1b. Therefore, N-terminally enhanced green fluorescent protein (eGFP)-tagged DrrA₈₋₅₃₃ constructs (wt, R70_{DrrA}, Q71_{DrrA}, and K74_{DrrA}) were generated and transfected with eukaryotic H1299 cells.

To precisely evaluate the AMPylation-mediated cytotoxicity by different tested constructs, fluorescence-activated cell sorting (FACS) (Gating strategy for FACS can be seen in Figure 21) was applied for the collection of GFP-positive cells. Subsequently, the relative cell viability was determined by the absorbance-based MTS (3-(4,5-dimethylthiazol-2-yl)-5-(3-

carboxymethoxyphenyl)-2-(4-sulfophenyl)-2H-tetrazolium) assay. Wild type DrrA₈₋₅₃₃ caused severe cytotoxicity (Figure 20F). However, the single mutants, such R70A_{DrrA}, Q71A_{DrrA}, and K74A_{DrrA} still caused similar level of cytotoxicity as wild type DrrA (Figure 20F). Indeed, these single mutants are not active as wt DrrA in the kinetic assays, but not dead. When these mutants are overexpressed in H1299 cells for 48 hours, they should cause pronounced cytotoxicity. Consistently, *in vitro* Rab1b AMPylation by these single mutants with extended time (72 hours) resulted full AMPylation of Rab1b (Supplementary Figure 4).

Guiding by the non-canonical complex structure, I found that R70_{DrrA}, Q71_{DrrA}, and K74_{DrrA} interact with each other and then form a delicate network to stabilize the interaction with D44 from Rab1b or Rab8a. Thus, I asked that if one triple alanine mutant R70A/Q71A/K74A_{DrrA} is designed and tested, this mutant will cause cytotoxicity or not. As expected, the triple mutant R70A/Q71A/K74A_{DrrA} of DrrA₈₋₅₃₃ did not induce any cytotoxicity in H1299 cells (Figure 20G). Therefore, the MTS data show that active Rab1b binding to the non-catalytic site of turns the AMPylation activity of DrrA on.

Furthermore, it is interesting to ask whether AMP-Rab1b can also bind to the allosteric site of DrrA. Therefore, time-resolved crosslinking assay was performed by our collaboration partners⁶⁰. However, no significant differences can be observed, then probably both Rab1b and AMP-Rab1b can stimulate the AMPylation activity⁶⁰, suggesting the AMP group in the AMPylated Rab1b probably does not cause any structural conflicts in the back site of DrrA. Therefore, our data shows that both Rab1b and Rab1b-AMP can bind to the allosteric binding site of DrrA *in vitro*. However, the MTS data indicated that DrrA must be activated prior to the AMPylation of Rab1b in the catalytic site. Moreover, DrrA and Rab1b are LCV-bound proteins during the *Legionella* infection. Likely, when Rab1b was AMPylated by DrrA in the catalytic site, AMP-Rab1b is unlikely to go back to the allosteric site to activate DrrA. Taken together, the initial and main activator should be Rab1b:GTP, the product of DrrA GEF domain, not the product of DrrA AMPylation domain.

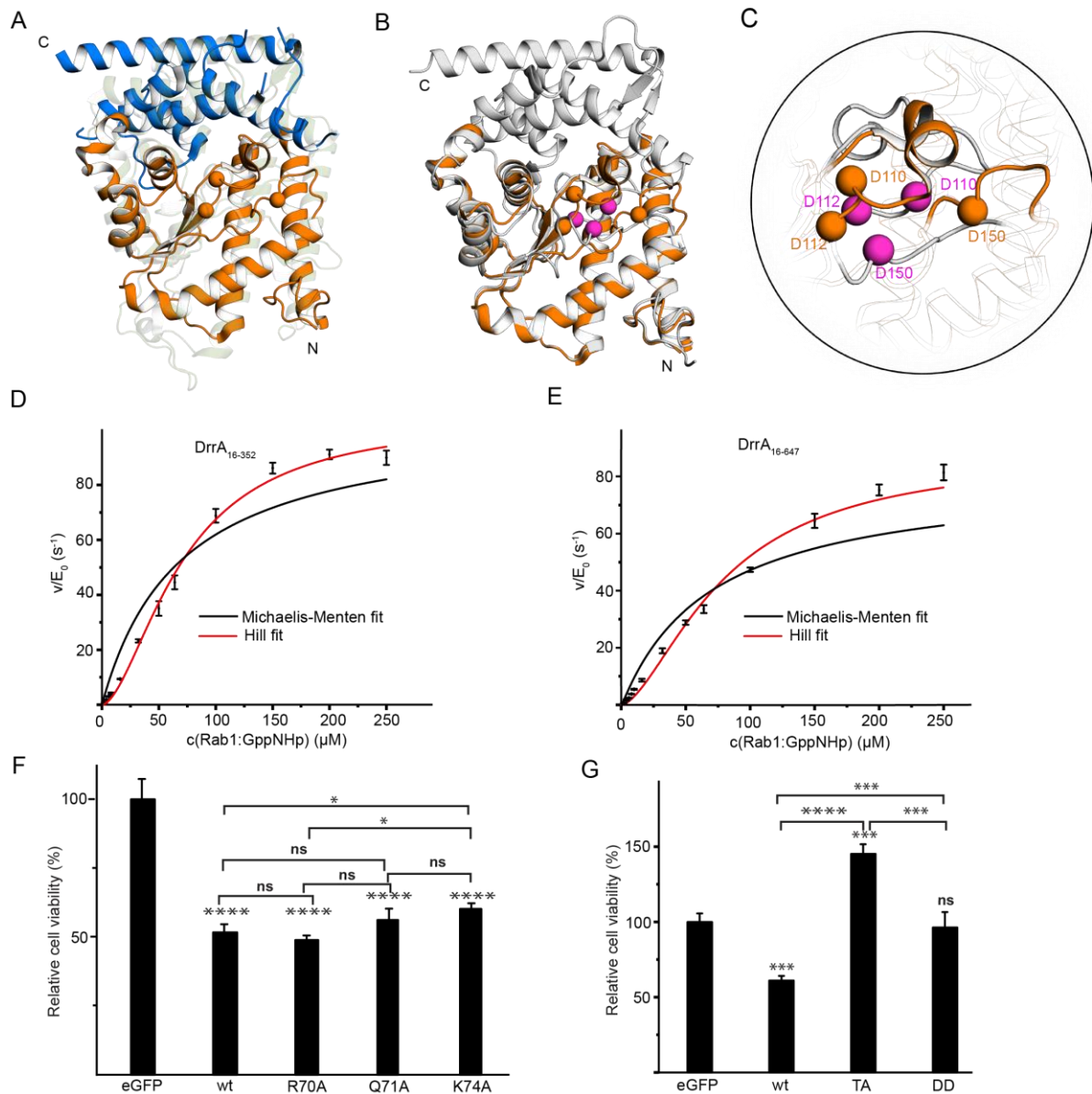


Figure 20 Allosteric activation of DrrA by active Rab1b. **(A)** Construction of the DrrA apo-form. DrrA₈₋₂₁₈ (PDB: 3NKU, orange) and DrrA₁₉₃₋₃₅₂ (PDB: 3LOI, blue) are superimposed onto GS-ATase (PDB: 3K7D, light green background). Orange spheres represent the catalytic Asp residues of DrrA₈₋₂₁₈. **(B)** Global structural changes in DrrA by binding to active Rab1b. DrrA₈₋₂₁₈ (PDB: 3NKU, orange) and DrrA₁₆₋₃₅₂ (grey) are shown. **(C)** Structural changes in the active centre of DrrA induced by Rab1b binding to the non-conventional site. Purple spheres represent the catalytic centre of DrrA₁₆₋₃₅₂ in the DrrA:TReND-1:Rab8a complex. Orange spheres represent the catalytic centre of DrrA₈₋₂₁₈ (PDB: 3NKU, orange). **(D)** Sigmoidal dependence of AMPylation on the active Rab1b concentration. The red curve represents the Hill fit with a cooperativity parameter of $n = 1.7 \pm 0.16$; the black curve is the Michaelis-Menten fit. Data are means \pm SEM from three independent experiments. **(E)** Full length DrrA₁₆₋₆₄₇ mediated AMPylation. The red curve represents the Hill fit with a cooperativity parameter of $n = 1.6 \pm 0.20$; the black curve is the Michaelis-Menten fit. Data

are means \pm SEM from three independent experiments. **(F)** Cytotoxicity analysis of DrrA single alanine mutants in H1299 cells. Cell viability values (determined by MTS assay) of DrrA-expressing cells (eGFP-positive) were determined in relation to the eGFP vector control. WT: DrrA₈₋₅₃₃; R70A: DrrA_{8-533_R70A}; Q71A: DrrA_{8-533_Q71A}; K74A: DrrA_{8-533_K74A}. Data are means \pm SEM from three independent experiments. One-way analysis of variance (ANOVA) was applied; ns, $p > 0.05$; ****, $p < 0.0001$. **(G)** Cytotoxicity analysis of DrrA mutants in H1299 cells. Cell viability values (determined by MTS assay) of DrrA-expressing cells (eGFP-positive) were determined in relation to the eGFP vector control. TA: DrrA_{8-533_R70A_Q71A_K74A}; DD: DrrA_{8-533_D110_D112A}. Data are means \pm SEM from three independent experiments. One-way analysis of variance (ANOVA) was applied; ns, $p > 0.05$; ***, $p < 0.001$; **, $p < 0.01$; *, $0.01 < p < 0.05$. Picture is a copy from my previous manuscript to Nature Communications⁶⁰.

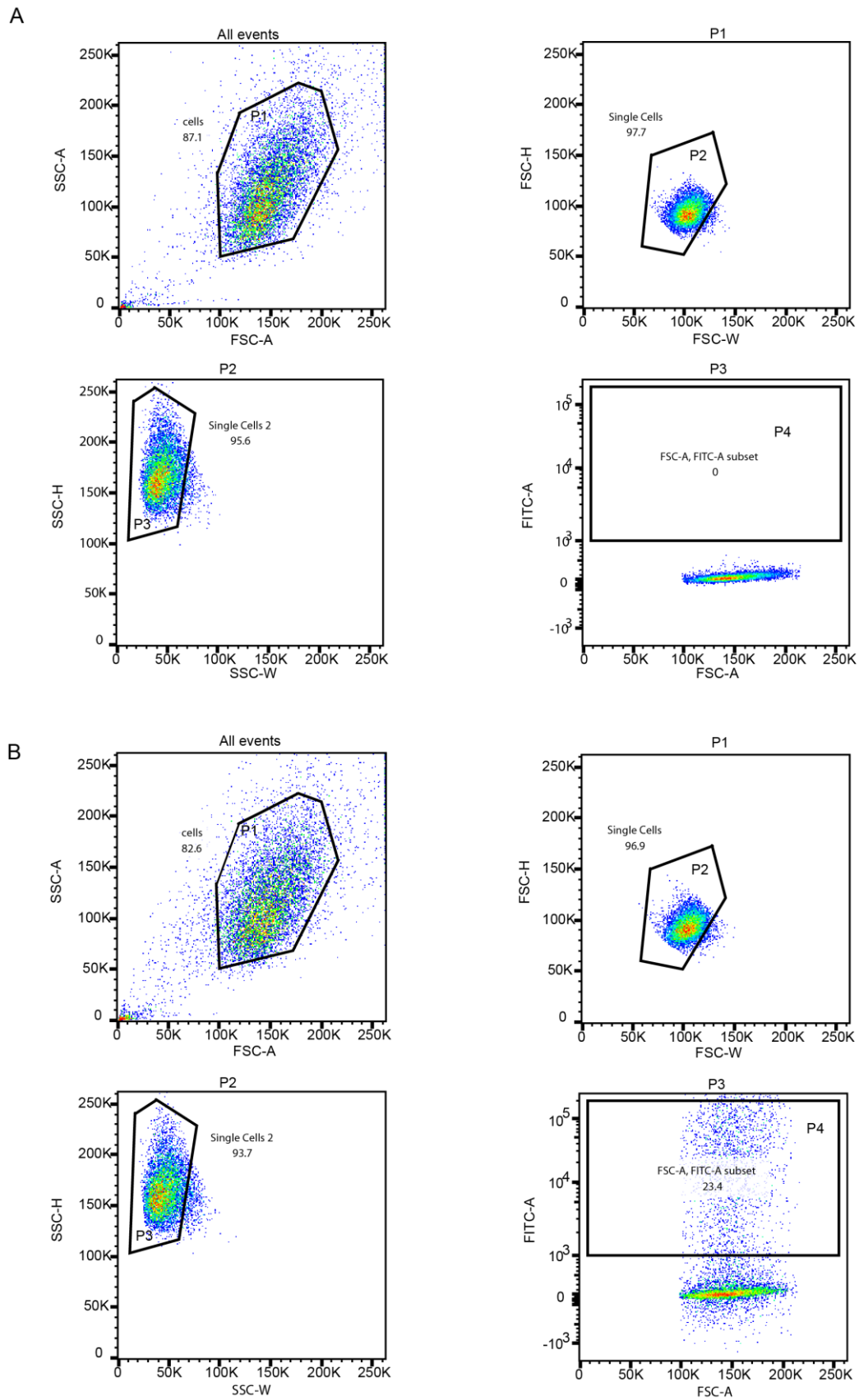


Figure 21 Representation of gating strategy for sorting GFP-positive H1299 cells. Side scatter area (SSC-A) versus forward scatter area (FSC-A) density plot was applied for excluding debris and dead H1299 cells. Selected population was named as P1. The plot

(forward scatter height (FSC-H) versus forward scatter width (FSC-W)) is used to discriminate doublets from single cells; selected population was marked as P2. The plot (side scatter height (SSC-H) versus side scatter width (SSC-W)) was further used to ensure the selection of single cells, selected population was labelled as P3. Subsequently, the last plot (FITC-A (GFP channel) versus FSC-A) was applied to separate the GFP-positive cells (P4 population) from the GFP-negative cells. The proper gating was set up using non-transfected cells as negative control. **(A)** Non-transfected H1299 cells was taken as negative control. **(B)** GFP- transfected H1299 cells as positive control. Picture is a copy from my previous manuscript to Nature Communications ⁶⁰.

2.2 Formation of the canonical complexes between DrrA AMPylation domain and Rab1b/8a

Structural study and kinetic study indicated that the AMPylation domain of DrrA contains two separated Rab1b binding platform. The previous unrecognized Rab1b binding site regulates the AMPylation activity by active Rab1b's binding. Therefore, we proposed that active Rab1b's binding causes structural changes in the catalytic center and then stimulate the AMPylation activity of DrrA.

Inspired by previous results, we further explored the DrrA-catalyzed Rab1b AMPylation mechanism by trapping the second covalent DrrA-Rab complex, which will be referred as canonical complex hereafter.

2.2.1 Design the potential cysteine substitutions for the DrrA-Rab1b/8a complex formation in the canonical site

I asked whether ATP can co-crystallize with the non-canonical DrrA-Rab8a complex. Such attempts failed due to the low affinity between ATP and DrrA. Again, since active Rab1b plays roles in regulating the AMPylation activity of DrrA, I decided to follow the same strategy to trap the second covalent complex as before (Figure 9). Based on my knowledge about DrrA, a model about ATP binding in DrrA was generated (Figure 22A): In this model, the γ phosphate group should interact with R303_{DrrA}. To test this ATP binding mode, R303A_{DrrA} was purified and tested. Indeed, R303A_{DrrA} significantly impairs the AMPylation activity of DrrA compared with wt DrrA₁₆₋₃₅₂ (Figure 22B). Therefore, guiding by this model, we designed the following cysteine mutants for trapping the canonical complex: T187C_{DrrA}, K219C_{DrrA}, and K223C_{DrrA}. However, none of these mutants can form a covalent complex in the presence of TReND-1 and Rab1b (Figure 22C).

Therefore, this ATP binding mode in the above-mentioned model should be wrong (Figure 22A). Of note, the orientation about the adenosine group of ATP is not conserved in the AMP-transferases ^{32, 34}. However, M174C and V175C in DrrA can form the second covalent complex with TReND-1 and Rab1b, although the yield is significant low (Figure 16B). Hence,

I created a new model about ATP binding mode in the catalytic center of DrrA by autodock Vina⁸⁶ (Figure 22D). In this new model, the adenosine group of ATP is located in the vicinity of D177_{DrrA}. Probably D177_{DrrA} interacts with the hydroxyl group in the adenosine group of ATP, since D177A moderately decreases its AMPylation activity (Figure 15). Interestingly, R303 also interacts with the phosphate group of ATP in this model. Based on this new model, three additional cysteine mutants were designed: A176C_{DrrA}, D177C_{DrrA}, and T181C_{DrrA} (Figure 22E). A176C_{DrrA}, but not other cysteine mutants, can form a covalent complex in the catalytic site (Figure 22F). It is worth mentioning that A176C_{DrrA} can only form a complex at high concentration (200 μ M or higher) of active Rab1b. Differently, the active Rab1b concentration was generally set at 100 μ M or lower concentrations in the previous non-canonical complex formation assays. Indeed, the K_M in the allosteric site is surely smaller than the one in the catalytic site. Therefore, our TReND-1 crosslinking assay for DrrA is affinity-dependent. However, the yield of this covalent complex is lower than the yield of the non-canonical complex in the presence of high concentration of active Rab1b. Therefore, the previous purification strategy (size exclusion chromatography) for the non-canonical complex cannot be applied for the purification of this canonical complex. Thus, in order to uncover the DrrA-catalyzed Rab1b AMPylation in a more detailed manner, the canonical complex has to be purified at the first place.

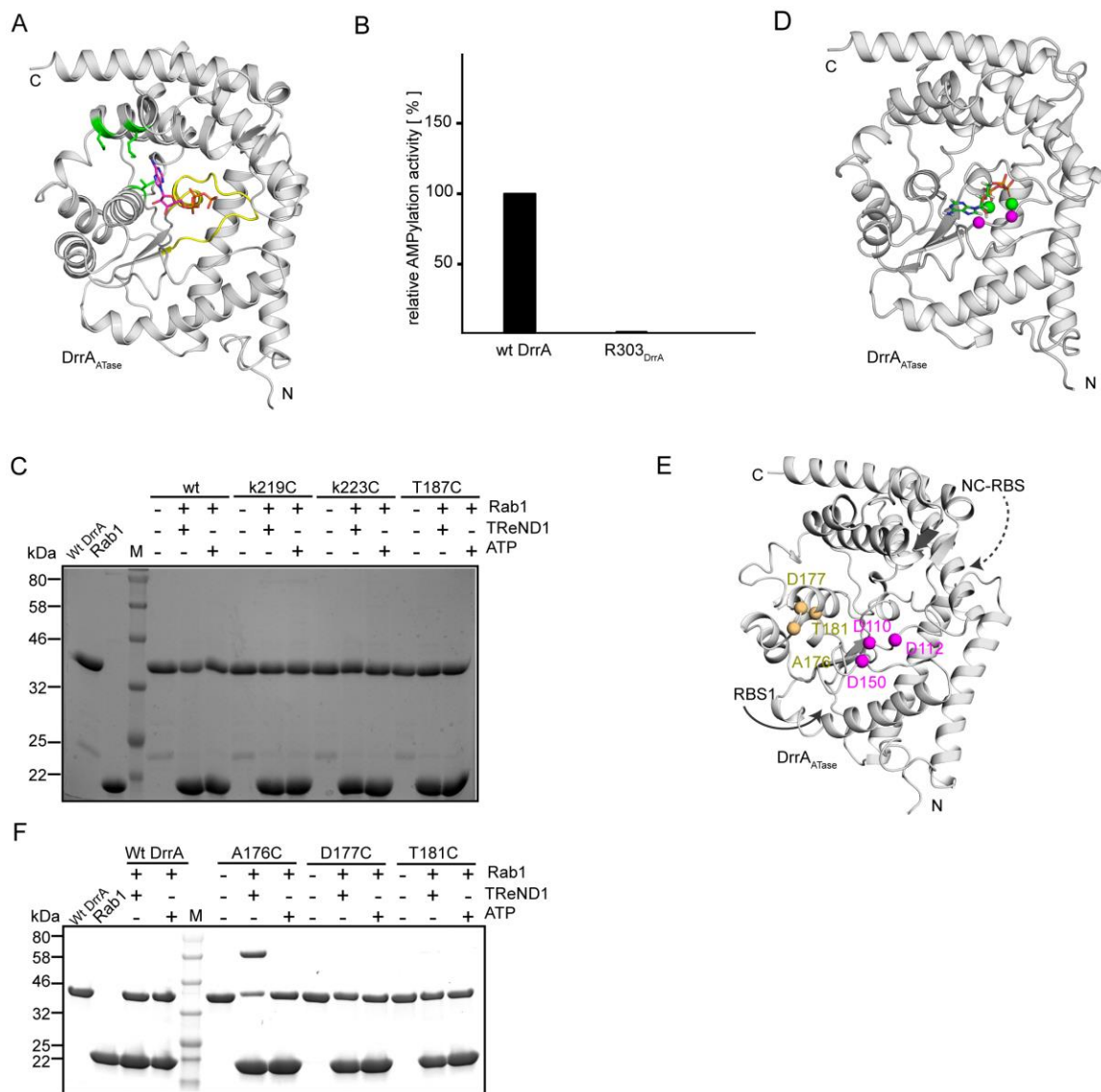


Figure 22 Strategy for the formation of the covalently linked complex. **(A)** The ATP binding mode in DrrA₁₆₋₃₅₂. DrrA fragment is from the non- canonical DrrA- Rab8a complex, PDB: 6YX5. Green residues are T187C_{DrrA}, K219C_{DrrA}, and K223C_{DrrA}. Yellow region is the catalytic center. Stick is ATP. **(B)** Catalysis kinetics of wt DrrA and R303A_{DrrA} toward Rab1b:GTP. The k_{cat}/K_M value of DrrA₁₆₋₃₅₂ was normalized to 1. The k_{cat}/K_M value of DrrA₁₆₋₃₅₂ is $8.0 \times 10^5 \text{ M}^{-1} \text{ s}^{-1}$. The k_{cat}/K_M value of R303A_{DrrA} is $1.1 \times 10^3 \text{ M}^{-1} \text{ s}^{-1}$. **(C)** SDS-PAGE shift analysis for complex formation with cysteine mutants based on previous model. **(D)** A new ATP binding mode in DrrA₁₆₋₃₅₂. DrrA fragment is from the non-canonical DrrA-Rab8a complex, PDB: 6YX5. Purple spheres are D110 and D112. Green spheres are Mg^{2+} . Stick is ATP. This model is generated by Autodock⁸⁶. **(E)** Cys substitution sites (A176, D177 and T181, light orange) in DrrA_{ATase}. Pink spheres represent the catalytic center of DrrA. RBS1 indicates the conventional site, which contains the catalytic center. NC-RBS represents the non-canonical site, which is located at the back face of the catalytic center. **(F)** SDS-PAGE shift analysis of

DrrA:TReND-1:Rab1b complex formation in the catalytic side (RBS1). Picture E and F are copies from my previous manuscript to Nature Communications⁶⁰.

2.2.2 Strategy for the purification of DrrA_{A176C}-Rab1b/8a complex

DrrA_{A176C} shares similar biochemical features (e.g. charge and isoelectric Point) with the DrrA_{A176C}-Rab complexes, which makes it difficult to be separated from the canonical covalent complexes. Indeed, we failed to purify the covalent complex by applying cation exchange chromatography or size exclusion chromatography.

Previously our co-worker separated AnkX from AnkX:Rab1b complex by introducing additional affinity tags into Rab1b²⁵. Introducing additional affinity tags into Rab proteins may help the complex separated from DrrA. Hence, a small tag (His₆-tag) was introduced to Rab1b protein. In order to make this flexible His tag removable, a PreScission cleavage site between this His₆-tag and Rab1b/Rab8a protein construct was also introduced.

Therefore, A176C_{DrrA}, TReND-1 and Rab1b or Rab8a are incubated at room temperature for the formation of complexes. After 48 hours, the sample was subjected to the Ni-chelating column. After getting rid of DrrA by washing extensively with low percentage imidazole containing buffer, the complex and Rab1b were eluted by high concentration of imidazole. Then the complex and Rab proteins will be digested with high concentration of PreScission enzyme in order to liberate the His₆-tag. Last, the complex can be separated from the Rab proteins by size exclusion chromatography (Figure 23A). By applying this approach, we were able to obtain preoperative amounts of DrrA-Rab1b/Rab8a complexes, demonstrated by intact mass spectrometry analysis (Figure 23B and 23C).

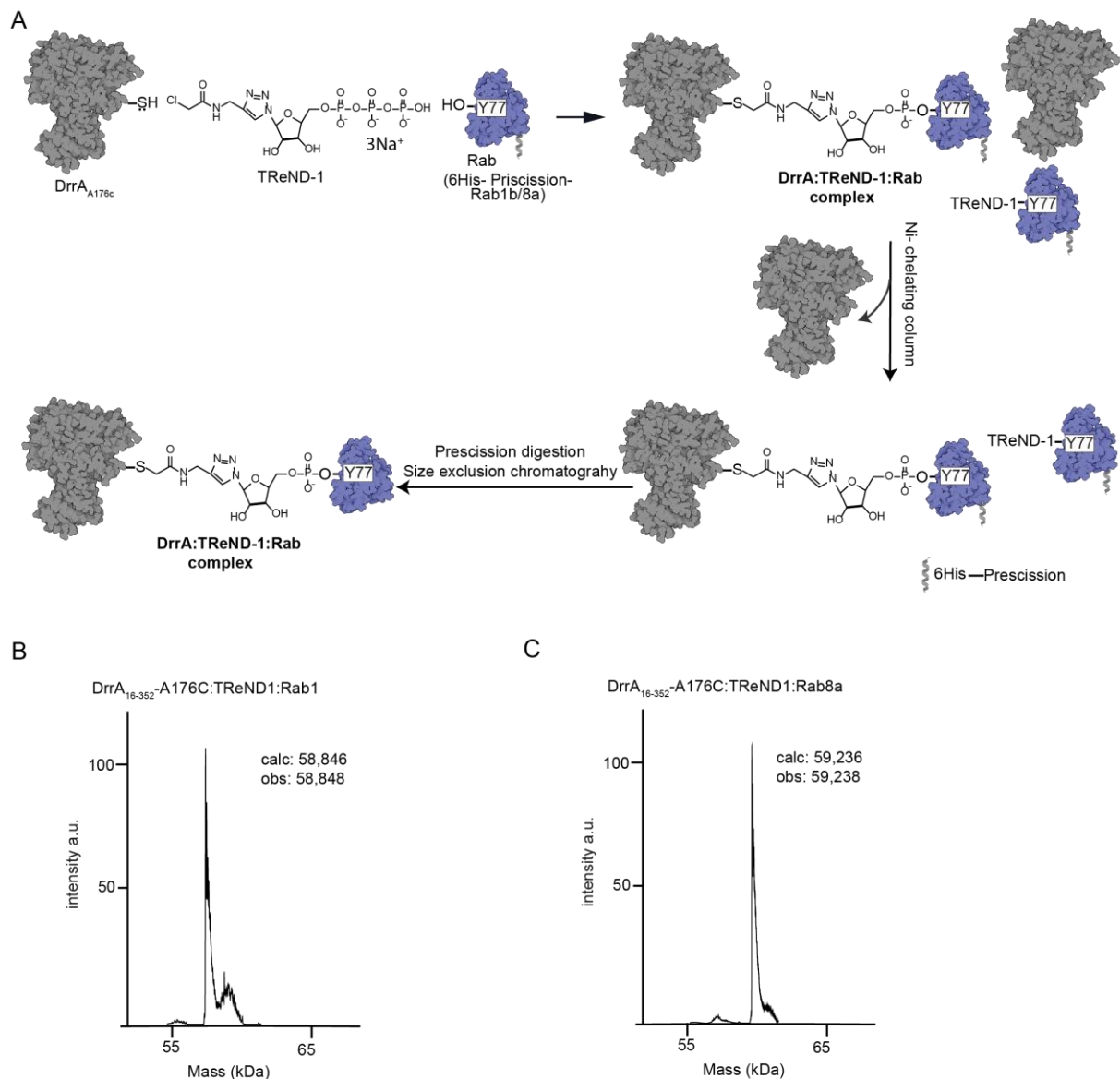


Figure 23 Strategy for the purification of the covalently linked complex. **(A)** Procedures for obtaining pure canonical complex. By Ni-chelating column, DrrA is separated from the canonical complex and Rab. After PreScission digestion, size exclusion chromatography was performed to get the pure complex. **(B)** Intact mass spectrometry analysis of the DrrA₁₆₋₃₅₂-A176C:TReND-1:Rab1b complex. **(C)** Intact mass spectrometry analysis of the DrrA₁₆₋₃₅₂-A176C:TReND-1:Rab8a complex.

2.2.3 Biochemical characterization of DrrA_{A176C}-Rab1b complex

To further assess the significance of the NC-RBS in DrrA and uncover the AMPylation mechanism of DrrA, we attempted to characterize the canonical complex biochemically.

2.2.3.1 Crystallization of the covalent DrrA_{A176C}-Rab1b/8a complexes and the methylated DrrA_{A176C}-Rab1b/8a

Encouraged by the previous results, we attempted to determine the interaction mode of DrrA and Rab proteins by solving the structures of the canonical complexes.

Interestingly, DrrA_{A176C}-Rab1b complex, but not DrrA_{A176C}-Rab8a complex, can yield crystals in different buffer conditions (Table 2). However, structure determination of the complex failed due to a lack of diffracting crystals. As mentioned before, DrrA possess numerous lysine residues in the surface, probably methylation of the complex may result diffracted crystals. Again, methylated DrrA_{A176C}-Rab1b complex, but not methylated DrrA_{A176C}-Rab8a complex, can yield crystals in different buffer conditions (Table 2). However, none of these crystals diffracted properly.

Although the structure determination of the canonical DrrA_{A176C}-Rab1b/8a complexes failed, probably replacing Rab1b or Rab8a with other *in vitro* AMPylation Rab target proteins, e.g. Rab3A, Rab6A, Rab4B, Rab13, Rab14, and Rab37, will result in diffracted crystals. Alternatively, changing the crosslinker in the canonical complex may work.

Table 2 Buffer conditions for obtaining crystals of the covalent complexes.

0.1 M Tris, 15 %(w/v) PEG 6000, pH 7.5 for DrrA _{A176C} -Rab1b
0.1 M Tris, 0.2 M Ammonium sulfate, 12 %(w/v) PEG 8000, pH 8.5 for DrrA _{A176C} -Rab1b
0.1 M Na/K phosphate, 0.2 M Sodium chloride, 10 %(w/v) PEG 8000, pH 6.2 for DrrA _{A176C} -Rab1b
0.085 M Sodium HEPES, 17 %(w/v) PEG 4000, 15 %(v/v) Glycerol, 8.5 %(v/v) Isopropanol pH 7.5 for methylated DrrA _{A176C} -Rab1b
0.1 M Tris, 0.1 M Potassium chloride, 15 %(w/v) PEG 2000 MME, pH 8 for methylated DrrA _{A176C} -Rab1b

2.2.3.2 Comparison of the catalytic activity of DrrA_{A176C}-Rab1b with the non-canonical complex

Although I used the kinetic assay to confirm two separate Rab binding sites in DrrA, I further validated the two separate Rab binding sites in DrrA by comparing the catalytic activity of these two different complexes (Figure 24A). Compared with free DrrA₁₆₋₃₅₂, the non-canonical DrrA:Rab1b complex stimulated the AMPylation activity by a factor of 1.5. In contrast to the non-canonical complex, the canonical complex did not AMPylate Rab1b, suggesting that the catalytic center of DrrA is covered by the currently linked Rab1b. Therefore, the results further indicate that DrrA₁₆₋₃₅₂ does possess two separate Rab-binding sites.

Hence, I proposed that the GEF activity of DrrA first recruits Rab1b protein from Rab1b: GDI complex in the cytosol of the host cells. Then active Rab1 is generated by the exchange of nucleotide from GDP to GTP in the LCV. Subsequently, allosteric binding of active Rab1b to the NC-RBS switches the active site of DrrA_{ATase} from an unstructured AMPylation-deficient state to an organized AMPylation-competent state, which further mediates the AMPylation of Rab1b (Figure 24B and 24C).

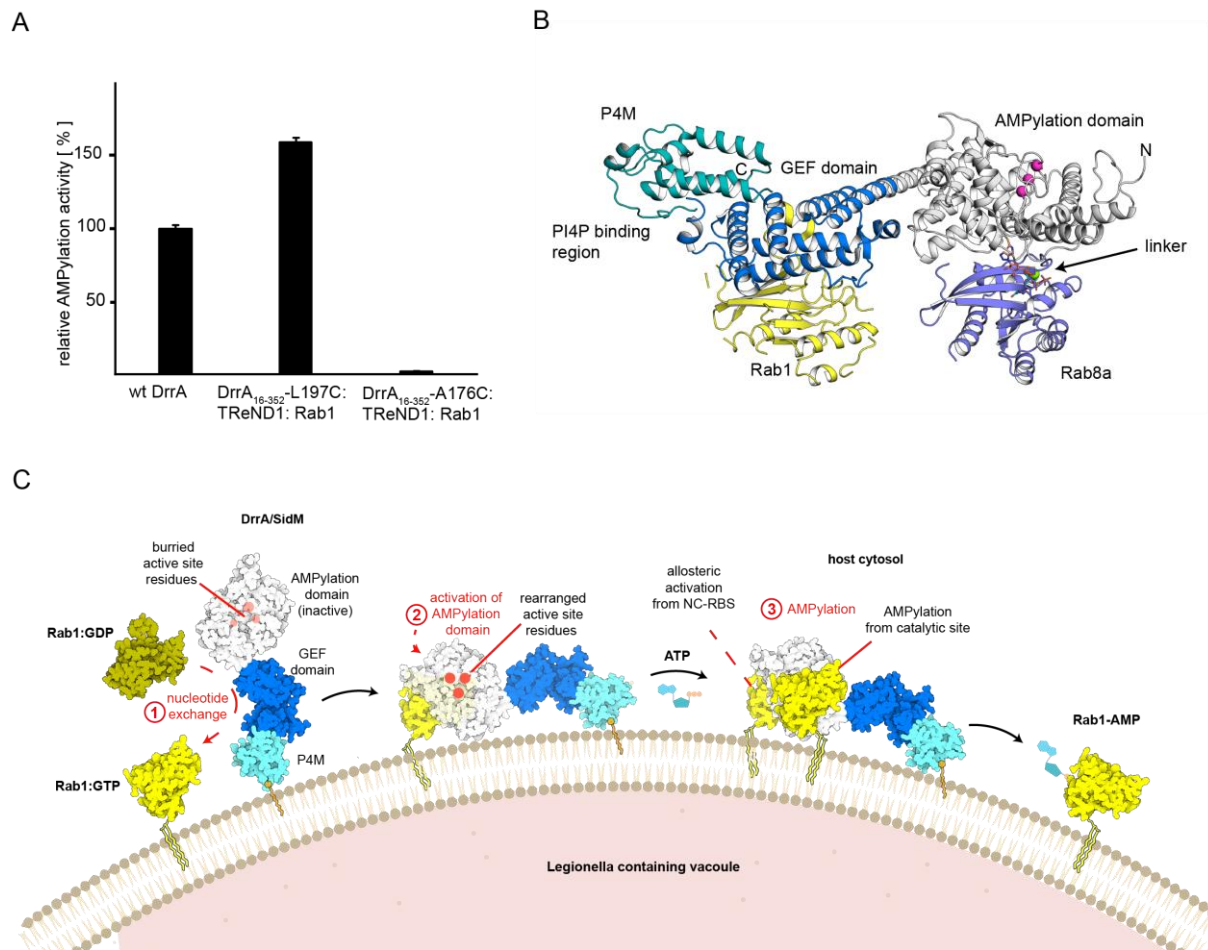


Figure 24 Biochemical characterization of DrrAA176C-Rab1b complex. **(A)** Comparison of the catalytic activity of DrrA_{A176C}-Rab1b with the non-canonical complex. **(B)** Composite model of DrrA produced from the following crystal structures PDB: 6YX5, 3LOI, 3N6O. The different binding sites of Rab-molecules is indicated at the GEF-domain and the NC-RBS. The catalytic site of the AMPylation domain (composed by D110, D112, D150) is indicated by magenta spheres. GEF: Guanine nucleotide exchange factor; P4M: phosphatidylinositol-4-phosphate (PI4P) binding of DrrA. **(C)** Model of DrrA action at the membrane. The P4M localizes DrrA to the membrane by binding to PI4P. The GEF-domain activates Rab1b by GDP-to-GTP exchange, thereby displacing it from GDI and creating membrane-bound Rab1b:GTP (yellow ribbons indicate geranylgeranyl lipids). Binding of Rab1b:GTP to the NC-RBS of DrrA putatively results in structural rearrangement of the catalytic site, which stimulates the subsequent AMPylation of another Rab1b:GTP-molecule. This picture is a copy from my previous manuscript to Nature Communications⁶⁰.

3. Discussion

As mentioned before, DrrA is secreted in the early infection phase, thus its enzymatic activity must be well controlled to fulfill two requirements: maximize its enzymatic activity and must not cause any cytotoxicity in the infected host cells. Therefore, it is not surprising that the expression level of DrrA cannot be detected in an early time point of *L. pneumophila* infection^{23, 39, 40}. It is also not surprising that *L. pneumophila* will coordinate the AMPylation activity of DrrA with other effectors. Therefore, the AMPylation activity of DrrA is under control by transcription regulation and the competitions between DrrA and other effectors^{23, 45}. However, intrinsic regulation in the AMPylation activity of DrrA has never been reported.

By using the TReND analogues combined with strategically designed DrrA_{cys} mutants, I found that active Rab1b binding to the noncanonical site of DrrA regulates the AMPylation activity of DrrA. Thus, the AMPylation event is primed by the GEF function, which provides the activator for the following AMPylation. Therefore, the current study provides answers to the long-standing question that why active Rab1b serves as the preferred AMPylation target of DrrA: active Rab1b allosterically activates the AMPylation activity of DrrA. Moreover, the GEF function of DrrA may render the DrrA-catalyzed Rab1 AMPylation restrained in the LCV. Presumably such controlling may help DrrA-catalyzed not cause any cytotoxicity, which can be further supported by the fact that overexpression of AMPylation-competent DrrA constructs cause severe cytotoxicity¹³, which may result in necrosis or pyroptosis *in vivo*.

Indeed, numerous pathogenic effectors are activated by host proteins. After host protein-mediated activation, these effectors can cause polyglutamylation^{55, 87, 88, 89}, lipid degradation^{90, 91}, ADP-ribosylation^{92, 93}, phosphorylation^{94, 95}, acetylation⁹⁶, and proteolytic cleavage^{97, 98}. However, AMPylation has not been shown as a PTM which is dependent on activation by a host protein. Of note, AMPylation by DrrA is directly activated by its target Rab1b, which is different from the above-mentioned PTMs.

The allosteric regulation of DrrA's AMPylation activity is different from other AMPylators. For instance, the AMPylation activity of GS-ATase is regulated by protein PII instead of its substrate glutamine synthetase^{3, 99}. Some of the Fic enzymes can regulate the AMPylation activity of Fic enzymes by the cycling between oligomeric state and monomeric state³⁷, which has never been observed in the study of DrrA. Although the AMPylation activity of some Fic enzymes can be activated by the auto-AMPylation in the so-called inhibitory helix^{36, 37}, the general regulation mechanisms of this inhibitory motif are unknown so far. Pseudokinase SelO regulates its enzymatic activity by reverse intramolecular disulfide bond formation²². In conclusion, the regulation mode of DrrA by its substrate Rab1b represents a unique example among AMP-transferases.

In conclusion, I successfully used the TReND analogues to trap two different states of complexes between the AMPylation domain of DrrA and Rab1b: the first one is that the non-canonical complex in the allosterically regulation state, and the second one is that the canonical complex in the AMPylation state (or post-AMPylation state). By the extensive biochemical characterization, this previously unrecognized allosterically regulatory site in the AMPylation domain of DrrA was further validated for the first time. The allosteric activation of DrrA AMPylation activity by active Rab1b represents a yet unprecedented mechanism, which may shed light on other AMPylation enzymes.

4. Outlook

As mentioned before, the regulation mode of DrrA by its substrate Rab1b is unique among AMP-transferases. Therefore, further investigation in DrrA-catalyzed AMPylation will be interesting. Hence, solving the structure of the canonical complex from the catalytic site is important. The kinetic study indicated that the affinity between DrrA and Rab1b is low (64 μM). Possibly, the low affinity makes the interactions between the canonical site of DrrA and Rab1b unstable, which further renders the crystals heterogeneous. Thus, how to stabilize the trapping complex will be important to get diffracted crystals for structural determination. Probably, due to the stimulatory effect of active Rab1b, co-crystallization of Rab1b and the canonical complex can stabilize the interactions in the canonical site of DrrA and Rab1b. Also, attempts to crystalize double ternary complex Rab1b-TReND-1-DrrA_{L197C_A176C}-TReND-1-Rab1 may be helpful.

TReND analogues serve as a powerful tool for trapping AMPylators' targets and uncovering the AMPylation mechanism by structural determination. Also, the allosteric activation of DrrA by its substrate active Rab1b depicts a mechanism that has no equivalent in other pathogenic systems and constitutes an original advance in the AMPylation field. Moreover, the TReND analogs probably can be further modified to expand the target identification *in vivo*. Furthermore, the concept of covalent trapping by TReND analogs can be applied to other fields, for instance target capture for kinases or other enzymes. However, it remains to be answered that TReND analogs can serve as a chemical tool to decipher the unknown activation mechanisms for AMPylation in Fic enzymes or not. If not, probably designing novel chemical tools is necessary in the coming future.

Currently AMPylation is appreciated as a widely shared PTM by diverse enzymes, however, its biological influence has never been shown as important as phosphorylation or other important post-transcriptional modifications. Although the AMPylation of Bip by HYPE has been shown to regulate the unfolded protein response in the ER and play a role in the recycling of the visual neurotransmitter histamine, current study cannot link these observations to more important cell signaling events, e.g. cell death or communication between ER and cytosol. Therefore, it may be interesting to further investigate the biological consequences of the intrinsic AMPylation events in the human cells or animal models.

5. Materials and methods

Full-length DrrA was amplified from *Legionella pneumophila* genomic DNA before. Then optimized DrrA truncated constructs were cloned into a modified pSF vector (a gift from Stefanie Pöggeler lab) with Gibson assembly by using Gibson assembly master mix from New England Biolabs. Wild type Rab1b and Rab8a were the same as previously reported. Rab1b and Rab8a with additionally His₆-tag were designed by Gibson assembly master mix. All the point mutations were performed with the Q5 Site-Directed Mutagenesis Kit. All the plasmids were confirmed by DNA sequencing. GppNHp and GDP were purchased from Jena Bioscience. The ATP analogue TReNDs are provided by Christian Hedberg lab. MTS agent was purchased from Promega, Walldorf, Germany. Unless otherwise stated, all other reagents were purchased from Sigma (Taufkirchen, Germany), Carl Roth (Karlsruhe, Germany).

5.1 Molecular biological methods

5.1.1 Polymerase chain reaction

DNA cloning was performed by using the T100 Thermal Cycler (BioRad, Hercules, USA). Q5 polymerase (New England Biolabs, Ipswich, USA) was used according to the supplier's recommendation. After PCR, DNA was purified with the Monarch® DNA Gel Extraction Kit (New England Biolabs, Ipswich, USA).

5.1.2 Agarose gel electrophoresis

In order to purify the amplified DNA products, template DNA was digested by excess home-made DpnI in room temperature for 2 hours. Following, agarose gel electrophoresis was performed. PCR products were mixed with 10x DNA loading buffer (50% glycerol, 10 mM EDTA, 0.2% bromophenol blue, 0.2% xylene cyanol FF) and loaded on a GelStar Nucleic Acid Stain (Lonza, Basel, Switzerland) contained agarose gel (1%). DNA was separated in 1x TAE buffer (40 mM Tris pH 7.6, 20 mM acetic acid, 1 mM EDTA) at 150 V for 15 min. A Dark Reader DR22 Blue LED Transilluminator (Clare Chemical Research, Dolores, USA) was used for visualization of DNA. A 1 kb DNA ladder was used as a reference to estimate the size of DNA fragment (New England Biolabs, Ipswich, USA). If needed, different DNA ladder (100bp) would be used as the reference to estimate DNA fragments with small sizes.

5.1.3 Gibson assembly

Gibson assembly was used to clone vectors for recombinant gene expression in *E. coli* or eukaryotic cells. The vector is linearized by PCR for inserting the gene of interest. The insert part is amplified with overlaps (at least 30 bases), which are homologous to the desired integration site on the vector. After purification of DNA constructs, Gibson assembly enzyme mix is used to link vector and insert together. In general, a 1:1 molar ratio of vector and insert

(total 100 ng) at a total volume of 10 μ L are incubated at 50 °C for 60 min. Of note, heat shock transformation in *E. coli* will increase the transfection yield.

5.1.4 T4 SLIC

DNA fragments with overlaps (at least 30 bases) can be assembled by applying T4 SLIC cloning. In this method, the T4 DNA polymerase' exonuclease activity was used to introduce single-stranded 5'end overlaps that are complementary to another DNA fragment. Therefore, the incubation time of T4 SLIC reaction must be under precise control. After transformation into *E. coli*, the bacterial replication machinery allows the repair of gaps and overhangs based on regions of sequence homology, resulting in intact circular DNA plasmids.

5.1.5 Quick change mutagenesis

In some cases, quick change mutagenesis was used as one alternative approach to introduce mutations in genes. Generally, primers were designed according to the Agilent website. However, Q5 polymerase was still used for PCR. Following, PCR product was incubated with home-made DpnI overnight. The PCR product was directly submitted to heat shock transformation in *E. coli*.

5.1.6 Site-directed Q5 mutagenesis

Q5 site directed mutagenesis was performed to introduce mutations in genes. Generally, primers were designed with NEBaseChanger®. After DpnI digestion and gel cleaning, the PCR product was incubated with KLD enzyme mix according to the supplier's recommendation (New England Biolabs, Ipswich, USA). After 60 min incubation at 37 °C the reaction mixture was submitted to heat shock transformation in *E. coli*.

5.1.7 Plasmid purification

10 mL of antibiotic contained LB medium was used for single colony culture and grown for 8-16 h at 37 °C. For plasmid purification the PureYield™ Plasmid Miniprep (Promega, Fitchburg, USA) was used. For getting higher yield, elution buffer can be incubated at 37 °C or 50 °C prior to the elution step.

5.1.8 Sequencing of vectors

10 μ M of sequencing primer were mixed with 500-1000 ng of vector in a total volume of 15 μ L. Samples were analyzed by Microsynth Biotech (Göttingen, Germany) using Sanger sequencing. Data was analysis by snapgene software (GSL Biotech LLC, USA).

5.2 Protein chemical methods

5.2.1 Recombinant protein overexpression

Generally, the *E. coli* BL21 DE3 strain and *E. coli* Rosetta2 (DE3) strain were used for expression of recombinant proteins. Expression strain were transformed with confirmed plasmids and grown on corresponding plate overnight. A pre-culture of 50 mL Lysogeny

broth (LB) medium was cultured with one single colony and grown at 37 °C overnight. After 12-14 hours, the culture was transferred to 1 L LB. Cells were grown to OD₆₀₀ 0.6-0.8 before expression was induced by addition of 1 mM IPTG. Cells grew at 20 °C, 180 rpm for 20 h during expression. Finally, cells were harvested by centrifugation at 8000 rpm for 10 min and washed twice with PBS before pellets were frozen with liquid nitrogen and stored at -20 °C. In some untypical cases, such as the expression of full length DrrA, TB expression and auto-induction can yield a better protein expression¹⁰⁰.

Of note, Rab8a was expressed in BL21(DE3) *E. coli* in LB medium at 18°C overnight, and the expression was induced with 1 mM IPTG at OD_{600nm} = 0.6. In contrast to other proteins, Rab8a was co-expressed with the chaperone GroEL/S (plasmid M202, pGro7 from Takara). The expression of the GroEL/S chaperone was induced by the addition of 1 mg/mL arabinose when OD_{600nm} is 0.4.

5.2.2 Production of *E. coli* cell lysates

E. coli pellets were re-suspended in buffer A and homogenized at low temperature. The Constant Cell Disruption Unit (Constant Systems, Low March, UK), set at 1.8 -2.0 bar and 8°C, was used for production of *E. coli* lysate. 1 mM PMSF was immediately added into the *E. coli* lysate. Subsequently, the *E. coli* lysate was incubated with DNase I (AppliChem, Darmstadt, Germany) at room temperature for 30 min. The cell lysate was cleared by centrifugation (20,000 rpm, 45min, and 4°C). Cell lysate can also be prepared with sonication by following manufacturer's protocols.

5.2.3 Protein purification

Generally, proteins were expressed with a His-tag. Therefore, the first purification step was performed using the Ni-chelating column, Bio-Scale™ Mini Nuvia™ IMAC Cartridges 5 mL (BioRad, Hercules, USA). The clear cell lysate was loaded into the column. The Ni-chelating column was first washed with 5 column volume buffer A. In order to remove the remaining impurities, column was wash extensively by 25 column volume 8 % buffer B (500Mm imidazole contained buffers). Then target protein was eluted with a gradient to 100% Buffer B within 10 CV. Fractions were collected and concentrated after analysis via SDS-PAGE and submitted to buffer exchange and corresponding proteases digestion, respectively. After the cleavage of the tag, and proteins were further purified by size exclusion chromatography (SEC) on a 16/600 Superdex 75 pg column pre-equilibrated with different SEC buffers. If necessary, proteins were concentrated by using Amicon® Ultra Centrifugal Filters (Merck Millipore).

Proteins expressed with Twin Strep tag or MBP tag were purified with Strep-Tactin Magnetic Microbeads (IBA Lifesciences, Gottingen, Germany) and MBP MBPTrap HP columns (GE Healthcare, Munich, Bavaria, Germany) by following the manufacturer's protocols.

5.2.4 Buffer exchange

Imidazole was removed from the target protein via buffer exchange. According to the volumes, buffer exchange for proteins can be performed with HiPrep 26/10 Desalting column or NAP columns (GE Healthcare, Chicago, USA). When the buffers of proteins were exchanged to SEC buffer by applying a HiPrep 26/10 desalting column, the protein solution needs to be concentrated to 10 mL. Proteins need to be concentrated or diluted to suitable volumes for NAP column-mediated buffer exchange. Once buffer exchange was finished, the protein was collected for next steps or frozen in -80°C.

5.2.5 In vitro AMPylation assay

AMPylation of Rab1b or Rab8a was performed in AMPylation buffer (50 mM HEPES-NaOH pH 7.5, 100 mM NaCl, 1 mM TCEP, 1 mM MgCl₂) and in the presence of 2 mM ATP. After incubation for 15 mins, wild type DrrA was added. In general, substrates were set in at 50-fold excess to the DrrA, at final concentrations of 50 μM substrate and 1 μM DrrA. Samples were incubated at 25 °C for 2 h. AMPylation of Rab8a was performed at 20°C. In some cases, 5% glycerol was added to stabilize Rab8a. Confirmation of AMPylation was done by mass spectra measurement.

5.2.6 Modification of Rab proteins with TReND-1

Buffer exchange is necessary to remove all the components, which can react with TReND-1. Following, 5 μM DrrA, 100 μM Rab1b/Rab8a, and 500 μM TReND-1 were incubated in AMPylation buffer. Samples were incubated at 25°C for 2 h. For modification of Rab8a, an additional 5% (v/v) glycerol was added for stabilizing Rab8a.

5.2.7 Formation of DrrA_{cys}-TReND-1 binary complex

DrrA_{cys} constructs were kept in 20 mM HEPES-NaOH pH 8, 100 mM NaCl, 1 mM TCEP. If not, buffer exchange was performed. Following, 50 μM DrrA, 1 mM TReND-1 was incubated at 25°C for overnight. Samples were subjected to mass spectrometry for detecting the formation of binary complex. Fic enzyme IbpA₃₄₈₃₋₃₇₉₇ I3455C was used as the positive control. Wild type DrrA was used as the negative control. Confirmation of binary complex formation was done by mass spectrometry.

5.2.8 ATPase assay

In General, ATPase assays were performed in 1X ATPase buffer (20 mM Hepes-NaOH pH 8, 100 mM NaCl, 1 mM MgCl₂, 1 mM TCEP). Unless otherwise stated, ATP was set at final concentrations of 50 μM ATP and 5 μM enzyme. Samples were incubated at 25 °C for overnight analyzed by reverse phase chromatography (50 mM KPi (K₂HPO₄ and KH₂PO₄) buffer pH 6.6, 12%-17% ACN, and 10 mM Tetrabutylammonium bromide).

5.2.9 Cleavage of tag by TEV and PreScission protease

TEV protease was used for removing the tags of most proteins in this study. Notably, the presence of Mg ion inhibits the activity of TEV. Therefore, buffer exchange was performed for the proteins, which contained Mg ion in the purification buffer. The ration between proteins of interest and TEV can be adjusted from 1: 40 to 1: 20.

Wild type PreScission was used for purification of the DrrA₁₆₋₃₅₂A176C:TReND-1:Rab1b/Rab8a complexes. When complexes formation was finished, DrrA₁₆₋₃₅₂A176C:TReND-1:Rab1b/Rab8a can be purified by using Ni-chelating column, since there was a 6- His tag in Rab proteins. After that, home-made PreScission protease was added according to 1: 1 ratio. Last, complexes can be further purified by gel-filtration.

5.2.10 Nucleotide exchange for Rab1b and Rab8a

Nucleotide exchange for Rab1b and Rab8a was performed by following previous protocols. Briefly, 5 mM EDTA was added to Rab1b/8a (20 mM HEPES-NaOH pH 8, 100 mM NaCl, 1 mM TCEP, 1 mM MgCl₂, 1 μM GDP). A 20-fold excess of GppNHp was then added and incubated at 4°C overnight. For Rab8a nucleotide exchange assays, an additional 5% (v/v) glycerol was also added for stabilization, and the buffer was exchanged using NAP columns (GE Healthcare, Munich, Bavaria, Germany). Nucleotide binding to Rab was confirmed by HPLC with a C18 reversed-phase liquid chromatography column. If the efficiency of nucleotide exchange for Rab1b is low, another alternative method can be applied: 10-fold excess of excess of GppNHp and a His-tag contained DrrA₃₄₀₋₅₃₃ protein were added and incubated in room temperature for 2 hours. Following, another 10-fold excess of excess of GppNHp was added and samples were incubated at 4°C overnight. Nucleotide exchange efficiency can be confirmed by HPLC with a C18 reversed-phase liquid chromatography column. If required, the His- tag contained DrrA₃₄₀₋₅₃₃ protein can be removed by Ni-chelating column.

5.2.11 Preparative production of the DrrA:TReND-1:Rab complexes

A 200 μM sample of DrrA₁₆₋₃₅₂-L197C, 500 μM TReND-1, and 400 μM Rab1b or Rab8a (GppNHp) were incubated overnight at 25°C or 20°C. Once the ternary complexes were formed and confirmed by SDS-PAGE, size-exclusion chromatography was performed using a Superdex 26/600 75pg column (GE Healthcare) to further purify DrrA₁₆₋₃₅₂-L197C:TReND-1: Rab complexes. In order to obtain pure complexes for subsequent experiments (e.g. crystallization screening), a second run of size-exclusion chromatography was conducted. For preparing the DrrA₁₆₋₃₅₂-A176C:TReND-1:Rab complexes, a 200 μM sample of DrrA₁₆₋₃₅₂-A176C, 1 mM TReND-1, and 800 μM His₁₀-PreScission-Rab1b (GppNHp) or His₆-PreScission-Rab8a (GppNHp) were incubated overnight at 25°C or 20°C. Following, this complex was purified using Ni-NTA resin. Subsequently, PreScission protease was added to

cleave the His tag in Rab1b, and then the complex was further purified by size exclusion chromatography on a 16/600 Superdex 75 pg column (GE Healthcare).

5.2.12 Lysine methylation of DrrA₁₆₋₃₅₂ and DrrA_{A176C}-Rab1b/8a complex

DrrA_{A176C}-Rab1b/8a Complexes were prepared in the first step. Following, the lysine methylation reaction was performed in SEC-buffer (20 mM HEPES-NaOH pH 8, 100 mM NaCl, 1 mM TCEP, 1 mM MgCl₂, 1 μM GppNHp) with the DrrA_{A176C}-Rab1b/8a complexes (1 mg/mL). In general, 20 μL freshly prepared 1 M dimethylamine-borane complex in reaction buffer (ABC; Sigma Aldrich) and 40 μl 1 M methanol-free formaldehyde (made from 16% stock in reaction buffer; Sigma) were added for per milliliter protein solution, and the reaction was kept on ice and gently rotated for 2 h-3h. Following, these steps are repeated for the second time. After 2 hours, a final addition of ABC and formaldehyde, then the reaction was rotated overnight at 4 °C. Precipitations were removed by centrifugation and filtration, the supernatant was applied to a gel filtration (16/600 Superdex 75 pg column, GE Healthcare) pre-equilibrated with SEC-buffer. Fractions containing the complexes were concentrated to a total of 10- 11 mg/mL and immediately aliquoted and frozen for future protein crystallization

83, 101 .

Lysine methylation of DrrA₁₆₋₃₅₂ was similar to the lysine methylation of DrrA_{A176C}-Rab1b/8a Complexes. However, DrrA₁₆₋₃₅₂ was diluted to 0.5 mg/ml for further steps. Otherwise, the yield of methylated DrrA was low in some cases.

5.3 Analytical methods

5.3.1 SDS-PAGE

Protein samples were heated at 95 °C for 5 min after addition of 2x Laemmli buffer. After 2 min full speed spin, proteins samples were loaded and separated in 4-20% acrylamide gels using the Mini Protean™ Tetra System (BioRad, München, Germany) or home-made 12% acrylamide gels. Samples were run in SDS-Buffer at 50 mA per gel in 5 min. Then the parameters are set as 60mA and 1 hour. The Color pre-stained protein standard (New England Biolabs, Ipswich, USA) was used as a reference. Protein bands were visualized via Coomassie stain.

5.3.2 Coomassie staining of SDS gels

SDS-PAGE Gels were stained by cooking in Coomassie staining solution. In order to destain the gels, gels were cooking in 10% acetic acid and shaking at room temperature overnight.

5.3.3 High resolution mass spectrometry (HRMS)

The DrrA:TReND:Rab complexes was measured using high-resolution mass spectra recorded on an Agilent 6230 Series TOF MS instrument coupled to an Agilent 1290 Infinity II LC system equipped with an Agilent Poroshell C8 column (2.1 mm × 75 mm, particle size 5 µm). The flow rate was 600 µL/min, buffer A consisted of milliQ H₂O + 0.1% formic acid, and buffer B was composed of acetonitrile + 0.1% formic acid. The electrospray ionization method was employed. Samples (1 µL; 0.1 to 0.5 mg/mL) and corresponding buffer stock solutions were injected, and time-based (0–1 min to waste) online desalting was performed.

5.3.4 Temperature-scanning Circular Dichroism (CD) measurements

CD signals were recorded on a Chirascan CD Spectrometer (Applied Photophysics, Leatherhead, Surrey, UK) in a 1 mm cuvette with a bandwidth of 0.5 nm and a response of 0.5 s. Temperature scanning CD measurements were taken at 222 nm at a heating rate of 1 K/min. Data were analyzed using Origin (Origin software Inc, Northampton, MA 01060, USA) and evaluated by the Boltzmann equation to obtain melting temperatures.

5.3.5 Determination of catalytic efficiencies for Rab1b and Rab8a

To determine the AMPylation rates of different DrrA constructs, time-resolved tryptophan fluorescence was applied. In general, 200 µM GTP and 100 mM DrrA_{GEF} were added for the nucleotide exchange of Rab1b (5 µM) from GDP to GTP, and AMPylation was initiated by addition of different DrrA constructs (100 nM). Data evaluation was performed as previously described³⁰.

Rab8a is one of the *in vitro* AMPylation targets of DrrA. However, Rab8a is not the target of DrrA GEF domain. Therefore, the nucleotide of Rab8a needs to be exchanged to GppNHp prior to the time-resolved tryptophan fluorescence assay. In general, 5 µM Rab8a:GppNHp

was added to the cuvette, then 1 mM ATP was added. Once the tryptophan signal is stable, 100 nM DrrA constructs were added to start the AMPylation. Data evaluation was the same as before^{13, 30}. In brief, for the determination of catalytic efficiencies (k_{cat}/K_M) of AMPylation reactions measured by fluorescence spectrometry, reaction curves were fitted to a single exponential curve according to using the following equation:

$$F(t) = F_0 + F_A \cdot e^{-k_{obs} \cdot t}$$

Where $F(t)$ is the fluorescence intensity, F_0 is the minimum fluorescence intensity, F_A is the total fluorescence amplitude (i.e., $F_{max} - F_0$, with F_{max} as the maximum fluorescence intensity), and k_{obs} is the observed rate constant. The observed rate constant (k_{obs}) was divided by the applied DrrA concentration (100 nM), yielding k_{cat}/K_M (Supplementary Figure 5).

5.3.6 Enzyme kinetics of DrrA based on time-resolved tryptophan fluorescence

The kinetics of Rab1b: GppNHp AMPylation by DrrA was monitored via the change in intrinsic Rab1b tryptophan fluorescence using an F-2710 fluorescence spectrophotometer (Hitachi, Schaumburg, Illinois, USA) (excitation wavelength of 297 nm, emission wavelength of 370 nm, excitation slit width of 2.5 nm, an emission slit width of 5 nm). The Rab1b concentration was <64 μ M. However, for Rab1b: GppNHp concentration >64 μ M, the emission wavelength was shifted to 390 nm, while keeping other parameters constant. All measurements were conducted in the presence of 100 mM DrrA and 1 unit of pyrophosphate (New England Biolabs) at 25°C with GppNHp in buffer (20 mM HEPES, 100 mM NaCl, 1 mM MgCl₂, 1 μ M GppNHp, 1 mM TCEP, pH 7.5). Data evaluation was performed as previously described³⁰ (Supplementary Figure 5).

5.3.7 Analytical formation of DrrA:TReND-1:Rab complexes

To form the DrrA₁₆₋₃₅₂-L197C:TReND-1:Rab1b ternary complex, 50 μ M cysteine-modified DrrA mutants were incubated with 200 μ M TReND-1, 200 μ M Rab1b:GppNHp (20 mM HEPES-NaOH pH 8, 100 mM NaCl, 1 mM TCEP, 1 mM MgCl₂, 1 μ M GppNHp) overnight at 25°C. Similar to the formation of the DrrA₁₆₋₃₅₂-L197C:TReND-1:Rab1b ternary complex, an additional 5% (v/v) glycerol was added to stabilize Rab8a:GppNHp for the formation of the DrrA₁₆₋₃₅₂-L197C:TReND-1:Rab8a ternary complex. *In vitro* ternary complex reaction was confirmed by SDS-PAGE and MS.

To the formation of DrrA₁₆₋₃₅₂-A176C:TReND-1:Rab1b/ Rab8a ternary complexes, 250 μ M Rab proteins in GppNHp state were modified by 10 μ M wild type DrrA and 500 μ M TReND-1. Following, excess TReND-1 was removed by buffer exchange. Then 200 μ M cysteine-modified DrrA mutants were incubated with 800 μ M TReND-1 modified Rab1b/ Rab8a (20 mM HEPES-NaOH pH 8, 100 mM NaCl, 1 mM TCEP, 1 mM MgCl₂, 1 μ M GppNHp)

overnight at 25°C, 20°C respectively. Of note, an additional 5% (v/v) glycerol was added to stabilize Rab8a: GppNHp.

5.3.8 Analytical size exclusion chromatography

The Prominence HPLC system (Shimadzu, Kyōto, Japan) was applied for Analytical size exclusion. The Superdex 10/300 75 pg column (GE Healthcare, Chicago, USA) was used. Protein samples were run with the corresponding SEC buffers (20 mM HEPES-NaOH pH 8, 100 mM NaCl, 1 mM TCEP, 1 mM MgCl₂, 1 μM GppNHp or GDP) at a flow rate of 0.5 mL/min. The Gel filtration standard (BioRad, Hercules, USA) was taken as a reference to determine the sizes of proteins of interest.

5.3.9 ATP docking in DrrA₁₆₋₃₅₂

The structure of DrrA₁₆₋₃₅₂ is from the structure of DrrA: Rab8a complex. Details about ATP docking in DrrA₁₆₋₃₅₂ can be seen in reference 85⁸⁶. In briefly, structure of DrrA₁₆₋₃₅₂ from the current complex was first generated as a PDB file. Water molecules were removed and non-polar hydrogen molecules were added to the protein structure in Python molecule viewer setting of PyMOL, which obtained the active site of the protein with a size of 25 × 25 × 25 at 1Å grid spacing. Ligand ATP was obtained from PubChem on the NCBI database. ATP was converted to pdbqt format in Open Babel (<https://openbabel.org/>) GUI 2.3.2a setting. Protein-ligand docking was performed in AutoDock Vina, which predicts interactions between ATP and DrrA.

5.4 Cell biology methods

5.4.1 Cultivation of H1299 cells

H1299 cells (ATCC® CRL-5803™) between 5 passages and 25 passages are cultured according the protocol in ATCC^{102, 103}. In general, H1299 cells are cultured in 10% fetal bovine serum (FBS) supplemented Dulbecco's modified Eagle's medium (DMEM) and 1mM Sodium pyruvate. Every 72 hours, cells are sub-cultured according to the protocol in ATCC. And cells are cultured with 5% carbon dioxide (CO₂) at 37 °C.

5.4.2 Transient transfection of H1299 cells

Five passages after thawing, H1299 cells between 5 passages and 25 passages are good for transient transfection. 24 hours prior to the transfection, 2 million cells are seeded into one 10cm dish. Once the confluence of the cells becomes 80%-90%, cells are ready for transient transfection. Of note, the confluence of the cells is not determined by microscopy inspection. Proliferation curve was predetermined by co-workers from Sabine Windhorst lab. Lipofectamine LTX was used for transient transfection of H1299 cells with eGFP, wild type DrrA, and various other constructs. Four hours to 6 hours after transfection, the culture medium was replaced with 10% fetal bovine serum (FBS) supplemented Dulbecco's modified

Eagle's medium (DMEM). In addition, 1 mM sodium pyruvate was added to decrease the oxidative stress caused by GFP overexpression.

5.4.3 Collection of GFP-positive cells by FACS

In general, the expression of different DrrA constructs starts at 6 hours after adding the DNA: LTX complex. And the expression level is high at 17 hours after transfection (Supplementary Figure 7). Notably, the H1299 cells transfected with wild type DrrA construct starts to be dead by necrosis or pyroptosis. Therefore, in order to get enough living cells for further assays, cells were ready for sorting at 20-21 hours after transfection.

Prior to the sorting in the FACS facility of UKE (using a FACS Aria Fusion, see Figure 21 and Supplementary Figure 6 for gating strategy), cells were prepared as the following: First, DMEN medium was removed and H1299 cells were washed by DPBS (Gibco Biotech) and trypsinized by using trypsin/EDTA (Gibco Biotech). Notably, H1299 cells are difficult to be detached from the wall of dishes. Longer incubation with trypsin in the incubator is allowed. After centrifugation (10 min at 300 g and 4°C) cells were washed two times in DPBS and cells were kept with DPBS supplemented with 3% FBS on ice prior to sorting by FACS. A total of 40000 GFP- positive cells were collected in cool DMEN medium (20% FBS supplemented) for per sample, and FACSDiva™ software (BD Biosciences) was used for data analysis. After sorting, to confirm there is no contamination in the sorted GFP-positive population, microscopy inspection was performed (Supplementary Figure 8).

5.4.4 Cytotoxicity analysis of DrrA-mutants by MTS assay

Next, 24,000 cells with a 300 µL DMEN medium (10%- 20% FBS supplemented) were seeded into three wells of a 96-well plate. After 24 h, MTS assays were conducted for cytotoxicity analysis. 20 µL MTS agent was added to each well. 20 µL MTS was added into 100 µL DMEN medium, which was set as background. After 2 to 4 hours incubation, cell viability was estimated by measuring the OD value at 490nm. Further, cytotoxicity of DrrA-mutants was determined by calculating the ratio of the indicated sample relative to the eGFP vector control. MTS (3-(4,5-dimethylthiazol-2-yl)-2,5-diphenyltetrazolium bromide) data was recorded with TECAN Spark (SparkControl™).

5.4.5 Fixation and imaging of H1299 cells

After seeding the cells for the MTS assay, the rest cells were seeded into a 8- well chamber slide. After 24 hours, the culture medium was removed and cells were washed by DPBS. Then 200 µL 4% paraformaldehyde DPBS solution was added to each well. In general, cells need to be incubated at 37 °C for 10 min. Later, cells were washed by DPBS solution and ready for DAPI staining. DAPI staining was followed the standard DAPI staining protocol¹⁰⁴. Imaging was performed with Keyence BZ-9000 (KEYENCE, Japan).

Reference

1. Kingdon HS, Shapiro BM, Stadtman ER. Regulation of glutamine synthetase. 8. ATP: glutamine synthetase adenylyltransferase, an enzyme that catalyzes alterations in the regulatory properties of glutamine synthetase. *Proc. Natl. Acad. Sci. USA* **58**, 1703-1710 (1967).
2. Xu Y, Carr PD, Vasudevan SG, Ollis DL. Structure of the adenylylation domain of *E. coli* glutamine synthetase adenylyl transferase: evidence for gene duplication and evolution of a new active site. *J. Mol. Biol.* **396**, 773-784 (2010).
3. Stadtman ER. The story of glutamine synthetase regulation. *J. Biol. Chem.* **276**, 44357-44364 (2001).
4. Itzen A, Blankenfeldt W, Goody RS. Adenylylation: renaissance of a forgotten post-translational modification. *Trends Biochem. Sci.* **36**, 221-228 (2011).
5. Kawamukai M, *et al.* Cloning of the *fic-1* gene involved in cell filamentation induced by cyclic AMP and construction of a delta *fic* *Escherichia coli* strain. *J. Bacteriol.* **170**, 3864-3869 (1988).
6. Kawamukai M, Matsuda H, Fujii W, Utsumi R, Komano T. Nucleotide sequences of *fic* and *fic-1* genes involved in cell filamentation induced by cyclic AMP in *Escherichia coli*. *J. Bacteriol.* **171**, 4525-4529 (1989).
7. Komano T, Utsumi R, Kawamukai M. Functional analysis of the *fic* gene involved in regulation of cell division. *Res. Microbiol.* **142**, 269-277 (1991).
8. Roy CR, Cherfils J. Structure and function of Fic proteins. *Nat. Rev. Microbiol.* **13**, 631-640 (2015).

9. Harms A, Stanger FV, Dehio C. Biological Diversity and Molecular Plasticity of FIC Domain Proteins. *Annu. Rev. Microbiol.* **70**, 341-360 (2016).
10. Bhattacharjee RN, *et al.* VP1686, a Vibrio type III secretion protein, induces toll-like receptor-independent apoptosis in macrophage through NF-kappaB inhibition. *J. Biol. Chem.* **281**, 36897-36904 (2006).
11. Yarbrough ML, Li Y, Kinch LN, Grishin NV, Ball HL, Orth K. AMPylation of Rho GTPases by Vibrio VopS disrupts effector binding and downstream signaling. *Science* **323**, 269-272 (2009).
12. Xu H, *et al.* Innate immune sensing of bacterial modifications of Rho GTPases by the Pysin inflammasome. *Nature* **513**, 237-241 (2014).
13. Muller MP, Peters H, Blumer J, Blankenfeldt W, Goody RS, Itzen A. The Legionella effector protein DrrA AMPylates the membrane traffic regulator Rab1b. *Science* **329**, 946-949 (2010).
14. Tan Y, Luo ZQ. Legionella pneumophila SidD is a deAMPyase that modifies Rab1. *Nature* **475**, 506-509 (2011).
15. Neunuebel MR, Chen Y, Gaspar AH, Backlund PS, Jr., Yergey A, Machner MP. De-AMPylation of the small GTPase Rab1 by the pathogen Legionella pneumophila. *Science* **333**, 453-456 (2011).
16. Chen Y, *et al.* Structural basis for Rab1 de-AMPylation by the Legionella pneumophila effector SidD. *PLOS Pathog.* **9**, e1003382 (2013).

17. Harms A, *et al.* Adenylation of Gyrase and Topo IV by FicT Toxins Disrupts Bacterial DNA Topology. *Cell Rep.* **12**, 1497-1507 (2015).
18. Preissler S, Rato C, Perera L, Saudek V, Ron D. FICD acts bifunctionally to AMPylate and de-AMPylate the endoplasmic reticulum chaperone BiP. *Nat. Struct. Mol. Biol.* **24**, 23-29 (2017).
19. Perera LA, *et al.* An oligomeric state-dependent switch in the ER enzyme FICD regulates AMPylation and deAMPylation of BiP. *EMBO J.* **38**, e102177 (2019).
20. Preissler S, *et al.* AMPylation matches BiP activity to client protein load in the endoplasmic reticulum. *eLife* **4**, e12621 (2015).
21. Rahman M, Ham H, Liu X, Sugiura Y, Orth K, Kramer H. Visual neurotransmission in *Drosophila* requires expression of Fic in glial capitate projections. *Nat. Neurosci.* **15**, 871-875 (2012).
22. Sreelatha A, *et al.* Protein AMPylation by an Evolutionarily Conserved Pseudokinase. *Cell* **175**, 809-821 e19 (2018).
23. Mukherjee S, Liu X, Arasaki K, McDonough J, Galan JE, Roy CR. Modulation of Rab GTPase function by a protein phosphocholine transferase. *Nature* **477**, 103-106 (2011).
24. Campanacci V, Mukherjee S, Roy CR, Cherfils J. Structure of the Legionella effector AnkX reveals the mechanism of phosphocholine transfer by the FIC domain. *EMBO J.* **32**, 1469-1477 (2013).

25. Ernst S, *et al.* Legionella effector AnkX displaces the switch II region for Rab1b phosphocholination. *Sci. Adv.* **6**, eaaz8041 (2020).
26. Garcia-Pino A, Zenkin N, Loris R. The many faces of Fic: structural and functional aspects of Fic enzymes. *Trends Biochem. Sci.* **39**, 121-129 (2014).
27. Castro-Roa D, Garcia-Pino A, De Gieter S, van Nuland NAJ, Loris R, Zenkin N. The Fic protein Doc uses an inverted substrate to phosphorylate and inactivate EF-Tu. *Nat. Chem. Biol.* **9**, 811-817 (2013).
28. Cruz JW, Rothenbacher FP, Maehigashi T, Lane WS, Dunham CM, Woychik NA. Doc Toxin Is a Kinase That Inactivates Elongation Factor Tu. *J. Biol. Chem.* **289**, 7788-7798 (2014).
29. Xiao JY, Worby CA, Mattoo S, Sankaran B, Dixon JE. Structural basis of Fic-mediated adenylylation. *Nat. Struct. Mol. Biol.* **17**, 1004-1010 (2010).
30. Muller MP, *et al.* Characterization of Enzymes from Legionella pneumophila Involved in Reversible Adenylylation of Rab1 Protein. *J. Biol. Chem.* **287**, 35036-35046 (2012).
31. Morar M, Bhullar K, Hughes DW, Junop M, Wright GD. Structure and Mechanism of the Lincosamide Antibiotic Adenylyltransferase LinB. *Structure* **17**, 1649-1659 (2009).
32. Pedersen LC, Benning MM, Holden HM. Structural Investigation of the Antibiotic and Atp-Binding Sites in Kanamycin Nucleotidyltransferase. *Biochemistry* **34**, 13305-13311 (1995).

33. Gavriljuk K, Schartner J, Itzen A, Goody RS, Gerwert K, Kottling C. Reaction Mechanism of Adenylyltransferase DrrA from *Legionella pneumophila* Elucidated by Time-Resolved Fourier Transform Infrared Spectroscopy. *J. Am. Chem. Soc.* **136**, 9338-9345 (2014).
34. Stern AL, Van der Verren SE, Kanchugal PS, Nasvall J, Gutierrez-de-Teran H, Selmer M. Structural mechanism of AadA, a dual-specificity aminoglycoside adenylyltransferase from *Salmonella enterica*. *J. Biol. Chem.* **293**, 11481-11490 (2018).
35. Garcia-Pino A, *et al.* Doc of Prophage P1 Is Inhibited by Its Antitoxin Partner Phd through Fold Complementation. *J. Biol. Chem.* **283**, 30821-30827 (2008).
36. Engel P, *et al.* Adenylylation control by intra- or intermolecular active-site obstruction in Fic proteins. *Nature* **482**, 107-110 (2012).
37. Stanger FV, *et al.* Intrinsic regulation of FIC-domain AMP-transferases by oligomerization and automodification. *Proc. Natl. Acad. Sci. USA* **113**, E529-E537 (2016).
38. Goody RS, *et al.* The versatile *Legionella* effector protein DrrA. *Commun Integr Biol* **4**, 72-74 (2011).
39. Murata T, Delprato A, Ingmundson A, Toomre DK, Lambright DG, Roy CR. The *Legionella pneumophila* effector protein DrrA is a Rab1 guanine nucleotide-exchange factor. *Nat. Cell Biol.* **8**, 971-977 (2006).
40. Ingmundson A, Delprato A, Lambright DG, Roy CR. *Legionella pneumophila* proteins that regulate Rab1 membrane cycling. *Nature* **450**, 365-369 (2007).

41. Del Campo CM, Mishra AK, Wang YH, Roy CR, Janmey PA, Lambright DG. Structural basis for PI(4)P-specific membrane recruitment of the Legionella pneumophila effector DrrA/SidM. *Structure* **22**, 397-408 (2014).
42. Schoebel S, Blankenfeldt W, Goody RS, Itzen A. High-affinity binding of phosphatidylinositol 4-phosphate by Legionella pneumophila DrrA. *EMBO Rep.* **11**, 598-604 (2010).
43. Mishra AK, Del Campo CM, Collins RE, Roy CR, Lambright DG. The Legionella pneumophila GTPase activating protein LepB accelerates Rab1 deactivation by a non-canonical hydrolytic mechanism. *J. Biol. Chem.* **288**, 24000-24011 (2013).
44. Schoebel S, Cichy AL, Goody RS, Itzen A. Protein LidA from Legionella is a Rab GTPase supereffector. *Proc. Natl. Acad. Sci. USA* **108**, 17945-17950 (2011).
45. Isberg RR, O'Connor TJ, Heidtman M. The Legionella pneumophila replication vacuole: making a cosy niche inside host cells. *Nat. Rev. Microbiol.* **7**, 13-24 (2009).
46. Hsu F, Zhu W, Brennan L, Tao L, Luo ZQ, Mao Y. Structural basis for substrate recognition by a unique Legionella phosphoinositide phosphatase. *Proc. Natl. Acad. Sci. USA* **109**, 13567-13572 (2012).
47. Ivanov SS, Roy C. Host lipidation: a mechanism for spatial regulation of Legionella effectors. *Curr. Top. Microbiol. Immunol.* **376**, 135-154 (2013).
48. Tan Y, Arnold RJ, Luo ZQ. Legionella pneumophila regulates the small GTPase Rab1 activity by reversible phosphorylation. *Proc. Natl. Acad. Sci. USA* **108**, 21212-21217 (2011).

49. Goody PR, Heller K, Oesterlin LK, Muller MP, Itzen A, Goody RS. Reversible phosphocholination of Rab proteins by Legionella pneumophila effector proteins. *EMBO J.* **31**, 1774-1784 (2012).
50. Qiu J, *et al.* Ubiquitination independent of E1 and E2 enzymes by bacterial effectors. *Nature* **533**, 120-124 (2016).
51. Bhogaraju S, *et al.* Phosphoribosylation of Ubiquitin Promotes Serine Ubiquitination and Impairs Conventional Ubiquitination. *Cell* **167**, 1636-1649 e13 (2016).
52. Wan M, *et al.* Deubiquitination of phosphoribosyl-ubiquitin conjugates by phosphodiesterase-domain-containing Legionella effectors. *Proc. Natl. Acad. Sci. USA* **116**, 23518-23526 (2019).
53. Kubori T, Shinzawa N, Kanuka H, Nagai H. Legionella metaeffector exploits host proteasome to temporally regulate cognate effector. *PLOS Pathog.* **6**, e1001216 (2010).
54. Bhogaraju S, *et al.* Inhibition of bacterial ubiquitin ligases by SidJ-calmodulin catalysed glutamylation. *Nature* **572**, 382-386 (2019).
55. Gan N, *et al.* Regulation of phosphoribosyl ubiquitination by a calmodulin-dependent glutamylase. *Nature* **572**, 387-391 (2019).
56. Lucas M, *et al.* Structural basis for the recruitment and activation of the Legionella phospholipase VipD by the host GTPase Rab5. *Proc. Natl. Acad. Sci. USA* **111**, E3514-E3523 (2014).

57. Dorer MS, Kirton D, Bader JS, Isberg RR. RNA interference analysis of Legionella in Drosophila cells: exploitation of early secretory apparatus dynamics. *PLoS Pathog.* **2**, e34 (2006).
58. Zhu Y, Hu L, Zhou Y, Yao Q, Liu L, Shao F. Structural mechanism of host Rab1 activation by the bifunctional Legionella type IV effector SidM/DrrA. *Proc. Natl. Acad. Sci. USA* **107**, 4699-4704 (2010).
59. Schoebel S, Oesterlin LK, Blankenfeldt W, Goody RS, Itzen A. RabGDI displacement by DrrA from Legionella is a consequence of its guanine nucleotide exchange activity. *Mol. Cell* **36**, 1060-1072 (2009).
60. Du. J, *et al.* Rab1-AMPylation by Legionella DrrA is allosterically activated by Rab1. *Nat. Commun.*, in revision (2020).
61. Matozaki T, Nakanishi H, Takai Y. Small G-protein networks: their crosstalk and signal cascades. *Cell. Signal.* **12**, 515-524 (2000).
62. Itzen A, Goody RS. GTPases involved in vesicular trafficking: structures and mechanisms. *Semin. Cell Dev. Biol.* **22**, 48-56 (2011).
63. Eathiraj S, Pan XJ, Ritacco C, Lambright DG. Structural basis of family-wide Rab GTPase recognition by rabenosyn-5. *Nature* **436**, 415-419 (2005).
64. Touchot N, Chardin P, Tavitian A. Four additional members of the ras gene superfamily isolated by an oligonucleotide strategy: molecular cloning of YPT-related cDNAs from a rat brain library. *Proc. Natl. Acad. Sci. USA* **84**, 8210-8214 (1987).

65. Vielh E, Touchot N, Zahraoui A, Tavitian A. Nucleotide sequence of a rat cDNA: rab1B, encoding a rab1-YPT related protein. *Nucleic Acids Res.* **17**, 1770 (1989).
66. Cherfils J, Zeghouf M. Regulation of small GTPases by GEFs, GAPs, and GDIs. *Physiol. Rev.* **93**, 269-309 (2013).
67. Levin RS, Hertz NT, Burlingame AL, Shokat KM, Mukherjee S. Innate immunity kinase TAK1 phosphorylates Rab1 on a hotspot for posttranslational modifications by host and pathogen. *Proc. Natl. Acad. Sci. USA* **113**, E4776-E4783 (2016).
68. Lee MC, Miller EA, Goldberg J, Orci L, Schekman R. Bi-directional protein transport between the ER and Golgi. *Annu. Rev. Cell Dev. Biol.* **20**, 87-123 (2004).
69. Yang XZ, *et al.* Rab1 in cell signaling, cancer and other diseases. *Oncogene* **35**, 5699-5704 (2016).
70. Hao YH, *et al.* Characterization of a rabbit polyclonal antibody against threonine-AMPylation. *J. Biotechnol.* **151**, 251-254 (2011).
71. Yu X, *et al.* Copper-catalyzed azide-alkyne cycloaddition (click chemistry)-based detection of global pathogen-host AMPylation on self-assembled human protein microarrays. *Mol. Cell Proteomics* **13**, 3164-3176 (2014).
72. Lewallen DM, Steckler CJ, Knuckley B, Chalmers MJ, Thompson PR. Probing adenylation: using a fluorescently labelled ATP probe to directly label and immunoprecipitate VopS substrates. *Mol Biosyst* **8**, 1701-1706 (2012).

73. Grammel M, Luong P, Orth K, Hang HC. A chemical reporter for protein AMPylation. *J. Am. Chem. Soc.* **133**, 17103-17105 (2011).
74. Hu CW, *et al.* Electrophilic probes for deciphering substrate recognition by O-GlcNAc transferase. *Nat. Chem. Biol.* **13**, 1267-1273 (2017).
75. Gulen B, *et al.* Identification of targets of AMPylating Fic enzymes by co-substrate-mediated covalent capture. *Nat. Chem.* **12**, 732-739 (2020).
76. Cigler M, *et al.* Proximity-Triggered Covalent Stabilization of Low-Affinity Protein Complexes In Vitro and In Vivo. *Angew. Chem. Int. Ed.* **56**, 15737-15741 (2017).
77. England CG, Luo H, Cai W. HaloTag technology: a versatile platform for biomedical applications. *Bioconj. Chem.* **26**, 975-86 (2015).
78. S NP, Kwon K. The HaloTag: Improving Soluble Expression and Applications in Protein Functional Analysis. *Curr. Chem. Genom.* **6**, 8-17 (2012).
79. Chalfie M, Tu Y, Euskirchen G, Ward WW, Prasher DC. Green Fluorescent Protein as a Marker for Gene-Expression. *Science* **263**, 802-805 (1994).
80. Soundrarajan N, *et al.* Green fluorescent protein as a scaffold for high efficiency production of functional bacteriotoxic proteins in Escherichia coli. *Sci. Rep.* **6**, (2016).
81. Chavas LMG, *et al.* Structure of the small GTPase Rab27b shows an unexpected swapped dimer. *Acta Crystallogr. D Biol. Crystallogr.* **63**, 769-779 (2007).

82. Wittmann JG, Rudolph MG. Crystal structure of Rab9 complexed to GDP reveals a dimer with an active conformation of switch II. *FEBS Lett.* **568**, 23-29 (2004).
83. Walter TS, *et al.* Lysine methylation as a routine rescue strategy for protein crystallization. *Structure* **14**, 1617-1622 (2006).
84. Guo Z, Hou X, Goody RS, Itzen A. Intermediates in the Guanine Nucleotide Exchange Reaction of Rab8 Catalyzed by Rabin8/GRAB. *J. Biol. Chem.* **288**, 32466-32474 (2013).
85. Krissinel E, Henrick K. Inference of macromolecular assemblies from crystalline state. *J. Mol. Biol.* **372**, 774-797 (2007).
86. Forli S, Huey R, Pique ME, Sanner MF, Goodsell DS, Olson AJ. Computational protein-ligand docking and virtual drug screening with the AutoDock suite. *Nat. Protoc.* **11**, 905-919 (2016).
87. Black MH, *et al.* Bacterial pseudokinase catalyzes protein polyglutamylation to inhibit the SidE-family ubiquitin ligases. *Science* **364**, 787-792 (2019).
88. Sulpizio A, *et al.* Protein polyglutamylation catalyzed by the bacterial calmodulin-dependent pseudokinase SidJ. *eLife* **8**, e51162 (2019).
89. Liu YC, Luo ZQ. The Legionella pneumophila effector SidJ is required for efficient recruitment of endoplasmic reticulum proteins to the bacterial phagosome. *Infect. Immun.* **75**, 592-603 (2007).

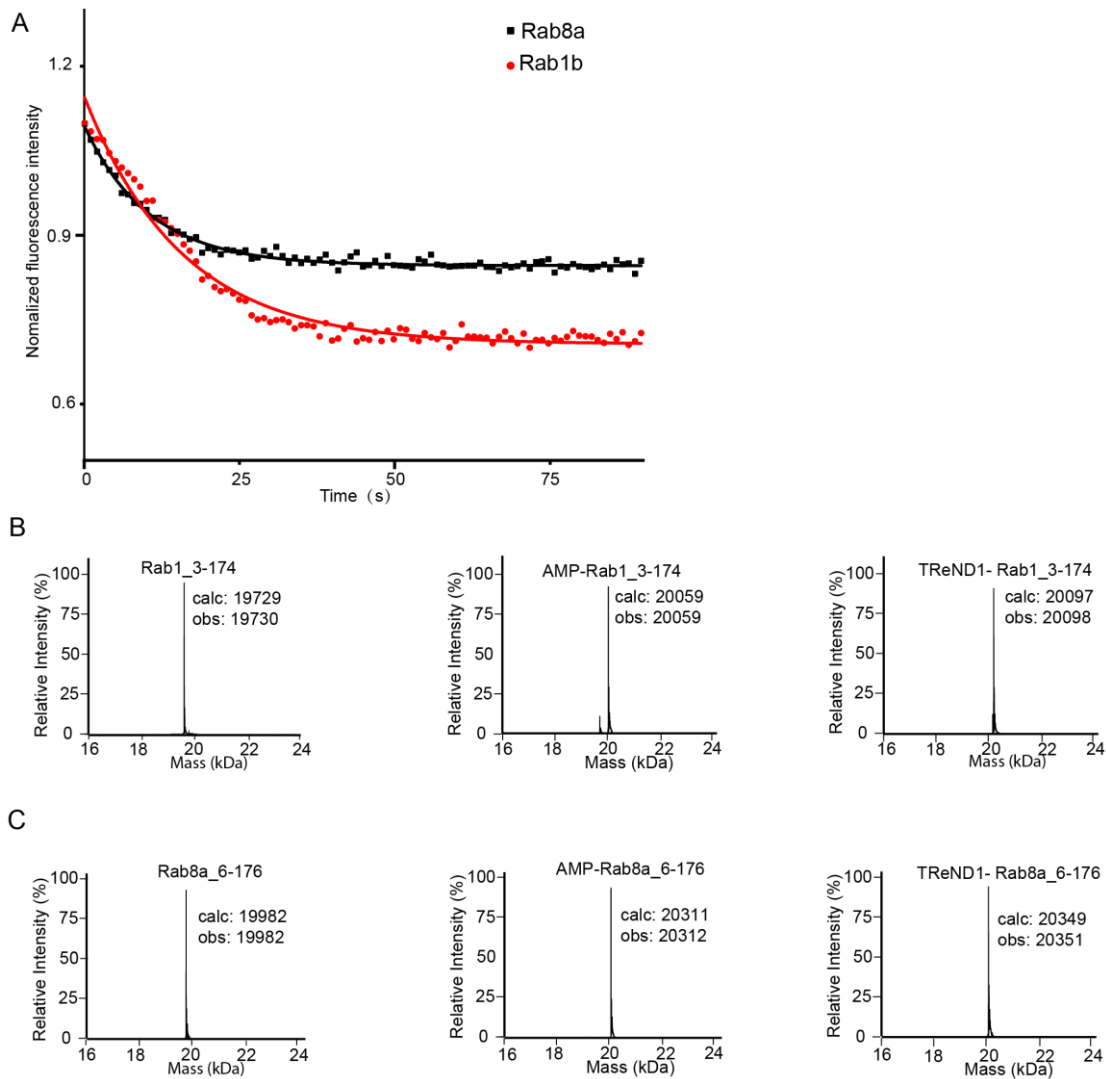
90. Gaspar AH, Machner MP. VipD is a Rab5-activated phospholipase A(1) that protects *Legionella pneumophila* from endosomal fusion. *Proc. Natl. Acad. Sci. USA* **111**, 4560-4565 (2014).
91. Anderson DM, Feix JB, Frank DW. Cross Kingdom Activators of Five Classes of Bacterial Effectors. *PLOS Pathog.* **11**, e1004944 (2015).
92. Fu H, Coburn J, Collier RJ. The Eukaryotic Host Factor That Activates Exoenzyme-S of *Pseudomonas-Aeruginosa* Is a Member of the 14-3-3 Protein Family. *Proc. Natl. Acad. Sci. USA* **90**, 2320-2324 (1993).
93. Kodama T, *et al.* Identification and characterization of VopT, a novel ADP-ribosyltransferase effector protein secreted via the *Vibrio parahaemolyticus* type III secretion system 2. *Cell. Microbiol.* **9**, 2598-2609 (2007).
94. Lee WL, Grimes JM, Robinson RC. *Yersinia* effector YopO uses actin as bait to phosphorylate proteins that regulate actin polymerization. *Nat. Struct. Mol. Biol.* **22**, 248-255 (2015).
95. Lopez VA, *et al.* A Bacterial Effector Mimics a Host HSP90 Client to Undermine Immunity. *Cell* **179**, 205-218 (2019).
96. Orth K, *et al.* Inhibition of the mitogen-activated protein kinase kinase superfamily by a *Yersinia* effector. *Science* **285**, 1920-1923 (1999).
97. Calder T, Kinch LN, Fernandez J, Salomon D, Grishin NV, Orth K. *Vibrio* Type III Effector VPA1380 Is Related to the Cysteine Protease Domain of Large Bacterial Toxins. *Plos One* **9**, e104387 (2014).

98. Coaker G, Falick A, Staskawicz B. Activation of a phytopathogenic bacterial effector protein by a eukaryotic cyclophilin. *Science* **308**, 548-550 (2005).
99. Itzen A, Blankenfeldt W, Goody RS. Adenylation: renaissance of a forgotten post-translational modification. *Trends Biochem. Sci.* **36**, 221-228 (2011).
100. Studier FW. Protein production by auto-induction in high density shaking cultures. *Protein Expr. Purif.* **41**, 207-34 (2005).
101. Wachtel R, *et al.* The protease GtgE from Salmonella exclusively targets inactive Rab GTPases. *Nat. Commun.* **9**, 44 (2018).
102. Giaccone G, Battey J, Gazdar AF, Oie H, Draoui M, Moody TW. Neuromedin-B Is Present in Lung-Cancer Cell-Lines. *Cancer Res.* **52**, S2732-S2736 (1992).
103. Lin DL, Chang CS. p53 is a mediator for radiation-repressed human TR2 orphan receptor expression in MCF-7 cells, a new pathway from tumor suppressor to member of the steroid receptor superfamily. *J. Biol. Chem.* **271**, 14649-14652 (1996).
104. Otto F. DAPI staining of fixed cells for high-resolution flow cytometry of nuclear DNA. *Methods Cell Biol.* **33**, 105-110 (1990).

Appendix

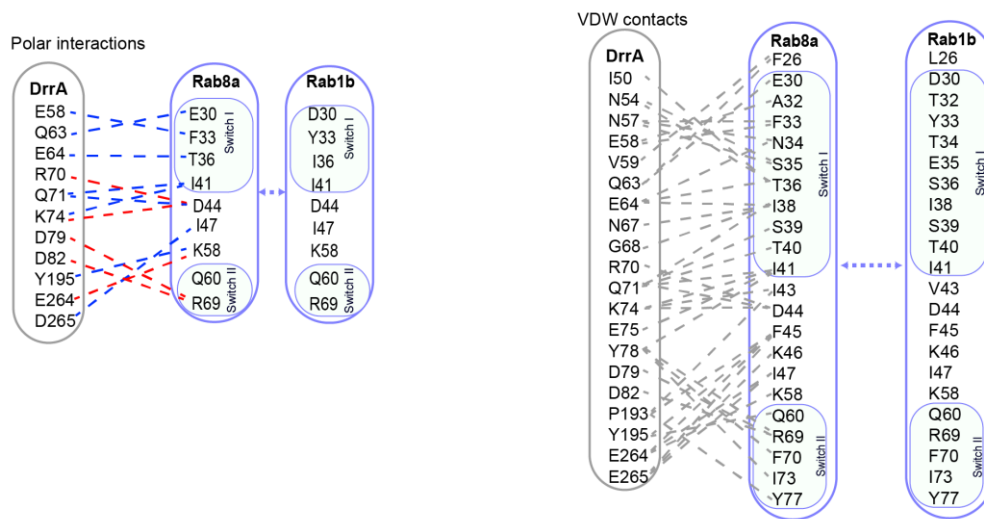
Supplementary Figures

Supplementary Figure 1



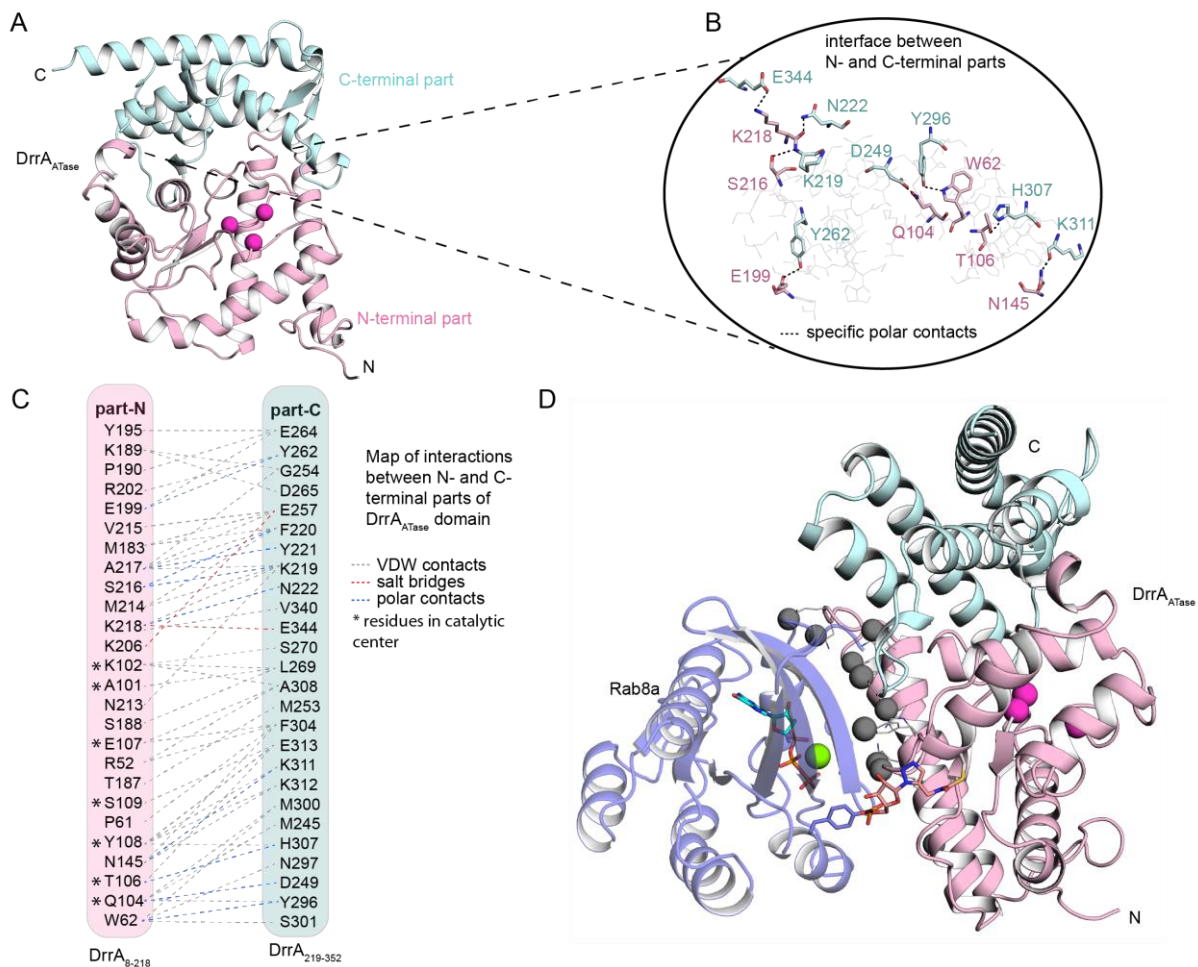
Supplementary Figure 1 DrrA-catalyzed AMPylation. (A) DrrA₁₆₋₃₅₂ AMPylates Rab8a and Rab1b with similar kinetics. Catalysis kinetics of DrrA toward Rab1b:GppNHp and Rab8a:GppNHp. The k_{cat}/K_M value of wt DrrA₁₆₋₃₅₂ toward Rab8a:GppNHp is $9.0 \times 10^5 \text{ M}^{-1} \text{ s}^{-1}$ ($\pm 1.2 \times 10^5 \text{ M}^{-1} \text{ s}^{-1}$). The k_{cat}/K_M value of wt DrrA₁₆₋₃₅₂ is $8.0 \times 10^5 \text{ M}^{-1} \text{ s}^{-1}$ ($\pm 2.0 \times 10^4 \text{ M}^{-1} \text{ s}^{-1}$). Data are means \pm standard error of the mean (SEM) from three independent experiments. (B) DrrA_{ATase} AMPylates Rab1b with adenosine triphosphate (ATP) or modified Rab1b with TReND-1. (C) DrrA_{ATase} AMPylates Rab8a with ATP or modified Rab8a with TReND-1. This picture is a copy from my previous manuscript to Nature Communications⁶⁰.

Supplementary Figure 2



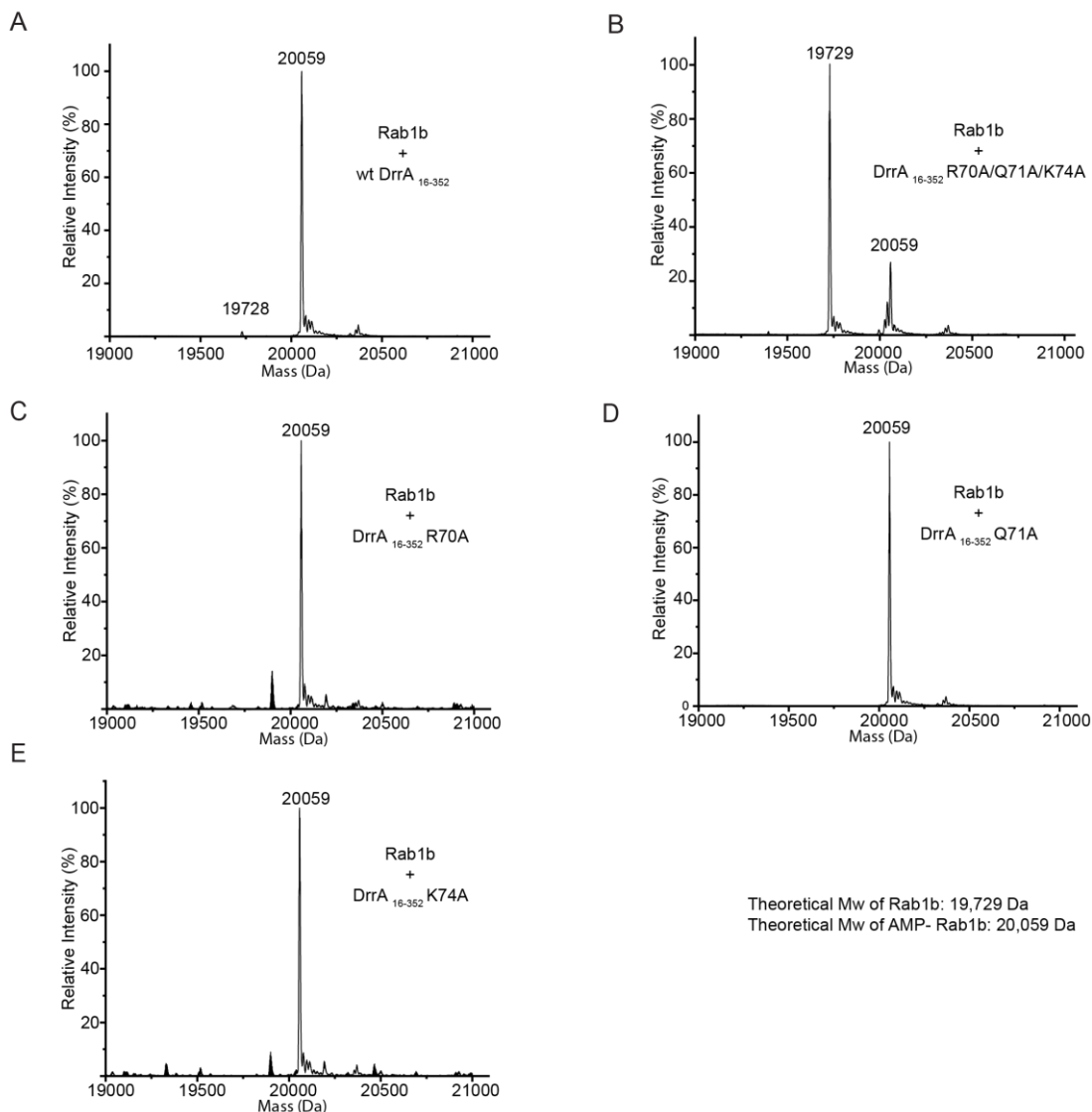
Supplementary Figure 2 Polar interactions and VDW contacts in DrrA:Rab8a complex. Polar interactions are shown with dashed lines: hydrogen bonds (blue), salt-bridges (red). VDW contacts are shown with grey dashed lines. The corresponding interaction residues in Rab1b are shown close to the Rab8a panels. This picture is a copy from my previous manuscript to Nature Communications ⁶⁰.

Supplementary Figure 3



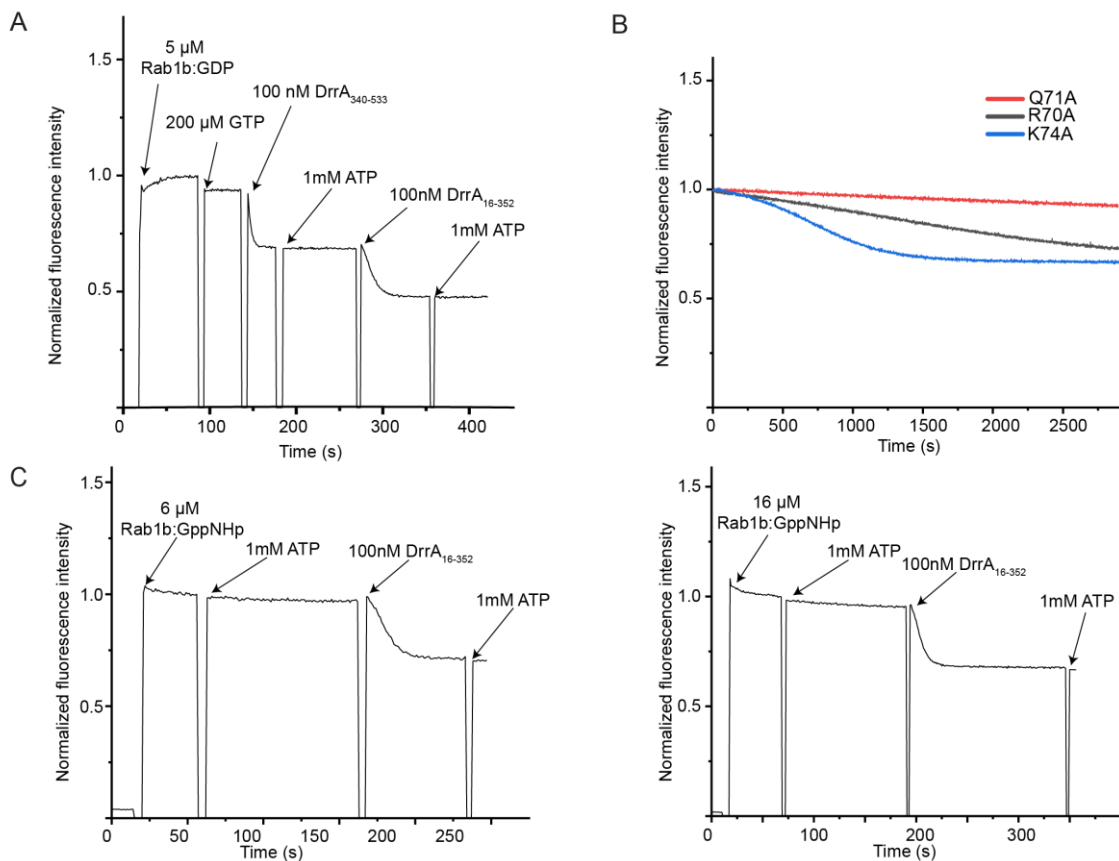
Supplementary Figure 3 Intra- and intermolecular interactions of N- and C-terminal parts of the DrrA ATase domain. (A) Schematic representation of N-terminal part (part-N, DrrA8-218, color pink) and C-terminal part (part-C, DrrA218-340, color cyan) in DrrA16-352. (B) Specific polar interaction involving sidechain-sidechain or sidechain-backbone between part-N (pink) and part-C (cyan). Interface between the parts is shown in transparent background. (C) Interaction map of part-N and part-C of DrrA_{ATase} domain. The residues within the catalytic site are illustrated with asterisks. Van der Waals contacts are gray, polar contacts are blue, salt bridges are red. (D) Mainly the residues in the part-N contacts Rab1b in the back site and only residue which contacts Rab1b in the back site from part-C is E264. Interacting residues are highlighted with black sphere. This picture is a copy from my previous manuscript to Nature Communications⁶⁰.

Supplementary Figure 4



Supplementary Figure 4 In vitro AMPylation of 100 μ M Rab1b₃₋₁₇₄:GppNHp by DrrA₁₆₋₃₅₂ (5 μ M) and DrrA NC-RBS-mutants (5 μ M). AMPylation was carried out for 72 h. The mass of AMPylated and non-AMPylated Rab1b₃₋₁₇₄ was determined by intact mass spectrometry. The triple-mutant R70A/Q71A/K74A has minor AMPylation activity, whereas the single mutants are still capable of producing AMPylated Rab1b (Mw(Rab1b₃₋₁₇₄)= 19,729 Da, Mw(AMP-Rab1b₃₋₁₇₄)=20,059 Da). (A) Rab1b AMPylated by wt DrrA₁₆₋₃₅₂. (B) Rab1b AMPylated by DrrA₁₆₋₃₅₂R70A/Q71A/K74A. (C) Rab1b AMPylated by DrrA₁₆₋₃₅₂R70A. (D) Rab1b AMPylated by DrrA₁₆₋₃₅₂Q71A. (E) Rab1b AMPylated by DrrA₁₆₋₃₅₂K74A. This picture is a copy from my previous manuscript to Nature Communications⁶⁰.

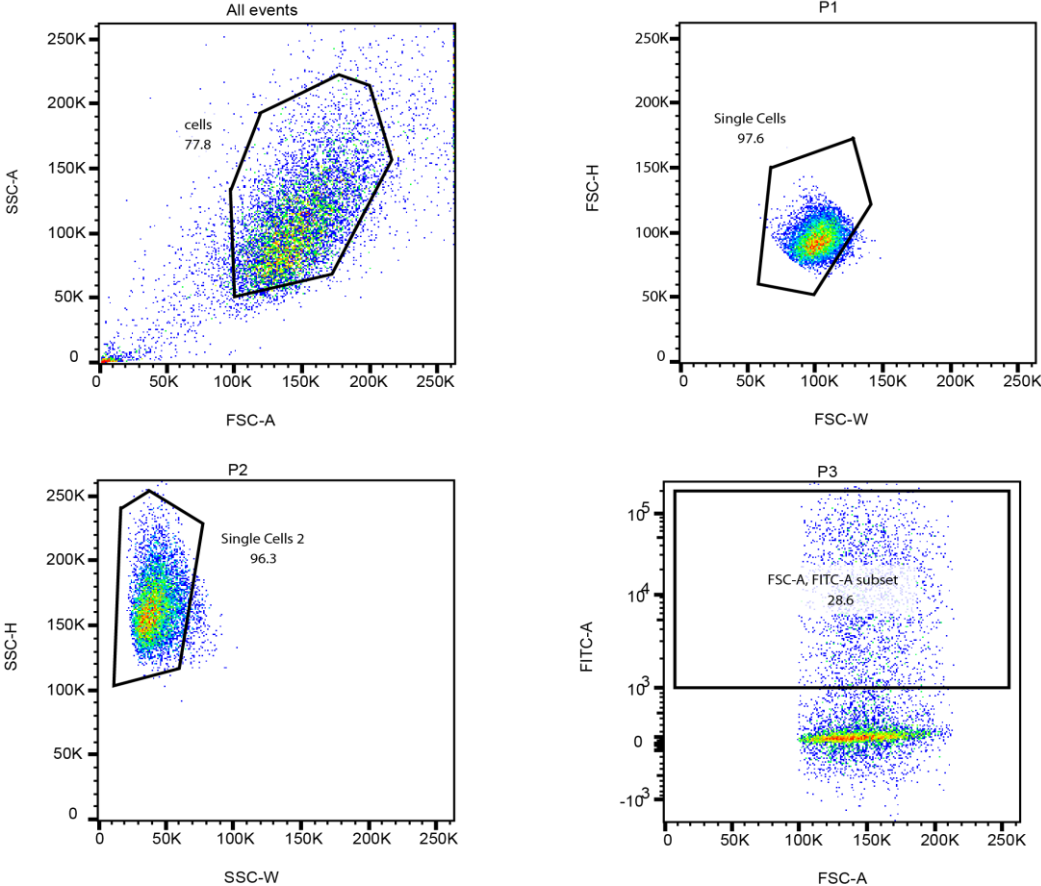
Supplementary Figure 5



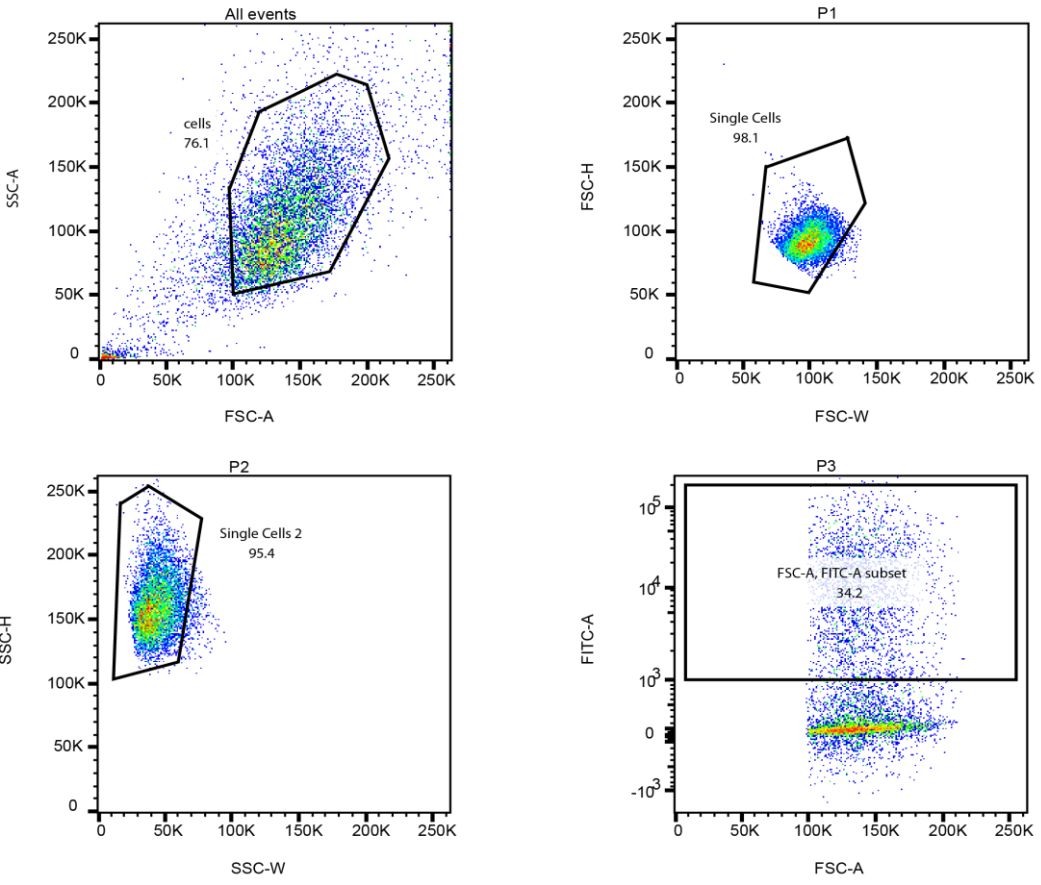
Supplementary Figure 5 Representative kinetics profiles for DrrA-catalyzed AMPylation of Rab1b by time-resolved tryptophan fluorescence. a) Standard procedure for studying the AMPylation activity of wt DrrA or DrrA alanine mutants in the allosteric binding site. b) Catalysis kinetics of DrrA mutants (R70A, Q71A, and K74A) toward Rab1b:GTP. The tryptophan fluorescence intensity is normalized to 1.0 before adding DrrA. c) Representative kinetic profiles for allosteric activation. The tryptophan fluorescence intensity of Rab1b:GppNHp is normalized to 1.0. This picture is a copy from my previous manuscript to Nature Communications⁶⁰.

Supplementary Figure 6

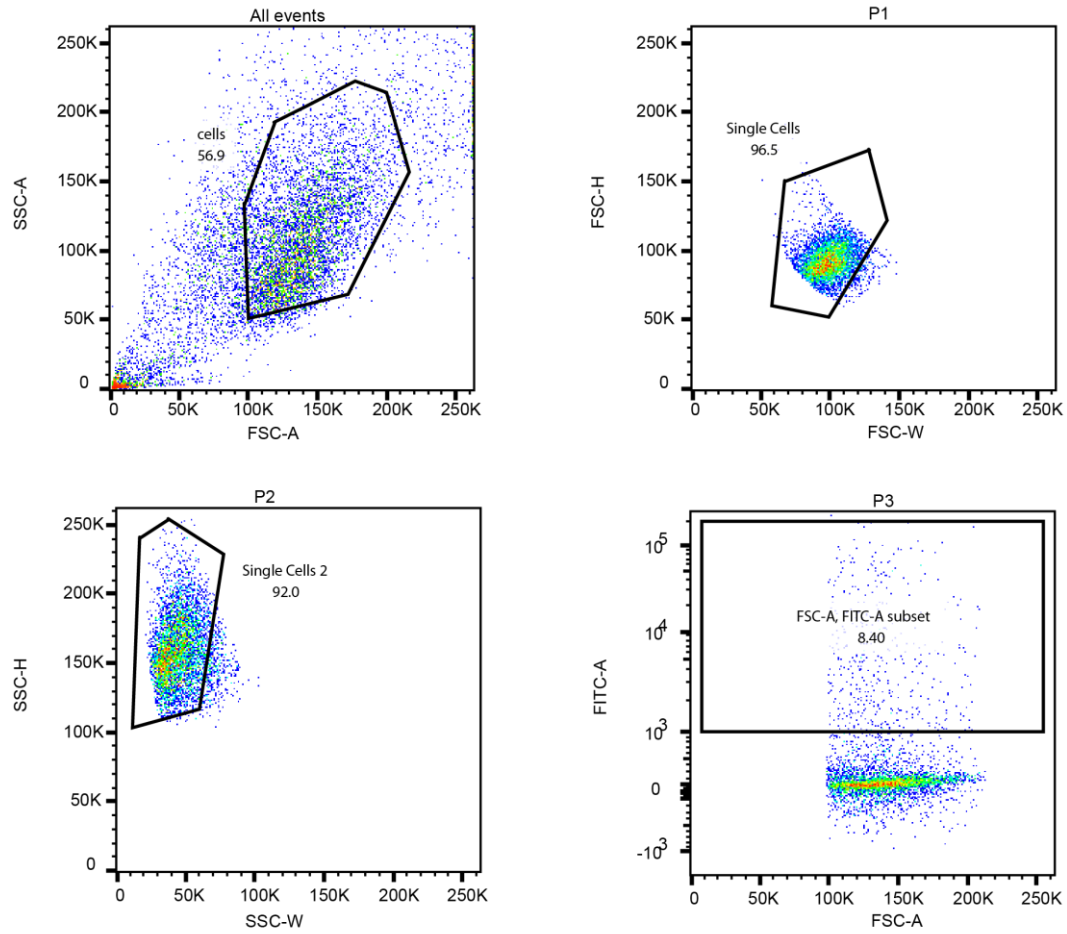
A



B

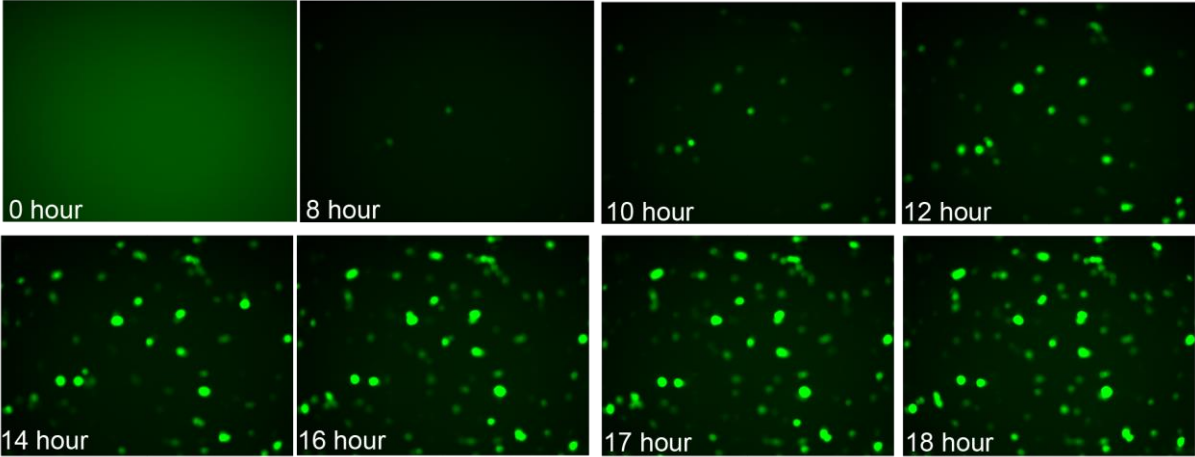


C



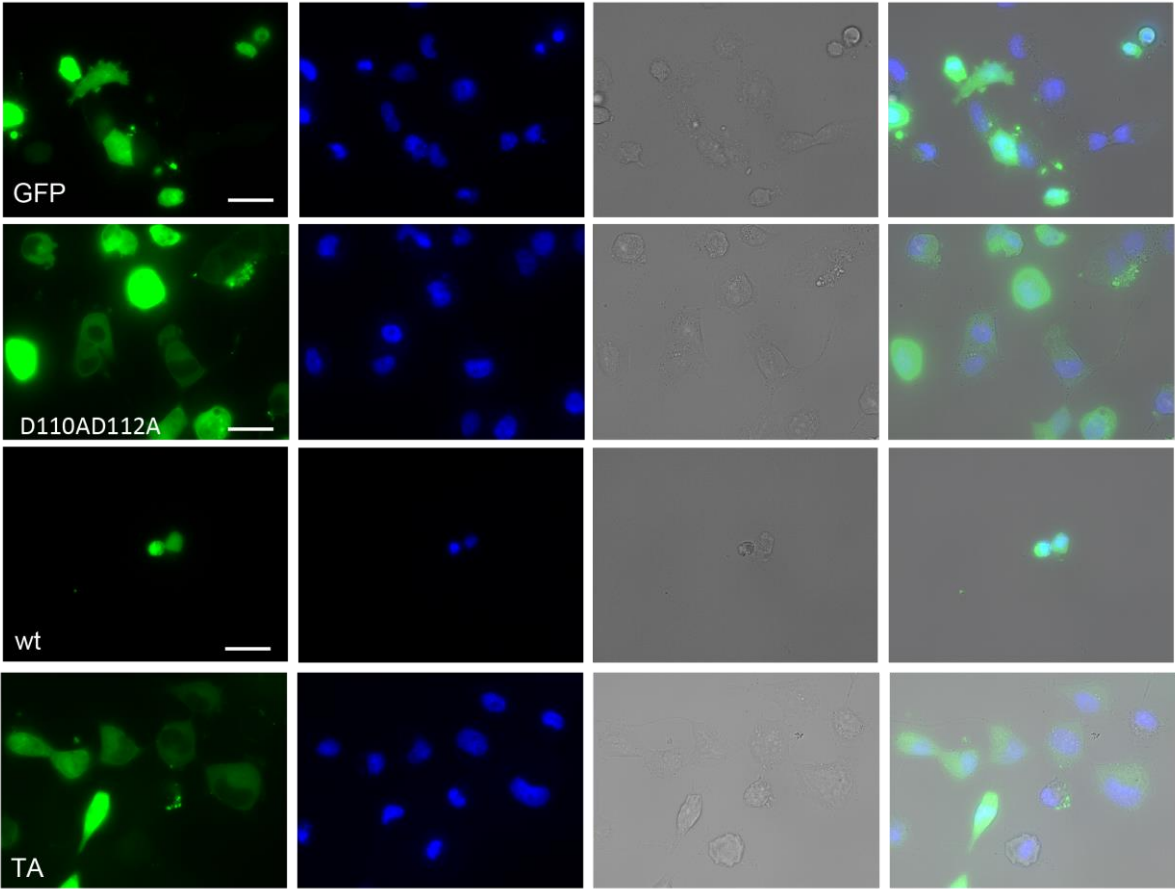
Supplementary Figure 6 Representation of gating strategy for sorting GFP-positive H1299 cells. (A) Sorting GFP-positive cells for DrrA₈₋₅₃₃R70A/Q71A/K74A transfected sample. (B) Sorting GFP-positive cells for DrrA₁₆₋₃₅₂D110A/D112A transfected sample. (C) Rab1b Sorting GFP-positive cells for DrrA₈₋₅₃₃ transfected sample.

Supplementary Figure 7



Supplementary Figure 7 Monitoring the expression level of GFP in H1299 cells. After transfection with the GFP control plasmid (M0786), cells were cultured with 5% carbon dioxide (CO₂) at 37 °C in Keyence BZ-9000 system. Cell images were taken in every 20 minutes. In general, cell starts to express GFP protein 8 hours after transfection.

Supplementary Figure 8



Supplementary Figure 8 Cell imaging for sorted cells from FACS. Cells were stained with DAPI for the observation of the nucleus. Cell images were taken at the same time when MTS assay was performed.

Supplementary Table 1

Data collection and refinement statistics (Data collection and refinement are contributed by Sabine Schneider)

	DrrA₁₆₋₃₅₂:TReND-1:Rab8a₆₋₁₇₆ PDB code 6YX5
Wavelength (Å)	0.966
Resolution range	48.02 - 2.14 (2.2 - 2.14)
Space group	P 3 2 1
Unit cell	142.3 142.3 76.6 90 90 120
Total reflections	980,292 (8,6871)
Unique reflections	49,091 (4,745)
Multiplicity	20.0 (18.3)
Completeness (%)	99.7 (97.0)
Mean I/sigma(I)	15.6 (0.93)
Wilson B-factor	43.5
R-merge	0.201 (2.43)
R-meas	0.206 (2.50)
R-pim	0.0458 (0.575)
CC1/2	0.999 (0.43)
CC*	1 (0.775)
Reflections used in refinement	49,075 (4,744)
Reflections used for R-free	2,440 (227)
R-work	0.23 (0.35)
R-free	0.25 (0.36)
CC(work)	0.95 (0.57)
CC(free)	0.93 (0.56)
Number of non-hydrogen atoms	4,353
macromolecules	4,146
ligands	94
solvent	113
Protein residues	512
RMS(bonds)	0.013
RMS(angles)	1.7
Ramachandran favored (%)	97.2
Ramachandran allowed (%)	2.7
Ramachandran outliers (%)	0.00
Rotamer outliers (%)	2.7
Clashscore	2.9
Average B-factor	32.32
macromolecules	31.26
ligands	66.34
solvent	43.06
Number of TLS groups	2

Statistics for the highest-resolution shell are shown in parentheses. This tabel is a copy from my previous manuscript to Nature Communications ⁶⁰.

List of figures

- Figure 1** Schematic representation of AMPylation. Hydroxyl-bearing side chains of target proteins are AMPylated by AMPylators. ATP is the co-substrate. 10
- Figure 2** Enzymatic mechanism of Fic enzymes. **(A)** Schematic representation of the general binding mode of the co-factor ATP. **(B)** Cartoon representation of complex structure IbpA: Cdc42. The green sphere represents the Mg^{2+} ion. Stick binds to Mg^{2+} ion: GDP. Cdc42 is AMPylated in Tyr32 by IbpA. **(C)** Schematic representation of interactions between the flap unit and the switch I region of Cdc42 (PDB: 4ITR). Red region indicates the catalytic center of IbpA. Purple region indicates the flap unit in IbpA. 12
- Figure 3** The potential AMPylation mechanism by AMP-transferases DrrA. Magnesium ions bridge the coordination between three aspartate residues and the triphosphate group of ATP. The second aspartate residue was suggested as the base to deprotonate the hydroxyl group. 14
- Figure 4** Representation of the interactions between ATP and pseudokinase SelO. The green sphere represents the Mg^{2+} ion. The sphere with wheat color represents the Ca^{2+} ion. Stick is ATP. 15
- Figure 5** Schematic representation of domain organization in full-length DrrA. Amino acid 1 to 340 is the AMPylation domain. GEF domain is from amino acid 340 to 533. The rest is the P4M domain. Picture is a copy from my previous manuscript to Nature Communications⁶⁰. 19
- Figure 6** Switch cycling of RabGTPases. Inactive Rab proteins bind to GDIs in the cytosol. GEF proteins convert Rab protein to active state by nucleotide exchange. In the active state, Rab proteins interact with downstream effectors in defined compartments. The active Rab proteins are deactivated by GAPs-mediated intrinsic GTPase activity. 20
- Figure 7** Cartoon representation of the structure of Rab proteins. Stick is GppNHp. Green sphere is Mg^{2+} . PDB: 1YZL⁶³. 21
- Figure 8** Chemical structures of TReND analogues and co-substrate-mediated covalent capture concept in Fic enzymes. **(A)** Chloroacetamide contained TReND analogues. The nomenclature of the TReND analogues is according to the linker length. **(B)** General strategy of co-substrate-mediated covalent capture in Fic enzymes. The chloroacetamide reacts with the engineered cysteine yield a binary complex. Following, targets can be trapped by the AMP-transfer reaction. Figure 8B is a courtesy of Burak Gulen and has been reprinted with his permission. 23
- Figure 9** Trapping the DrrA:Rab complex via thiol-reactive nucleotide analog 1. Rab1b or Rab8a will be modified with TReND-1 at the AMPylation site Y77. The strategically designed cysteine will react with thiol-reactive nucleotide analog 1. Picture is a copy from my previous manuscript to Nature Communications⁶⁰. 25
- Figure 10** Expression, purification and characterization of the DrrA AMPylation domain. **(A)** DrrA₁₋₃₄₀ and DrrA₈₋₃₄₀ share decreased AMPylation activity. The k_{cat}/K_M value of His tag DrrA is $5.6 \times 10^5 M^{-1} s^{-1}$. **(B)** Interactions between the long helix (light blue) and the other helices (pink). PDB: 3LOI. **(C)** DrrA₈₋₃₅₂ is an optimized construct. The k_{cat}/K_M value of His tag DrrA₈₋₅₃₃ is $5.6 \times 10^5 M^{-1} s^{-1}$ 29
- Figure 11** DrrA_{ATase} is a monomeric protein. **(A)** DrrA₈₋₃₄₀ shows the same monomer peak in analytical size exclusion chromatography in a concentration-independent manner. **(B)** DrrA₈₋₃₄₀ does not change its monomer state in the presence of Rab1b:GppNHp and nucleotide ATP. 30
- Figure 12** N-terminus of DrrA AMPylation domain plays a significant role in AMPylation. **(A)** Relative Tryptophan fluorescence change by different DrrA constructs. The k_{cat}/K_M value of DrrA₁₆₋₃₅₂ is $7.4 \times 10^5 M^{-1} s^{-1}$. The k_{cat}/K_M value of DrrA₃₀₋₃₅₂ is $2.4 \times 10^3 M^{-1} s^{-1}$. **(B)** DrrA₁₆₋₃₅₂

and DrrA₃₀₋₃₅₂ share identical ATase activities. 100 μM ATP and 5 μM DrrA constructs were incubated for overnight, samples were analyzed by reverse phase chromatography. **(C)** Important residues in the N-terminus of DrrA AMPylation domain for maintaining the AMPylation activity. R24_{DrrA} is important for interaction with Rab1b. **(D)** Interactions among D22DrrA, E23DrrA, R24DrrA, and R139_{DrrA}. Orange spheres are catalytic Asp residues. PDB: 3NKU (orange)..... 31

Figure 13 DrrA₁₆₋₃₅₂ show similar kinetic features with DrrA₈₋₃₄₀. **(A)** DrrA₁₆₋₃₅₂-catalyzed Rab1b:GppNHp AMPylation in the presence of pyrophosphatase. Sigmoidal dependence of AMPylation from active Rab1b-concentration. Red curve is the Hill-fit with the cooperativity parameter 1.8 ± 0.19 , black curve is the Michaelis-Menten-fit. **(B)** DrrA₈₋₃₄₀-catalyzed Rab1b AMPylation in the absence of pyrophosphatase. Sigmoidal dependence of AMPylation from active Rab1b-concentration. Red curve is the Hill-fit with the cooperativity parameter 2.2 ± 0.30 , black curve is the Michaelis-Menten-fit. 33

Figure 14 Mass spectrometry analysis of DrrA₁₆₋₃₅₂ and methylated DrrA₁₆₋₃₅₂. The increased mass indicated that all the 30 lysine residues in DrrA were methylated..... 34

Figure 15 Profiling substrate recognition and catalytic residues in DrrA AMPylation domain. Alanine mutations in the putative catalytic center inactive DrrA. R139A (not located in the catalytic center) also inactive the AMPylation activity of DrrA. 34

Figure 16 Detection of the potential ATP binding mode in DrrA AMPylation domain by forming DrrAcys-TReND-1 binary complex. **(A)** DrrA is deficient in ATP hydrolysis. Antarctic Phosphatase was used to generate adenosine as a reference. Snake venom phosphodiesterase was used to generate adenosine and AMP as another reference. **(B)** Rab1b can be modified with TReND-1 by wild type DrrA₁₆₋₃₅₂. **(C)** Schematic representation of the region of D249 and R246, and the region of R158 and D177. K223C, F228C, F250C, and M253C are located in the region of D249 and R246. Orange spheres are catalytic Asp residues. PDB: 3NKU (orange) and 3LOI (blue). Model is created by superimposing these two structures. Figure 16B and 16C are copies from my previous manuscript to Nature Communications⁶⁰..... 36

Figure 17 Conceptual design for stabilising the low affinity DrrA_{ATase}:Rab complexes. **(A)** Selection of Cys substitution sites (M169, M174, V175, L197 and G198, purple) in the model, and superimposition of DrrA₈₋₂₁₈ (PDB: 3NKU, orange) onto GS-ATase (PDB: 3K7D, light green background). **(B)** SDS-PAGE shift analysis of DrrA:TReND-1:Rab1b complex formation. **(C)** Demonstration of the positions of L197_{DrrA} (color blue) and D82_{DrrA} (color light blue). Pink spheres: the active site of DrrA_{ATase}. **(D)** SDS-PAGE shift analysis of preparative DrrA:TReND-1:Rab1b (DR1) / Rab8a (DR8) complex formation. **(E)** Intact mass spectrometry analysis of the DrrA:TReND-1:Rab8a complex. Picture is a copy from my previous manuscript to Nature Communications⁶⁰..... 40

Figure 18 Structure of the DrrA:Rab8a complex. **(A)** Orthogonal views of the Rab8-DrrA complex. Pink spheres denote the catalytic Asp residues of DrrA. The green sphere represents the Mg²⁺ ion. **(B)** Linker density from the unbiased simulated-annealing omit DFo-Fc electron density map contoured at 2.5 σ. The R subscript denotes Rab8a, and the D subscript denotes DrrA. **(C)** Schematic representation of the Rab8-DrrA interface. Interactions are shown with dashed lines; hydrogen bonds are blue and salt bridges are red. The corresponding interaction residues in Rab1b are shown in the panel on the right. Important residues for maintaining enzymatic activity are coloured cyan, and 'α' represents α-helix. **(D)** Demonstration of the conventional site (RBS1, containing the catalytic centre) and non-conventional site (RBS2, the back face of the catalytic centre). **(E)** Structural comparison between the catalytic centre in GS-ATase (PDB: 3K7D, green) and the catalytic centre in

DrrA in the DrrA-Rab8a complex. The catalytic centre of DrrA includes D110_{DrrA}, D112_{DrrA} and D150_{DrrA}. The catalytic centre of GS-AT includes D701_{GS-AT}, D703_{GS-AT} and D753_{GS-AT}. **(F)** Structural superposition of free AMP-Rab1b:GppNHp (PDB: 3NKV, yellow) and Rab8a (PDB: 4LHW, pink) with Rab8a (blue) from the complex with DrrA. Green spheres indicate Mg²⁺ ions, and GppNHp is shown in stick representation. Picture is a copy from my previous manuscript to Nature Communications ⁶⁰..... 43

Figure 19 Confirmation of the NC-RBS complex interface. **(A)** Melting point (T_m) determination of DrrA and DrrA alanine mutants by circular dichroism (CD). The melting point of wt DrrA is 60.1°C. Data are means ± standard error of the mean (SEM) from three independent experiments. **(B)** Determination of Rab1b-AMPylation rates in vitro by DrrA with mutations in the non-conventional site. The k_{cat}/K_M value of wt DrrA toward Rab8a:GppNHp is 9.0 × 10⁵ M⁻¹ s⁻¹ (± 1.2 × 10⁵ M⁻¹ s⁻¹). Data are means ± standard error of the mean (SEM) from three independent experiments. **(C)** Validation of the non-conventional (NC) site from DrrA mutation: AMPylation rates. The k_{cat}/K_M value of wt DrrA toward Rab1b:GppNHp is 8.0 × 10⁵ M⁻¹ s⁻¹ (± 2.0 × 10⁴ M⁻¹ s⁻¹). Data are means ± standard error of the mean (SEM) from three independent experiments. Picture is a modified copy from my previous manuscript to Nature Communications ⁶⁰..... 46

Figure 20 Allosteric activation of DrrA by active Rab1b. **(A)** Construction of the DrrA apo-form. DrrA₈₋₂₁₈ (PDB: 3NKU, orange) and DrrA₁₉₃₋₃₅₂ (PDB: 3LOI, blue) are superimposed onto GS-ATase (PDB: 3K7D, light green background). Orange spheres represent the catalytic Asp residues of DrrA₈₋₂₁₈. **(B)** Global structural changes in DrrA by binding to active Rab1b. DrrA₈₋₂₁₈ (PDB: 3NKU, orange) and DrrA₁₆₋₃₅₂ (grey) are shown. **(C)** Structural changes in the active centre of DrrA induced by Rab1b binding to the non-conventional site. Purple spheres represent the catalytic centre of DrrA₁₆₋₃₅₂ in the DrrA:TReND-1:Rab8a complex. Orange spheres represent the catalytic centre of DrrA₈₋₂₁₈ (PDB: 3NKU, orange). **(D)** Sigmoidal dependence of AMPylation on the active Rab1b concentration. The red curve represents the Hill fit with a cooperativity parameter of n = 1.7 ± 0.16; the black curve is the Michaelis-Menten fit. Data are means ± SEM from three independent experiments. **(E)** Full length DrrA₁₆₋₆₄₇ mediated AMPylation. The red curve represents the Hill fit with a cooperativity parameter of n = 1.6 ± 0.20; the black curve is the Michaelis-Menten fit. Data are means ± SEM from three independent experiments. **(F)** Cytotoxicity analysis of DrrA single alanine mutants in H1299 cells. Cell viability values (determined by MTS assay) of DrrA-expressing cells (eGFP-positive) were determined in relation to the eGFP vector control. WT: DrrA₈₋₅₃₃; R70A: DrrA_{8-533_R70A}; Q71A: DrrA_{8-533_Q71A}; K74A: DrrA_{8-533_K74A}. Data are means ± SEM from three independent experiments. One-way analysis of variance (ANOVA) was applied; ns, p > 0.05; ****, p < 0.0001. **(G)** Cytotoxicity analysis of DrrA mutants in H1299 cells. Cell viability values (determined by MTS assay) of DrrA-expressing cells (eGFP-positive) were determined in relation to the eGFP vector control. TA: DrrA_{8-533_R70A_Q71A_K74A}; DD: DrrA_{8-533_D110_D112A}. Data are means ± SEM from three independent experiments. One-way analysis of variance (ANOVA) was applied; ns, p > 0.05; ***, p < 0.001; **, p < 0.01; *, 0.01 p < 0.05. Picture is a copy from my previous manuscript to Nature Communications ⁶⁰..... 50

Figure 21 Representation of gating strategy for sorting GFP-positive H1299 cells. Side scatter area (SSC-A) versus forward scatter area (FSC-A) density plot was applied for excluding debris and dead H1299 cells. Selected population was named as P1. The plot (forward scatter height (FSC-H) versus forward scatter width (FSC-W)) is used to discriminate doublets from single cells; selected population was marked as P2. The plot (side scatter height (SSC-H) versus side scatter width (SSC-W)) was further used to ensure the selection of single cells, selected population was labelled as P3. Subsequently, the last plot

(FITC-A (GFP channel) versus FSC-A) was applied to separate the GFP-positive cells (P4 population) from the GFP-negative cells. The proper gating was set up using non-transfected cells as negative control. **(A)** Non-transfected H1299 cells was taken as negative control. **(B)** GFP- transfected H1299 cells as positive control. Picture is a copy from my previous manuscript to Nature Communications ⁶⁰ 52

Figure 22 Strategy for the formation of the covalently linked complex. **(A)** The ATP binding mode in DrrA₁₆₋₃₅₂. DrrA fragment is from the non- canonical DrrA- Rab8a complex, PDB: 6YX5. Green residues are T187C_{DrrA}, K219C_{DrrA}, and K223C_{DrrA}. Yellow region is the catalytic center. Stick is ATP. **(B)** Catalysis kinetics of wt DrrA and R303A_{DrrA} toward Rab1b:GTP. The k_{cat}/K_M value of DrrA₁₆₋₃₅₂ was normalized to 1. The k_{cat}/K_M value of DrrA₁₆₋₃₅₂ is $8.0 \times 10^5 \text{ M}^{-1} \text{ s}^{-1}$. The k_{cat}/K_M value of R303A_{DrrA} is $1.1 \times 10^3 \text{ M}^{-1} \text{ s}^{-1}$. **(C)** SDS-PAGE shift analysis for complex formation with cysteine mutants based on previous model. **(D)** A new ATP binding mode in DrrA₁₆₋₃₅₂. DrrA fragment is from the non-canonical DrrA-Rab8a complex, PDB: 6YX5. Purple spheres are D110 and D112. Green spheres are Mg²⁺. Stick is ATP. This model is generated by Autodock ⁸⁶. **(E)** Cys substitution sites (A176, D177 and T181, light orange) in DrrA_{ATase}. Pink spheres represent the catalytic center of DrrA. RBS1 indicates the conventional site, which contains the catalytic center. NC-RBS represents the non-canonical site, which is located at the back face of the catalytic center. **(F)** SDS-PAGE shift analysis of DrrA:TReND-1:Rab1b complex formation in the catalytic side (RBS1). Picture E and F are copies from my previous manuscript to Nature Communications ⁶⁰ 55

Figure 23 Strategy for the purification of the covalently linked complex. **(A)** Procedures for obtaining pure canonical complex. By Ni-chelating column, DrrA is separated from the canonical complex and Rab. After PreScission digestion, size exclusion chromatography was performed to get the pure complex. **(B)** Intact mass spectrometry analysis of the DrrA₁₆₋₃₅₂-A176C:TReND-1:Rab1b complex. **(C)** Intact mass spectrometry analysis of the DrrA₁₆₋₃₅₂-A176C:TReND-1:Rab8a complex. 57

Figure 24 Biochemical characterization of DrrAA176C -Rab1b complex. **(A)** Comparison of the catalytic activity of DrrAA176C -Rab1b with the non- canonical complex. **(B)** Composite model of DrrA produced from the following crystal structures PDB: 6YX5, 3LOI, 3N6O. The different binding sites of Rab-molecules is indicated at the GEF-domain and the NC-RBS. The catalytic site of the AMPylation domain (composed by D110, D112, D150) is indicated by magenta spheres. GEF: Guanine nucleotide exchange factor; P4M: phosphatidylinositol-4-phosphate (PI4P) binding of DrrA. **(C)** Model of DrrA action at the membrane. The P4M localizes DrrA to the membrane by binding to PI4P. The GEF-domain activates Rab1b by GDP-to-GTP exchange, thereby displacing it from GDI and creating membrane-bound Rab1b:GTP (yellow ribbons indicate geranylgeranyl lipids). Binding of Rab1b:GTP to the NC-RBS of DrrA putatively results in structural rearrangement of the catalytic site, which stimulates the subsequent AMPylation of another Rab1b:GTP-molecule. This picture is a copy from my previous manuscript to Nature Communications ⁶⁰ 59

List of Tables

Table 1 DrrA cysteine mutants for DrrAcys-TReND-1 binary complex formation. IbpA ₃₄₈₃₋₃₇₉₇ I3455C can form a binary complex with TReND-1, and was used as a positive control. Wild type DrrA ₈₋₅₃₃ was used as a negative control.....	37
Table 2 Buffer conditions for obtaining crystals of the covalent complexes.	58

Acknowledgement

From 2016.10.10, I started my PhD study at TU Munich, Germany. I thought that I could not graduate as a doctor since I switched my study from Organic Chemistry to Biochemistry. Therefore, I made up my mind that if it would be acceptable if I would fail after giving my best. However, I didn't realise that it would be such a colourful journey.

I am thankful to my supervisor, Prof. Aymelt Itzen. Prof. Itzen created this PhD project for me and gave me the opportunity to work on it. Prof. Itzen is open for scientific discussions and happy to help his co-workers. Also, Prof. Itzen helped me to get Prof. Kathrin Lang as my mentor, who had beautiful collaboration with us for this "old but new" project. Therefore, I would also like to express my gratitude to my mentor Prof. Kathrin Lang. I also want to thank Prof. Christian Hedberg to offer us the TReND analogues and provide me constructive advices. Importantly, I would like to say thank you to Sabine Schneider, since she was always optimistic about this project and happy to crystalize the samples for me.

Importantly, I want to thank our lab members, especially Burak. He has not only spent so much time to teach me all the basics at the beginning but also picked up a terrific "training project" for me. Moreover, he protected me as an elder brother in the lab. I am so thankful for all the things he did. Without his help and protection, I would have not been able to continue my PhD journey until today. After that, I want to say thank you to Joel, Sergey, Vivian, Doro, Sophie and Rudi. Without your support, it would be difficult for me to face all the challenges alone. I still remembered that Joel went to the renting company to ask renting offers for me in the early morning of winter in Munich; I still remembered that Sophie and Doro tried their best to find the student accommodation for me in Munich; I still remembered that all of lab members gave me help when I was in trouble in Munich or in Hamburg. Of note, I would like to express my gratitude to Themis and Steffi from UKE for great assistance in cell biology study.

I want to thank my family, especially my wife and my kid. Thanks for your strong support and love. In the end, I want to share my favourite motto with you: something that doesn't kill you makes you stronger.

Rights and permissions

Figures which are originally or modified from my previous manuscript are already specifically stated in the thesis ⁶⁰.

This work is licensed under the Creative Commons Attribution 4.0 International License. To view a copy of this license, visit <http://creativecommons.org/licenses/by/4.0/> or send a letter to Creative Commons, PO Box 1866, Mountain View, CA 94042, USA.

Statutory declaration

I hereby affirm that I have prepared the present work independently and only using the specified aids. All literal or substantive citations are marked as such and listed in the bibliography. This work has not yet been submitted to an examination committee for assessment.

Hamburg, October of 2020

Jiqing Du

(Jiqing Du)